Testing and Analysis of a Fiber-Reinforced Polymer (FRP) Bridge Deck

By

Zihong Liu

Dissertation submitted to the Faculty of

Virginia Polytechnic Institute and State University

in partial fulfillment for the requirements for the degree of

Doctor of Philosophy

in

Civil Engineering

Thomas E. Cousins, Co-Chair

John J. Lesko, Co-Chair

Raymond H. Plaut

Carin L. Roberts-Wollmann

Elisa Sotelino

June 27, 2007

Blacksburg, VA

Keywords: Fiber-reinforced polymer (FRP), composite, pultrusion, structure, bridge deck, rehabilitation, finite element

Testing and Analysis of a Fiber-Reinforced Polymer (FRP) Bridge Deck

Zihong Liu

Dr. Thomas E. Cousins, Co-Chair

Civil Engineering

(ABSTRACT)

A fiber reinforced polymer (FRP) composite cellular deck system was used to rehabilitate a historical cast iron thru-truss structure (Hawthorne St. Bridge in Covington, Virginia). This research seeks to address following technical needs and questions to advance FRP deck application.

The critical panel-to-panel connections were developed and evolved through a four-stage study and finally realized using full width, adhesively bonded tongue and groove splices with scarfed edges. Extensive experimental study under service, strength and fatigue loads in a full-scale two-bay mock-up test and a field test was performed. Test results showed that no crack initiated in the joints under service load and no significant change in stiffness or strength of the joint occurred after 3,000,000 cycles of fatigue loading. Various issues related to constructability of FRP deck systems were investigated and construction guidelines and installation procedures for the deck system were established.

The structural performance of the FRP-on-steel-superstructure system was examined in the laboratory and field under service load. Tests results confirmed the following findings: (1) the clip-type of panel-to-stringer connection provides little composite action as expected, which fulfilled the design intention; (2) local effects play an important role in the performance of FRP deck; (3) the FRP deck design is stiffness driven rather than strength driven like traditional concrete deck.

Finally, an FEM parametric study was conducted to examine two important design issues concerning the FRP decks, namely deck relative deflection and LDF of supporting steel girders. Results from both FEM and experiments show that the strip method specified in AASHTO LRFD specification (AASHTO 2004) as an approximate method of analysis can also be applied to unconventional FRP decks as a practical method. However, different strip width equations have to be determined by either FEM or experimental methods for different types of FRP decks. In this study, one such an equation has been derived for the Strongwell deck. In addition, the AASHTO LDF equations for glued laminated timber decks on steel stringers provide good estimations of LDFs for FRP-deck-on-steel-girder bridges. The lever rule can be used as an appropriately conservative design method to predict the LDFs of FRP-deck-on-steel-girder bridges.

ACKNOWLEDGEMENTS

I would like to sincerely thank my advisor and co-chair of my committee, Dr. Cousins. It was you who brought me into the door and guided me through my research endeavors. Your suggestions were always constructive and beneficial, no matter in my research or in my life. Your humor and generosity made my life much easier than I thought be. Thank you for all of the once-in-a-lifetime opportunities and I could not have made a better choice that will forever guide my future.

Dr. Lesko, my committee co-chair, for your time, patience and knowledge in helping me complete my research. Your perspective in the field of composite materials brought a great deal to my research.

I would also like to thank my committee members Dr. Sotelino for providing me such a strong foundation on Finite Element Modeling that was invaluable to my research. I appreciate all the guidance and encouragement from the other members of my committee: Dr. Roberts-Wollmann and Dr. Plaut. It was a pleasure working with you and I learned a tremendous amount from your classes.

Thanks to my friend Prasun Majumdar. It was you who worked with me to drill hundreds holes on the steel and build the mock-up structure in the lab. I'd also like to thank all the folks working in the Structures and Materials Lab. at Virginia Tech: Brett Farmer and Dennis Huffman for their tremendous help on my tests and their jokes and country music make the lab a so good place to work. Clark Brown for his expertise on electronic instruments; Thanks to other friends that also supported me in my studies: Devin Harris, Joshua Boggs and Charles Newhouse.

I am grateful for my family and their support, especially my wife. You made great sacrifice in your career to help me finish my degree here. Without your love and support, I could not become a Ph.D. holder.

I am very thankful to the financial support of the Federal Highway Administration's (FHWA) Innovative Bridge Research & Construction Program, the technical and financial support of the Virginia Transportation Research Council (contract # VTRC-MOA-03-010) and Virginia Department of Transportation (VDOT). The continued support of Strongwell Corporation, Bristol, Virginia for the application of FRP composites in bridges is greatly appreciated.

TABLE OF CONTENTS

ABSTRACT ii
ACKNOWLEDGEMENTS iii
TABLE OF CONTENTS iv
LIST OF FIGURES viii
LIST OF TABLES xii

CHAPTER 1 INTRODUCTION AND LITERATURE REVIEW 1

1.1 Introduction 1
1.2 Scope of Research 2
1.3 Introduction of the Bridge Rehabilitation Project 4
1.4 Review of Development of Fiber-reinforced Polymer Composites in Bridge Engineering 6
1.5 Review of FRP Deck Systems on the Market 7
1.5.1 Background 7
1.5.2 General introduction to FRP deck systems 7
1.5.3 Comparison of Decks 10
1.6 Review of Previously Conducted FRP Deck Research 12
1.6.1 Structural behavior of FRP deck systems 12
1.6.2 Joining issues for FRP bridge deck systems 19
1.7 Review of Development of Design Philosophy for FRP Bridge Deck Systems 31
1.8 Need for Research 35

CHAPTER 2 DEVELOPMENT AND EVOLUTION OF AN ADHESIVELY-BONDED PANEL-TO-PANEL CONNECTION FOR AN FRP BRIDGE DECK SYSTEM 37

2.1 Background 37
2.2 Stage II: Weak-direction (beam) Bending Test 40
2.2.1 Specimen description 40
2.2.2 Test setup and instrumentation 43
2.2.3 Experimental procedure and results 46

2.2.4 Summary of Stage II Testing 53
2.3 Stage III: Plate Bending Test 54
2.3.1 Specimen description 54
2.3.2 Study on connection geometry: scarfed vs. butt joint behavior 54
2.3.3 Construction for adhesively-bonded panel-to-panel connections 56
2.3.4 Test setup and instrumentation 58
2.3.5 Experimental procedure and results 61
2.3.6 Summary of Stage III Testing 65
2.4 Stage IV:Full-scale Mock-up Test 66
2.4.1 Purpose and Scope 66
2.4.2 FRP Bridge Deck System 66
2.4.3 Construction of Adhesively-bonded Panel-to-panel Connections 68
2.4.4 TEST SETUP AND INSTRUMENTATION 72
2.4.5 Results and Discussion 81
2.4.6 Bridge Installation 99
2.4.7 Summary of Stage IV Test 99

CHAPTER 3 GLOBAL STRUCTURAL PERFORMANCE OF THE HAWTHORNE ST. BRIDGE 102

3.1 Laboratory Full-Scale Mock-up Test 102
3.1.1 Objective of Testing Program 102
3.1.2 Specimen Description 102
3.1.3 Test setup and Instrumentation 102
3.1.4 Experimental Procedure and Results 105
3.2 Field Test 117
3.2.1 Bridge Rehabilitation 117
3.2.2 FRP Deck System 117
3.2.3 Field Testing Objectives 119
3.2.4 Instrumentation 119
3.2.5 Summary 132

CHAPTER 4 DESIGN RECOMMENDATIONS FOR FRP BRIDGE DECK SUPPORTED ON STEEL SUPERSTRUCTURE 134

4.1 Objectives 134
4.2 Strongwell FRP Deck System 135
4.3 Bridge Finite Elment Model 135
4.4 FRP Deck Design – Deck Relative Defleciton 143
4.4.1 Design Procedures and its limitations for FRP Decks 143
4.4.2 Strip Method 144
4.4.3 Parametric Study and Strip Width Determination 145
4.4.4 Example: Live Load Deflection Determination 148
4.4.5 Comparison: values from strip methods vs. laboratory measurements 150
4.5 Steel Girder design - Load Distribution Factor 151
4.5.1 Need for research 151
4.5.2 LDF equations in current provisions 151
4.5.3 Parametric study 152
4.6 Summary 157

CHAPTER 5 CONCLUSIONS AND RECOMMENDATIONS FOR FUTURE RESEARCH 159

5.1 Conclusions 159
5.1.1 Development and Evolution of an Adhesively-bonded Panel-to-panel connection for an FRP Bridge Deck System 160
5.1.2 Global Structural Performance of the FRP-deck-on-steel-superstructure system 162
5.1.3 Design Rcommendations for FRP Bridge Deck Supported on Steel Superstructure 163
5.2 Recommendations for Future Research 164

REFERENCES 166

APPENDICES 173

Appendix A: Testing Results of Stage III (Plate Bending Test) 173

A.1 Results of Service Load Tests 173

A.2 Results at Crack Initiation 173

A.3 Results at Ultimate Failure 174

Appendix B: Testing Results of Stage IV (Full-scale Mock-up Test) 174

B.1 Results of Strength Test on the As-received Deck 174

B.2 Results of Strength Test on Panel-to-panel Connections 175

Appendix C: Global Structural Performance of the Hawthorne St. Bridge 176

C.1 Results of Stringer and Deck Deflection under Service Load Case 1 to 5 at Location A176

C.2 Results of Stringer and Deck strains under Service Load Case 1 to 5 at Location A ... 177

C.3 Results of Stringer and Deck Deflection under Service Load Case 1 to 5 at Location B178

C.4 Results of Stringer and Deck strains under Service Load Case 1 to 5 at Location B ... 179

Appendix D: Field Testing 180

D.1 Results of Deck Strains under different load paths 180

D.2 Results of Stringer Strains under different load paths 182

VITA 183

LIST OF FIGURES

Figure 1.1 The Hawthorne Street Bridge in Covington, VA 5
Figure 1.2 Examples of two types of sandwich construction:(a) generic foam core; (b) proprietary (KSCI) corrugated core (Bakis et al. 2002) – used with permission 8
Figure 1.3 FRP decks produced from adhesively bonded pultrudedshapes: (a) EZSpan (Atlantic Research); (b) Superdeck (Creative Pultrusions); (c) DuraSpan (Martin Marietta Materials); (d) square tube and plate deck (Strongwell) (Bakis et al. 2002) – Reproduced with permission 9
Figure 1.4 FRP deck cross-section analyzed by previous researchers (Temeles 2001) 14
Figure 1.5 Cross section of some FRP Deck System in market - Reproduced..... 19
Figure 1.6 Component-to-component level connections (a) Bonded pultrusion shapes (Keller and Schollmayer 2004) – used with permission.; (b) Bonded sandwich (Davalos et al. 2001) – used with permission.; (c) Bonding with fastening. 21
Figure 1.7 Panel-to-panel connections..... 26
Figure 1.8 Redesigned adhesive bonded connection recommend by Link (2003) - reproduced27
Figure 1.9 Two shear stud type of connections 28
Figure 1.10 Mechanical (clamped) connection (Righman et al. 2004) – used with permission 30
Figure 1.11 Mechanical (bolted) connection (Zhou et al. 2005) 31
Figure 2.1 Evolution of panel-to-panel connections at Virginia Tech..... 39
Figure 2.2 Cross Section of Adhesive Connection 41
Figure 2.3 Adhesive Gun PPA-300A..... 42
Figure 2.4 Adhesive Arrangement..... 42
Figure 2.5 Assembling the Adhesive Connection..... 42
Figure 2.6 Setup of three-point bending test..... 43
Figure 2.7 Instrumentation for six deck specimens 45
Figure 2.8 Representative plots of load vs. strain in service load test (Deck #3)..... 48
Figure 2.9 Representative plots of load vs. strain in failure test (Deck #1)..... 49
Figure 2.10 Representative plots of LVDT vs. SG#3 Strain in failure test (Deck #1) 49
Figure 2.11 Progressive failure of Deck #1 51
Figure 2.12 The groove shape after brittle failure 52

Figure 2.13 The bonded face after brittle failure 52
Figure 2.14 Implementation of scarf geometry for panel-panel connections 55
Figure 2.15 Critical load and displacement increased as scarf angle decreased, under 4-point bend test. 56
Figure 2.16 Adhesive layout 57
Figure 2.17 Adhesively-bonded joints after curing 58
Figure 2.18 Test setup and tire loading patch. 59
Figure 2.19 Instrumentation key for two specimens 60
Figure 2.20 Typical load versus strain behavior until initiation of crack. 63
Figure 2.21 Representative load versus deflection until failure (Deck #2, second seam) 64
Figure 2.22 An undamaged seam on the bottom of the deck and local damage at the load patch. 64
Figure 2.23 Cross section of the Strongwell FRP Deck System 67
Figure 2.24 FRP deck panels and joints of the Hawthorne St. Bridge mock-up. 68
Figure 2.25 Fitting of the adhesively-bonded panel-to-panel connection. 69
Figure 2.26 Adhesive construction for panel-to-panel connection. 70
Figure 2.27 Adhesive squeezing out from joints during adhesive construction. 71
Figure 2.28 Adhesive layout pattern. 72
Figure 2.29 Steel superstructure of the Hawthorne St. Bridge mock-up. 73
Figure 2.30 Load Cases for service load test. 74
Figure 2.31 Experimental Setup for service load test (Load Case 5) on Seam #3 75
Figure 2.32 Special tire patches used to mimic the cushioning effect of a pneumatic tire 75
Figure 2.33 Strength and fatigue tests locations 76
Figure 2.34 Experimental setup for strength tests 77
Figure 2.35 Load Cases for strength tests on as-received deck. 78
Figure 2.36 Experimental Setup for strength tests on as-received deck 78
Figure 2.37 Experimental setup for fatigue test. 79
Figure 2.38 Instrumentation for three adhesively-bonded panel-to-panel connections 80
Figure 2.39 Instrumentations at one adhesive joint below the deck. 80
Figure 2.40 Location of instrumentation for failure tests on as-received deck 81
Figure 2.41 Representative plots in service load tests 85

Figure 2.42 Mid-span longitudinal strain and deflection versus load in as-received deck strength test at mid-span between Stringer #1 and #2 88
Figure 2.43 Mid-span longitudinal strain and deflection versus load in strength test performed at mid-span between Stringer #4 and #5 on Seam #2. 90
Figure 2.44 Maximum strain and deflection at service load after interrupted fatigue loading.. 92
Figure 2.45 Deck load vs. strain and deflection from interrupted fatigue cycling. 93
Figure 2.46 Crack gauge and deflection results after 3,000,000 cycles 94
Figure 2.47 Crack gauge and deck deflection results in residual strength test after 3,000,000 cycles..... 95
Figure 2.48 Failure mode in as-received strength tests..... 97
Figure 2.49 Failure mode in strength test after fatigue (a) Highly localized surface failure (b) Failure detail on top surface of the deck (c) Side view of the flexural failure of top surface 98
Figure 2.50 Field installation of the FRP bridge deck (a) Dry fit (b) Adhesive application (c) Seam curing (d) Jacking system 99
Figure 3.1 Location of instrumentation for global performance of FRP deck systems. 104
Figure 3.2 A representative load vs. stringer deflections..... 106
Figure 3.3 Deflection distribution on stringers at Locations A and B during Load Cases 1 through 5 108
Figure 3.4 A representative plot of load vs. stringer strain..... 109
Figure 3.5 Maximum longitudinal and transverse strain at the bottom of the deck under loading patch at Locations A and B during Load Cases 1 to 5. 110
Figure 3.6 Load distribution factors at Locations A and B..... 114
Figure 3.7 Deck-to Girder connection. 116
Figure 3.8 Location of neutral axis for Stringers 1 to 4 during Load Case 5 116
Figure 3.9 The Hawthorne Street Bridge rehabilitation..... 118
Figure 3.10 Plan view of deck and supporting steel superstructure 119
Figure 3.11 Location of instrumentation for field testing..... 121
Figure 3.12 Field Test Truck 122
Figure 3.13 Summary of Loading Paths for Live Load Tests..... 123
Figure 3.14 Mid-span deflection measurement during field test 124

Figure 3.15 Mid-span stringer deflections 125
Figure 3.16 Top and bottom flange strains of Stringer #5 following load path 2..... 126
Figure 3.17 Deck longitudinal and transverse strains at Location C between Stringer #3 and #4 following Load Path 6..... 128
Figure 3.18 Longitudinal strain on both sides of the panel-to-panel joint..... 129
Figure 4.1 Finite Element Model..... 137
Figure 4.2 Test setup and instrumentation plan for a full-scale laboratory investigation..... 138
Figure 4.3 Comparison of FEM results to experimental measurements (mock-up test) 140
Figure 4.4 Comparison of Stringer deflections: FEM analysis vs. average field measurements 141
Figure 4.5 Comparison of Stringer strains: FEM analysis vs. average field measurements ... 142
Figure 4.6 Deck relative deflection comparison 147
Figure 4.7 Strip width curve fit..... 147
Figure 4.8 Design truck positioned for maximum deck relative deflection 149
Figure 4.9 Loading cases for model M1 to M4 154
Figure 4.10 Comparison of LDFs: FEM results vs. design estimations 155

LIST OF TABLES

Table 1.1 Summary of Deck Characteristics for Two Fabrication Methods (Bakis et al. 2002) – Reproduced with permission..... 12
Table 1.2 Summary of road bridges with FRP deck systems constructed between 1997 and 2000 (Keller 2001) – used with permisssion 23
Table 1.3 Summary of Standards Committees for FRP composites..... 34
Table 2.1 Instrumentation used in each deck..... 44
Table 2.2 Strain Values from Previous Research –Reproduced with permission (Coleman 2002) 47
Table 2.3 Behavior Comparison during Failure Stage..... 50
Table 2.4 Strain & deflection data of service load test..... 61
Table 2.5 Data of initial crack test..... 63
Table 2.6 Data of failure test..... 64
Table 2.7 Material Properties of Strongwell's Deck Components 67
Table 2.8 Data from Service Load Tests 86
Table 2.9 Strength Tests on As-Received Deck 87
Table 2.10 Strength Tests Results on the panel-to-panel connections..... 89
Table 2.11 Strength Tests Results..... 96
Table 3.1 Data of Service Load Test 109
Table 3.2 Calculated Distribution Factors 111
Table 3.3 Summaries of DFs for interior stringers 113
Table 3.4 Stringer deflections at mid-span of the bridge in field test (unit: in)..... 125
Table 3.5 Top and bottom flange average strains of Stringer #5..... 126
Table 3.6 The average maximum longitudinal and transverse strains at Location C and D .. 128
Table 3.7 Longitudinal strain on both sides of the panel-to-panel join 129
Table 3.8 Live Load Test Distribution Factors..... 131
Table 3.9 Summaries of critical distribution factors..... 132
Table 4.1 FRP deck material properties summary..... 137
Table 4.2 Stringer deflections and strains: FEM vs. average experimental results (mock-up test) 141

Table 4.3 Deck relative deflection: FEM vs. average test results (mock-up test) 141
Table 4.4 Stringer deflections and strains: FEM vs. average experimental results (field test) 142
Table 4.5 Recommended limits of live load deflection in AASHTO LRFD Bridge Design Specifications 144
Table 4.6 Equivalent Strip (unit: in.) 145
Table 4.7 Equivalent Young's modulus E11 and moment of inertia for Strongwell's FRP deck 148
Table 4.8 Deck relative deflection: strip method vs. laboratory measurement 151
Table 4.9 Summary of equations for calculating interior girders' LDFs 153
Table 4.10 Bridge models used to investigate LDFs 154
Table 4.11 LDFs: FEM results vs. design estimations 156
Table 4.12 Summaries of critical distribution factors (interior stringers) 156

CHAPTER 1 INTRODUCTION AND LITERATURE REVIEW

1.1 Introduction

The deteriorating state of transportation infrastructure systems is a serious concern worldwide. In the United States, nearly 180,000 of the 600,000 bridges are either structurally deficient or functionally obsolete (Transportation Research Board 2006). Corrosion of steel reinforcement is one of the major reasons for these deficiencies. A 2002 FHWA/USDOT (2002) study estimates the direct cost of repairing corrosion on highway bridges to be $8.3 billion annually, including $3.8 billion over the next 10 years to replace structurally deficient bridges and $2.0 billion for maintenance of concrete bridge decks. In addition to these direct costs, the study's life-cycle analysis estimates indirect costs to the user due to traffic delays and lost productivity at more than 10 times the direct cost of repair. In the face of funding shortfalls, there is a growing interest among state and federal agencies to find cost-effective and durable technologies for bridge repair, rehabilitation and replacement.

In recent years, high-performance fiber reinforced polymer (FRP) composite materials have been identified as an excellent candidate for rehabilitating deteriorated bridges. One of the most promising applications for this high-performance material is bridge decking. Since 1996 approximately 83 vehicular bridges in the United States have been constructed or rehabilitated using FRP decks (Composite Growth Initiative of the American Composites Manufactures Association (ACMA) 2004). Although many demonstration projects are based on new bridges, FRP decks hold greatest promise as a method of deck replacement on older structures (Moses et al. 2006).

The superior material properties, such as high fatigue resistance, and excellent corrosion resistance are desirable characteristics for bridge deck application, which has the potential to prolong the service life of FRP bridge decks as long as 50 to 60 years, while steel-reinforced concrete decks typically last for 15 to 20 years in North America (Lopez-Anido 2002). Their high strength-to-weight ratio and low self-weight (480-1440 N/m^2 or 10-30 lb/ft^2) compared to conventional concrete decks (about 5300 N/m^2 or 110 lb/ft^2) is particularly attractive for rehabilitating posted bridges because the live load-carrying capacity of existing

bridges can be increased by replacing an existing concrete deck with an FRP deck. Another advantage the low self-weight can bring is a decrease in construction time, which can reduce the inconvenience to the traveling public (Zhang and Cai 2006).

An in-depth literature review (in following sections) shows that both the general design standards and efficient analysis procedures are still lacking due to the relatively limited experience with composites in the bridge engineering community and the scarce data on long-term durability for composites. The development of FRP bridge decks is still in the experimental phase. Several technical needs and questions have to be addressed before FRP decks receive wide spread use. These technical needs are: (1) development of design standards and guidelines; (2) efficient design and characterization of panel-to-panel joints and deck-to-girder joints; (3) fatigue behavior of panels and connections; (4) durability characteristics under combined mechanical and environmental loads; (5) failure mechanisms and ultimate strength, including local and global buckling modes; and (6) efficiency and durability of surface overlays (e.g., polymer concrete) and application of hot-mix asphalt in relation to the glass-transition temperature of the polymer(Bakis et al. 2002).

1.2 Scope of Research

The purpose of this research is to develop and investigate the performance of an FRP deck system (Strongwell Decks) used to rehabilitate the Hawthorne St. Bridge in Covington, Virginia. Based on the findings of this research, the author seeks to address some of the technical needs and questions listed above. The objectives of the research are as follow:

1. Develop an effective panel-to-panel connection in a four-stage study and investigate the performance and failure mechanism of the final-proposed adhesively-bonded tongue-and-groove, panel-to-panel connection under service, strength and fatigue loads. Explore various issues related to constructability of FRP deck systems. Establish construction and installation procedures for this adhesively bonded panel-to-panel connection.
2. Monitor and examine global structural performance of the FRP-deck-on-steel-superstructure system both in laboratory and in field. Various issues concerning design of the FRP-deck-on-steel-superstructure bridges are investigated, such as global structural

deflections and strains, effectiveness of the clip-type deck-to-stringer connections and load distribution factors under service load.

3. Address two important design issues concerning the design of FRP-deck-on-steel-superstructure bridges, namely FRP deck relative deflection and load distribution (LD) to supporting steel stringers. Provided relevant practical design recommendations to help design engineers overcome any reluctance to adopt FRP decks due to limited experience and design approaches.

Chapter 1 is the introduction and literature review of the research, which briefly introduces the general background, status and technologies in FRP bridge deck application. The objectives and needs for research are also provided in this part.

Chapter 2 presents four-stage development and evaluation of an adhesively-bonded panel-to-panel connection for the FRP bridge deck system to rehabilitate the Hawthorne St. Bridge. The panel-to-panel connections were finally accomplished using full width, adhesively (structural urethane adhesive) bonded tongue and groove splices with scarfed edges. To ensure proper construction, serviceability, and strength of the splice, a full-scale two-bay section of the bridge with three adhesively bonded panel-to-panel connections was constructed and tested in the Structures Laboratory at Virginia Tech. Test results showed that no crack initiated in the joints under service load and no significant change in stiffness or strength of the joint occurred after 3,000,000 cycles of fatigue loading.

In Chapter 3, various design issues related to global structural performance of the FRP-deck-on-steel-superstructure system in the laboratory and in the field are investigated and discussed. The following conclusions are drawn from this study: (1) the clip-type of panel-to-stringer connection provides little composite action as expected, which fulfilled the design intention; (2) the AASHTO LDFs equations for the category of glued laminated timber deck on steel stringers can give good estimations on LDFs of FRP-deck-on-steel-girder bridges; (3) the lever rule can be used as an appropriately conservative design method to predict the LDFs of FRP-deck-on-steel-girder bridges; (4) local effects play a important role in the performance of FRP deck. The strains of the cellular type of deck system changed rapidly and experienced longitudinal double curvature when the loading truck crossed the instrumented area; (5) the average peak longitudinal and transverse strains under truck loading did not even come close to

reaching the ultimate strain in the material, which indicates that the FRP deck design is stiffness driven rather than strength driven like conventional concrete decks.

The design recommendations for FRP bridge decks supported on steel superstructure are summarized in Chapter 4. In this chapter, an extensive FEM parametric study was conducted to examine two design issues concerning the FRP deck design, namely deck relative deflection and steel structural design, i.e. LDF of supporting steel stringers. Results show that the strip method specified in the AASHTO LRFD specification (AASHTO 2004) as an approximate method of analysis can also be applied to unconventional FRP decks as a practical method. However, different strip width equations have to be determined by either FEM or experimental methods for different types of FRP decks. In this study, one such an equation has been derived for the Strongwell deck. In addition, both FEM results and experimental measurements show that the AASHTO LDFs equations for glued laminated timber decks on steel stringers provide good estimations of LDFs for FRP-deck-on-steel-girder bridges. The lever rule can be used as an appropriately conservative design method to predict the LDFs of FRP-deck-on-steel-girder bridges.

Chapter 5 gives the summary of this research and recommendations for future research on this subject.

This research seeks to advance FRP deck application and enhance the performance of the FRP deck system based on the findings from a bridge rehabilitation project. Therefore, a brief introduction to the bridge rehabilitation project will be helpful before getting into deeper discussion.

1.3 Introduction of the Bridge Rehabilitation Project

The focus of this research is to investigate the performance of an FRP deck system used to rehabilitate the Hawthorne Street Bridge in Covington, Virginia (see Figure 1.1). This is one of many structurally deficient bridges in Virginia, however, the historical significance of its Phoenix Columns has ruled out bridge replacement. The thru-truss bridge has a 75 ft clear span Pratt-truss structure, with a roadway width of 22 ft, running over three rail-lines. It also serves as the only emergency lifeline to parts of downtown Covington during periods of high water, and thus must support emergency vehicles.

The bridge was posted at a maximum load of 7 tons before rehabilitation. The structure has a condition rating of 5 on a scale of 0 to 9 (fair condition with all primary elements experiencing only minor section loss). Inspections have shown that the existing W10x33 stringers supporting the deck of the bridge are no longer sufficient to meet the deflection requirements of the American Association of State Highway and Transportation Officials (AASHTO) Standard Specification (2002). The inspections have also revealed that the connections of the truss members are rusted to a rigid condition, causing tension members in the truss to sustain compressive loads. Additionally, the reinforced concrete deck is severely deteriorated; several large pieces of it fell from the structure in February 2001 onto the railroad tracks, causing the Virginia Department of Transportation (VDOT) to close the bridge for repairs.

Figure 1.1 The Hawthorne Street Bridge in Covington, VA

Based on the condition of the deck and superstructure, VDOT has determined that the Hawthorne Street Bridge requires rehabilitation or replacement. However, they have ruled out replacement because the bridge is historically significant and because of alignment challenges at each approach. Consequently, the focus has shifted towards finding a rehabilitation alternative. VDOT plans to replace the bridge superstructure with a new deck/beam/girder system and keep the historical thru-truss. They plan to replace the aging beams and girders with new steel sections and to replace the existing, deteriorating reinforced concrete deck with

an FRP composite bridge deck system. The most important characteristic of the deck/beam/girder replacement is the reduction in self-weight of the bridge, which will increase the posting and allow for use by emergency vehicles.

The following sections will review the general background, research status and technologies in FRP bridge deck application.

1.4 Review of Development of Fiber-reinforced Polymer Composites in Bridge Engineering

Composite materials are made by combining at least two different constituent materials, with one or more materials as reinforcements, and one or more materials as the matrix. The first composite material appeared approximately 4500 years ago; the Egyptians combined mud from the River Nile with straw to build the Sakkara pyramids, which are still standing today. Reinforced concrete (RC) is another example of composite material, which combines reinforcing steel and concrete matrix to create a composite material having some of the advantages of both steel and concrete. Fiber-reinforced polymer (FRP) composite is similar to RC, with a fiber as the reinforcement and a polymer as the matrix. The fiber reinforcement carries load in pre-designed directions and the polymer matrix serves as a medium to transfer loads between adjacent fibers and to provide protection for the fiber. Current FRP composite materials typically have high-strength and high-stiffness structural fibers embedded in light-weight, low-cost, and environmentally resistant polymers, which have better mechanical and durability properties than either of the constituents alone. FRP materials were developed primarily for aerospace and defense industries in the 1940s and are widely used in many industries today, including aeronautic, marine, automotive and electrical engineering. With the continuing cost reduction in high-performance FRP materials and the growing need for new materials to renovate civil infrastructures, FRP materials are now finding wider acceptance among civil engineers. One current application of FRP research is to help rebuild the American transportation infrastructure, and in particular, to rehabilitate existing bridges (Tang and Podolny 1998).

Civil engineers have used FRP composites for several decades. In 1976, Israel built the first FRP composite bridge (Munley 2000). In 1986, Germany built the world's first

highway bridge using FRP composite reinforcing tendons and in 1982, China constructed the first FRP composite bridge deck (Karbhari and Zhao 2000). In 1992, Scotland demonstrated the first all-FRP cable-stayed pedestrian bridge. In the US, the first FRP-reinforced concrete bridge deck was built in 1996 in McKinleyville, West Virginia. In the same year, the first all-composite (FRP) vehicular bridge deck was installed in Russell, Kansas (Tang and Podolny 1998).

Today, there are hundreds of completed and ongoing bridge projects using FRP composite materials all over the world. These projects belong to two categories (Karbhari and Zhao 2000):

(1) Bridge Renewal: primarily bridge structure rehabilitation and bridge superstructure replacement.

(2) New Bridge Construction: bridge structures made entirely of FRP composites (primarily for pedestrian bridges); concrete bridges with FRP-rebar reinforcement, FRP-wrapped concrete piles or pylons, and external FRP cable stays; protective or secondary structural systems; etc.

Within the vast applications for FRP in bridge engineering, this research focuses on bridge deck systems. Reviews of state-of-the-art use of FRP for various other bridge applications are available (Bakis et al. 2002; Karbhari and Zhao 2000; Lopez-Anido et al. 1997) and the author will not repeat them here. In the following, only the literature concerned with FRP bridge deck systems will be reviewed.

1.5 Review of FRP Deck Systems on the Market

1.5.1 Background

The author will focus on the bridge deck, which serves as the structural element that transfers vehicular loads transversely to the superstructure members, such as stringers or floor beams.

1.5.2 General introduction to FRP deck systems

The most commonly used reinforcements in FRP deck systems are glass fibers/fabrics, occasionally carbon fibers, or a hybrid of carbon and glass for higher stiffness. Carbon fibers

are attractive for their very high specific strength and stiffness as well as fatigue resistance. However, glass fibers/fabrics currently dominate the market due to their low cost compared with carbon fibers. Polyester or vinyl ester matrices are commonly employed as binders. Detailed fiber and resin properties are available in a number of books, such as mechanics of laminates by Jones (1999), materials and manufacturing aspects by Mallick (Mallick 1993), and Theory of Composites Design by Tsai (1992).

In the U.S. there are six major competitive suppliers of FRP deck systems. The FHWA website (Link: http://www.fhwa.dot.gov/bridge/frp/frppract.htm) lists the known suppliers and completed projects. Each uses one of three current manufacturing techniques: pultrusion, vacuum-assisted resin transfer molding (VARTM), and open- or closed-mold hand lay-up.

There are two major types of FRP decks currently in use: sandwich structures and adhesively bonded, pultruded shapes. Sandwich structures consist of strong, stiff face sheets that can carry flexural loads and a low-density, shear-resistant core bonded between a top face sheet and a bottom face sheet that can provide composite action of the deck. Face sheets are usually composed of E-glass mat and/ or roving infused with a polyester or vinyl ester resin. Core materials are rigid foams or thin-wall cellular FRP materials, such as those shown in Figure 1.2. Cellular materials are the most efficient core materials for weight-sensitive applications. Open- or closed-mold hand lay-up manufacturing methods used in sandwich construction make it easy to change materials, orientations, and thickness of FRP face sheets or core. This gives designers great flexibility to meet depth and deflection requirements.

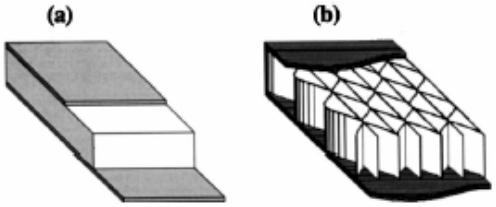

Figure 1.2 Examples of two types of sandwich construction:(a) generic foam core; (b) proprietary (KSCI) corrugated core (Bakis et al. 2002) – used with permission from ASCE

The pultrusion processing method can fabricate high performance, continuous length, and constant cross-section FRP structural parts. However, this method cannot produce larger parts such as bridge deck panels, because of technical difficulties and cost considerations (Bakis et al. 2002).

Most currently available commercial decks are constructed using assembly of adhesively bonded, pultruded shapes. This technique gives design flexibility through changes in the constituents (such as fiber types, fiber volume fraction and fiber orientations) and/or the cross-section of the shapes. However, because of the potentially high cost of pultrusion dies and fiber guides, variations in the cross sections of the shapes are feasible only if sufficiently high production warrants the tooling investment (Bakis et al. 2002).

Figure 1.3 shows typical cross-sections of FRP decks from bonded pultrusion components. DuraSpan and Superdeck use woven and stitched fabrics for precise placement of multi-axial reinforcement to improve delamination resistance. EZSpan employs the through-the-thickness braided pre-forms as the reinforcement for the triangular tubes. Strongwell's deck system combines off-the-shelf shapes composed of continuous strand mat (CSM) and roving. This research will investigate Strongwell's deck system, as discussed in more detail later.

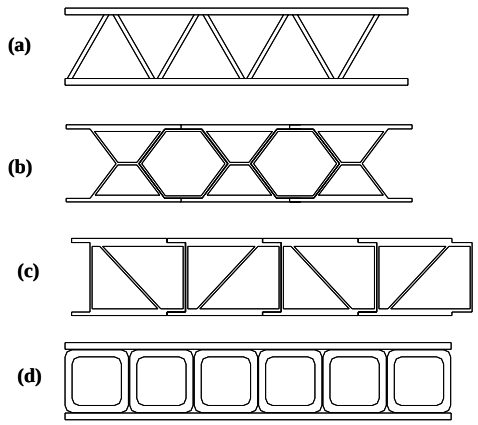

Figure 1.3 FRP decks produced from adhesively bonded pultrudedshapes: (a) EZSpan (Atlantic Research); (b) Superdeck (Creative Pultrusions); (c) DuraSpan (Martin Marietta Materials); (d) square tube and plate deck (Strongwell) (Bakis et al. 2002) – Reproduced with permission from ASCE

1.5.3 Comparison of Decks

Table 1.1 compares the characteristics of sandwich and pultruded FRP decks. The weight per unit surface area listed in Table 1.1 is about 98 kg/m2 (20 lb/ft2), except for the KSCI (Kansas Structural Composites, Inc.) corrugated core deck system. The latter has a value of 76 kg/m2 (15.5 lb/ft2), which shows more efficiency in material use.

High initial cost is the first concern that hinders the use of FRP bridge deck systems. From Table 1.1, the lower bound for current FRP decks is approximately $700/m2 ($65/ft2). This cost is more than twice that typically quoted for the new construction or replacement of a deck with conventional materials, $322/m2 ($30/ft2). However, other cost advantages of FRP bridge decks may partially, or completely, compensate for this high initial cost, especially when there is a need for light weight, strong corrosion resistance, and/or rapid installation (Lopez-Anido 2002).

The literature suggests that a life cycle cost analysis (LCCA) can demonstrate the cost competitiveness of FRP bridge deck system (Ehlen 1999). This analysis considers the major costs throughout the entire life cycle of the bridge deck, namely, the initial construction costs, maintenance costs and disposal costs. Due to limited cost data available at present, the development of LCCA for FRP bridge deck systems is still underway. As FRP becomes more widely used in civil engineering, production quantities and manufacturing advances will help to reduce the high initial project costs.

Although limited field experience and concerns over costs have slowed the introduction of FRP decks into mainstream bridge application, the specifications for deflections have presented the greatest number of questions in the design of these systems (Bakis et al. 2002). As shown in Table 1.1, there is no current consensus on deck deflections (normalized) by the manufacturers. There is also uncertainty in defining the deflection limits in existing design guidelines for conventional structures. The AASHTO load and resistance factor design (LRFD) Bridge Design Specifications (2004) has recommended limits of live load deflection for steel, aluminum, and concrete construction.

- Vehicular load, general: Span/800
- Vehicular and/or pedestrian loads: Span/1,000
- Vehicular and/or pedestrian loads on cantilever arms: Span/375

For wood construction, the following deflection limits apply:

• Vehicular and pedestrian loads: Span/425

• Vehicular load on wood planks and panels relative deflection between adjacent edges: 0.10 in.

No limit is set for FRP composites construction. As stated in the commentary to the specification, the purpose of the above criteria is twofold: (1) to prevent excessive deflections that may cause damage to wearing surfaces applied to the bridge decks; and (2) to provide for rider comfort (Hayes et al. 2000). The criteria are stated as recommended limits because, at present, there are no definitive guidelines for the limits of tolerable static deflection or dynamic motion due to vehicular traffic (Taly 1998).

For the time being, FRP bridge deck designers quantify deck performance in terms of criteria developed for conventional materials. As shown in Table 1.1, most of the deck systems built by adhesively bonded pultrusion shapes cannot meet this L/800 requirement. The literature suggests that a direct application of L/800 criteria to advanced composite materials is inadvisable without understanding the dynamic response of the component. Proper deflection limitation (an equivalent L/x) imposed on composite bridge components should be derived from human tolerance on static deflection or dynamic motion due to vehicular traffic (Demitz et al. 2003). Also, the proper deflection limit should be investigated with regard to any wearing surface applied on FRP deck.

Table 1.1 Summary of Deck Characteristics for Two Fabrication Methods (Bakis et al. 2002) – used with permission from ASCE

	Deck system	Depth (mm)	kg/m^2 [a]	Dollars/m^2	Deflection[b] (reported)	Deflection[c] (normalized)
(a) Sandwich Construction	Hardcore composites	152–710	98–112	570–1,184	L/785[d]	L/1,120
	KSCI	127–610	76[e]	700	L/1,300[f]	L/1,300
(b) Adhesively Bonded Pultrusions	DuraSpan	194	90	700–807	L/450[g]	L/340
	Superdeck	203	107	807	L/530[h]	L/530
	EZSpan	229	98	861–1,076	L/950[i]	L/950
	Strongwell	120–203	112	700 [j]	L/605[k]	L/325

a Without wearing surface.
b Assumes plate action.
c Normalized to HS201IM for a 2.4-m center-to-center span between supporting girders.
d HS20+IM loading of a 203-mm-deep section at a center-to-center span between girders of 2.7 m.
e For a 203-mm-deep deck targeted for RC bridge deck replacements.
f HS20+IM loading of a 203-mm-deep deck at a center-to-center span between girders of 2.4 m.
g HS20+IM loading of a 203-mm-deep deck at a center-to-center span between girders of 2.2 m.
h HS20+IM loading at a center-to-center span between girders of 2.4 m.
I HS20+IM loading at a center-to-center span between girders of 2.4 m.
j For a 171-mm-deep deck with a wearing surface under experimental fabrication processes.
k HS20+IM loading of a 171-mm-deep section at a center-to-center span between girders of 2 m.

1.6 Review of Previously Conducted FRP Deck Research

Many academic institutions in North America, and around the world are actively engaged in research involving FRP applications for civil infrastructure. Notably among them in the U.S. are: North Carolina State University, California State University-Long Beach, West Virginia University, the University of California - San Diego, the University of Illinois – Urbana Champaign, University of Missouri-Rolla, Georgia Institute of Technology, Virginia Polytechnic Institute and State University, and the University of Wisconsin–Madison. Universities, manufacturers, and state Departments of Transportation often collaborate on the evaluation and implementation of FRP composites that best meet the needs of the State. This section discusses in some detail previous research.

1.6.1 Structural behavior of FRP deck systems

This section discusses the theoretical and experimental structural behavior of FRP decks subjected to an applied load, focusing on those studies that have significant impact on FRP deck development.

The initial research on FRP deck systems conducted in the U.S. dealt with the development of effective deck configurations in terms of finite-element methods. Henry (1985), Bakeri and Sunder (1990), McGhee et al. (1991) and Zureick (1997) tried to identify the desired performance of FRP decks by varying the cross-section configurations and/or the constituents of the shapes (such as fiber types, fiber volumes fraction and fiber orientations).

Henry (1985) analyzed five single-span (7 ft), E-glass/epoxy deck panels (9-in. thick) with various cross-section configurations, shown in Figure 1.4(a) under HS20-44 wheel load. He modeled FRP decks as a truss member along the traffic direction and a beam member transverse to the traffic direction, and compared the effects of using truss elements versus plate elements on stresses and deflections. He found that two sections with the X-shaped panels underwent the smallest deflection (L/583) and that none of these cross–section configurations could deflect less than L/800 deflection index.

Bakeri and Sunder (1990) developed four truss-shaped glass/polyester decks with parabolically varying depth, seen in Figure 1.4(b). The deck had a 7-ft span and a maximum thickness of 10.25 in. Their finite-element method (FEM) analysis showed that the deflection for all cases exceeded the L/800 deflection index, but that all stresses were under the safety region.

McGhee et al. (1991) developed a software package to optimize deck design by a trial- and-error method. They found the minimum weight of the deck from varying thicknesses of the web, top and bottom plates under constraints from ultimate strength, local buckling and, L/800 deflection limit. Their study involved four cross-section configurations, and they found that the Type 2 cross section is the most efficient design, seen in Figure 1.4(c).

Zureick (1997) conducted a finite-element analysis on FRP decks with box-shaped cells, seen in Figure 1.4(d) Deck 1. He considered four cases with different fiber directions and orientation of cells. His results show that deflections control the design of this type of FRP deck, and that deflections are much lower for the two cases where the cells are aligned perpendicular to traffic. Through an optimization study, Zureick found box-celled deck and the V-celled deck to be the most efficient sections. Finally, he tested these box-celled and V-celled decks at 10-ft and 12-ft stringer spacing, and found that none of the decks was able to satisfy the L/800 deflection index.

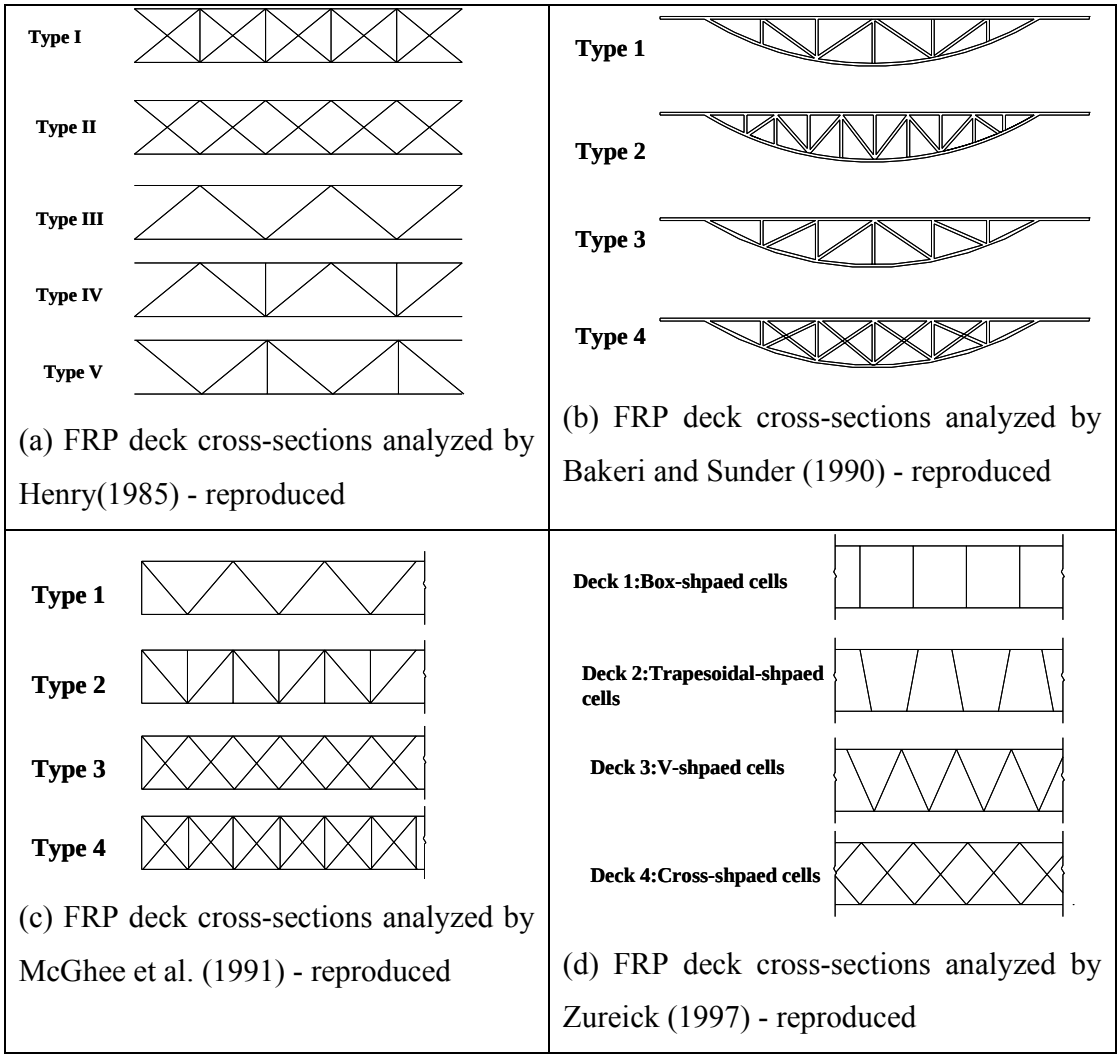

(a) FRP deck cross-sections analyzed by Henry(1985) - reproduced

(b) FRP deck cross-sections analyzed by Bakeri and Sunder (1990) - reproduced

(c) FRP deck cross-sections analyzed by McGhee et al. (1991) - reproduced

(d) FRP deck cross-sections analyzed by Zureick (1997) - reproduced

Figure 1.4 FRP deck cross-section analyzed by previous researchers

The subsequent FRP deck research dealt with the development of viable products for a specific project or for a particular manufacturing need.

Researchers at West Virginia University began to study thin-walled FRP sections in the early 1990s. They used both micro- and macro- mechanics models and coupon tests to investigate the stiffness properties of the components and the pultruded composite sections (Salim et al. 1997).

Brown (1998) did a combined analytical and experimental study of FRP composite bridges consisting of cellular box decks and wide-flange I-beams as stringers. His study led to the development of simplified design equations for bridge applications. These equations are

applicable to the global design of a deck and stringer super-structure system and account for transverse load distribution.

Lopez-Anido et al. (1997) developed an FRP deck system composed of hexagonal-shaped cells and double-trapezoidal-shaped cells (Superdeck^{TM} System); they used this system to construct two bridges in West Virginia in 1997: the Laurel Lick Bridge and the Wichwire Run Bridge. Figure 1.5(a) shows the cross section. The hexagonal and double-trapezoidal components are composed of E-glass fibers embedded in a vinylester resin and adhesively bonded together to form 8-inch thick FRP deck modules. The fiber architecture is in the form of stitched fabrics, continuous roving and chopped strand mats.

Harik et al. (1999) conducted static tests on three Superdeck^{TM} FRP deck panels (36 in. along the traffic direction and different effective spans: 8, 10 and 12 ft). They found that none of the decks could satisfy the L/800 deflection index under HS25-44 loading and the safety factors for all the specimens were above five. For consistency throughout this proposal, the safety factor was calculated as ultimate failure load divided by the design service load.

In addition to Harik's static tests, GangaRao et al. (1999) did static and fatigue tests on small Superdeck^{TM} deck panels (36 in. along the traffic direction, 9-ft simply supported span). One panel was loaded at a rate of 3 cycles per second for up to 2 million cycles. The load range was 2 to 35 kips. After fatigue loading on this panel, a residual strength test was conducted and another strength test was performed on a panel that was not subjected to a fatigue loading. Results showed less than 4% stiffness loss and no significant strength loss after the fatigue loading (failure load 124.5 kips and maximum deflection of 1.54 in. for the fatigued deck compared with 126.7 kips and 1.57 in. for the deck without fatigue loading).

Cassity et al. (2002) demonstrated another FRP bridge deck system (DuraSpan system) that could be compositely connected to steel girders. The deck panels were composed of pultruded rectangular tubes (each having a "male" and "female" end) bonded together by polyurethane adhesive as shown in Figure 1.5(b). The tubes were 7 $^{5}/_{8}$ in. thick and consisted of E-glass fibers embedded in isophthalic polyester resin. Prior to the construction of the full-scale bridge, Cassity et al. performed static and fatigue tests on smaller scale deck panels. A 3-ft 4-in. by 8-ft (7-ft 4-in. effective span) panel was loaded up to 110 kips (without failure) under a 3-point bending test setup, which showed a safety factor of five compared to service loads (AASHTO Standard Specification HS20 wheel load plus impact). For fatigue testing,

after 10.5 million cycles, local bending of the top face of the panel in the vicinity of the loading patch resulted in interlaminar shear cracking on the underside of the top face sheet at a ply drop-off detail and at mid-depth of the top face sheet. The cracks did not grow far beyond the loading patch region, and did not affect the overall stiffness of the specimen. After fatigue loading, a residual strength test was performed on the specimen, which responded linearly up to failure at 116 kips.

Figure 1.5(c) shows the EZ-span deck system developed by Brown and Zureick (1999). The 9 in thick deck panel was composed of pultruded triangular shapes adhesively bonded together with hand lay-up top and bottom face sheets. They used E-glass braided fabrics embedded in a vinylester resin for the triangular elements and E-glass knitted fabrics in a vinylester resin for the face sheets. Brown and Zureick tested a square (9.84 ft) deck panel under a 3-point bending test setup. They observed no failure up to 140 kips and recorded a maximum deflection of 0.7 in. After the static test, they placed two 10 ft by 20 ft (3 m by 6 m) deck panels in the Troutville, Virginia weigh station on I-81 to investigate long-term durability issues.

Since 1997, researchers at Virginia Polytechnic Institute and State University (Virginia Tech) have worked with Strongwell Corporation (Bristol, Virginia), the Federal Highway Administration (FHWA) and the Virginia Department of Transportation (VDOT) to develop and test FRP deck panels made from pultruded, off-the-shelf components. This system is unique, as it is built from readily available pultruded Strongwell FRP "EXTREN" shapes (Strongwell Inc. 2002), which shows the potential for a cost-competitive product.

The Virginia Tech team developed the first Strongwell prototype for use as replacements for the existing decking in the Schuyler Heim Vertical Lift Bridge in Long Beach, California. This system was built from Strongwell's Extren 500 product line of shapes, 4-in. x 4-in. x 1/4-in. tubes sandwiched between 3/8-in. plates. The tubes and plates were made of E-glass mats (continuous) and roving embedded in an isophthalic polyester resin.

The assembly procedures for the prototype were to: (1) prepare the bonding surfaces of tubes and plates by roughening; (2) bind together the tubes using an epoxy adhesive and fasten them mechanically with 1-in. diameter fiberglass thru-rods (running through the sidewalls of the tubes) spaced at 12 in.; (3) bind the top and bottom plates to the tubes using the epoxy adhesive to form an FRP deck panel; and (4) put the deck panel into a vacuum bag

and apply pressure until the completion of the curing process. The prototype deck panel size was 4-ft long (traffic direction) by 14-ft wide with 4-ft effective spans (Hayes et al. 2000).

Hayes et al. (2000) conducted three different tests on the prototype: (1) stiffness test (2) as-received strength test and (3) fatigue test followed by a residual strength test. Load was transferred to the deck through a 12-in. by 20-in. steel plate over a neoprene pad. The designed service load was 20.8 kips, which was calculated based on AASHTO Standard Specification HS20 wheel load plus a 30% impact allowance. For the stiffness test, the maximum deflection was 0.15 in., corresponding to a deflection index of L/320. The strength test on the as-received panel showed failure at 78 kips with a punching shear failure mode. After 3-million cycles of fatigue loading (2.5 kips to 25 kips at a rate of 2 to 3 Hz), there was no apparent loss in stiffness and the residual strength was 83 kips with the same failure mode. Because the prototype maintained good structural performance, it might make excellent candidates for future field application. However, there was still the need to optimize its configurations to meet specific stiffness requirement. Also, it is important that the long-term behavior and durability—in a field application—of the FRP deck concept be studied (Temeles 2001).

The Strongwell deck system has evolved through four phases after the prototype referred to as Phases I to IV; Each iteration sought to maximize its short- and long-term performance. Phase I to IV decks were all constructed from 6-in. x 6-in. x 3/8-in. pultruded Extren tubes, with varied thickness for the top and bottom pultruded Extren plate (3/8-in. thick top and bottom plate for Phase I and II decks, 1/2-in. top plate and 1/4-in. bottom plate for Phase III and IV decks). Each deck panel was 5 ft wide, 15.25 ft long, and 6 ¾ in. deep (not including the wearing surface). Because the standard size of pultruded plates used for top and bottom face sheet was 4 ft by 8 ft, the top and bottom face sheets were not monolithic plates. Several sections of plate were cut and sized to properly fit the top and bottom surfaces of the deck panel in a way to avoid joining in the maximum moment area. Phase I to IV decks were all supported during tests to create two 6 ft 6in clear spans (center-of-support to center-of-support). Three different deck-to-support (girder) connections were used and evaluated and will be discussed later.

Temeles (2001) tested the Phase I and II decks. There were some characteristic differences between Phase I Deck and Phase II Deck: the quality of pultruded tubes (higher quality control in Phase II deck), adhesive types used to bond components, types of thru-rods

(Phase I: GFRP rods and Phase II, steel thru-rods) and curing methods for plate-to-tube bonding (Phase I: weights place on top of deck and Phase II: cured in vacuum bag) etc. Detailed information can be found in Temeles thesis (Temeles 2001).

Pre-service stiffness tests conducted on Phase I to II decks in the laboratory showed that the maximum deflections for all cases exceeded L/800 deflection index at 26 kips service load (AASHTO Standard Specification HS-25 wheel load plus impact). A maximum deflection of L/470 was recorded when loaded at panel center. The Phase II deck was transported to and placed in the field test facility at the Troutville, Virginia interstate I-81 weigh station, to investigate the deck performance under actual loading and environmental effects. It was left in place for eight months and underwent approximately 4-million load cycles. Next the deck was returned to the laboratory for post-service stiffness tests; no indications of a loss of stiffness were observed. Strength tests were conducted on both the Phase I and II deck panels. The safety factors were all above 4 when loaded at the panel center with the failure mode as punching shear under the steel loading patch. From the testing results, Temeles (2001) concluded that the design of this FRP deck system was governed by stiffness rather than strength. He also suggested that it may not be appropriate to use L/800 as a deflection limit for FRP deck systems because L/800 limit is for conventional structures. It was pointed out that a definitive deflection limit for composite construction needs further research.

Coleman (2002) tested the Phase III and IV decks. Figure 1.5(d) shows the typical Phase III and IV decks. The only structural difference between Phase III and IV deck systems is the spacing of the thru-rods. Laboratory stiffness testing was performed on both decks under an AASHTO Standard Specification HS-25 service load. The Phase III deck was installed at the weigh station mentioned above; it was then tested immediately after installation, about two months after installation and approximately 14 months after installation. During the 14 months, the deck experienced about 11.7 million load cycles with about 8 percent of the cycles produced by trucks over the legal weight limit (Coleman 2002). The aim of this long-term monitoring was to investigate the deck performance under actual interstate load and environmental effects. The results showed that the strains and deflections of the Phase III deck did not increase after 14-month service, indicating no ascertainable loss in stiffness. Phase IV deck was loaded to failure after the stiffness test in the laboratory. The results showed the safety factors were more than 4. The failure modes during the strength testing in Phase IV deck

when using the rubber tire load patch were drastically different from those observed in the strength tests for Phase I and II decks. Although Phases I and II decks failed under punching shear, the top flange of the Phase IV deck system (both plate and tube flange) failed as a fixed-ended beam between the tube webs. This more accurately reproduces the failure which would occur due to an actual truck tire loading (Coleman 2002). Coleman also concluded from the testing data that the thru-rods do not contribute to the strength of the deck, and can be reduced in number to the minimum required for fabrication purposes and for connecting the deck to the supporting girders.

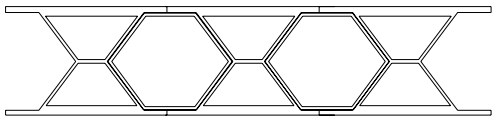

(a) Superdeck by Creative Pultrusions (Lopez-Anido et al. 1997) - reproduced

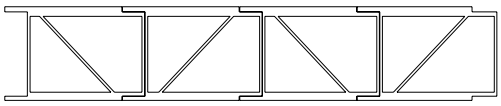

(b) DuraSpan by Martin Marietta Composites (MMC 2002) - reproduced

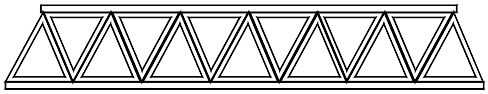

(c) EZ Span system (Brown and Zureick 1999) - reproduced

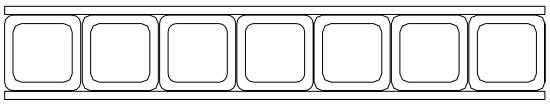

(d) Strongwell system

Figure 1.5 Cross section of some FRP Deck System in market

1.6.2 Joining issues for FRP bridge deck systems

Due to the limitations imposed by the fabrication process and by shipping requirements, connections are inevitable in FRP bridge decks. There are three types of joints in FRP bridge deck construction: component-to-component connections to form modular deck panels, panel-to-panel connections to form bridge deck systems and deck-to-support connections to form bridge superstructures (including deck-girder, deck-abutment and deck-barrier connections) (Zhou and Keller 2005). All these load-carrying connections influence the performance of FRP deck systems in terms of stiffness, strength and service time. Without properly-designed and well-constructed connections, the advantages of advanced FRP

composites cannot be realized. Thus the author reviewed the research about these three types of connections below.

1.6.2.1 Component-to-component level connections

Modular FRP bridge deck panels are usually shop-fabricated. The CCL (Component-to-component level) connections link together deck elements such as pultruded shapes, sandwich core and face sheets to form modular FRP bridge deck panels. These connections ensure the integrity of the modular deck panel and the local load transfer efficiency between the jointed deck elements.

Figure 1.6 shows adhesive bonding for CCL connections. Zetterberg et al. (2001) have found that bonded joints have a simpler design and a greater safety margin than bolted joints. The criterion for designing adhesively-bonded CCL connections is that failure should occur in the FRP substrate before failure in the adhesive or at the interface. This criterion has been achieved by a number of researchers (Hayes et al. 2000; Keller and Schollmayer 2006; Zhou et al. 2005). The failure modes varied case by case. Examples include punching shear failure, plate bending failure, delamination, and bucking of the FRP components. In all failure modes, the adhesive layer and interface were stronger than the FRP components. No pre-mature adhesion or cohesion failure occurred. All these studies showed that factory-performed adhesive bonding is a viable technique for joining CCL connections in FRP deck applications. Successful CCL connections have been developed and implemented by many researchers; therefore this type of connections will not be discussed further.

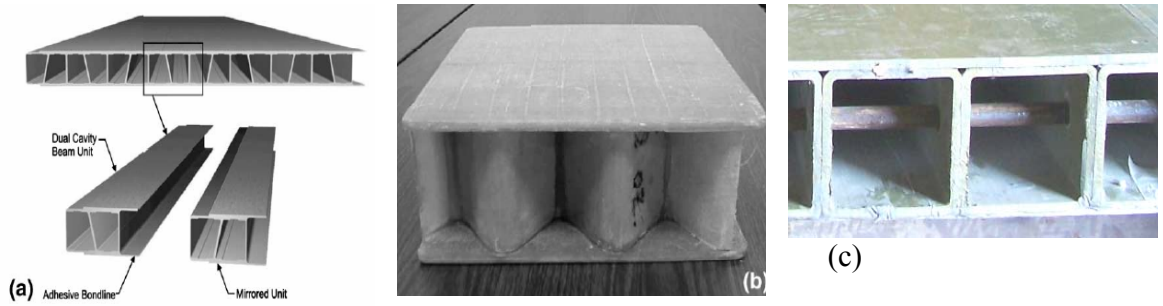

Figure 1.6 Component-to-component level connections (a) Bonded pultrusion shapes (Keller and Schollmayer 2004) – used with permission.; (b) Bonded sandwich (Davalos et al. 2001) – used with permission.; (c) Bonding with fastening.

1.6.2.2 Panel-to-panel connections

Due to the limitations imposed by the modular fabrication process and shipping requirements, manufacturers typically provide FRP bridge decks in modular panel forms. At the bridge site, the modular panels are connected together using panel-to-panel connections to form the FRP deck system. Panel-to-panel connections are designed to efficiently transfer bending moments and shear forces between joined modular panels; to ensure deformation compatibility due to thermal effect; and to simplify on-site installation. Several techniques have been developed for panel-to-panel connections, including adhesively bonded splicing tongue-groove connection and shear key or clip-joint mechanical fixing connection (Zhou and Keller 2005). Because this research seeks to develop an effective panel-to-panel joint, the following reviews this research in this area.

Between 1997 and 2000, six different FRP deck systems were used in the US. As classified by construction techniques, four systems (Superdeck^{TM}, Duraspan, EZ-Span and Strongwell systems) were constructed by adhesively-bonded pultruded shapes, and two systems (Hardcore and Kansas systems) were sandwich structures, as shown in Table 1.2 (Keller 2001). For each system, the details of the panel-to-panel joints are discussed.

The Superdeck^{TM} system was developed by researchers at West Virginia University and manufactured by Creative Pultrusions, Inc. This system was installed in seven bridges from 1997 to 2000. Figure 1.7(a) shows that pultruded tubes made from E-glass fibers and

vinyl ester resin are adhesively bonded together to form the cross section. The deck panels are joined together using a built-in panel-to-panel connection that provides both shear key interlock and a bonding surface. A two-part polyurethane adhesive joins the panels (Lopez-Anido et al. 1997). This reference did not report any laboratory or field test data on the performance of this panel-to-panel joint, and only presented some data indicating that the deck system has sufficient capacity to carry HS20-44 Loading.

The DuraSpan deck system from Martin Marietta Composites is fabricated with adhesively bonded tubes pultruded with E-glass fibers and isopthalic polyester resin. These rectangular tubes with diagonal members are alternated to form a truss-like structure when fully assembled. Figure 1.7(b) shows that this deck system has a panel-to-panel connection similar to the Superdeck^{TM} system. The adhesive joint was subjected to static, fatigue and environmental durability testing by the manufacturer; the failure of each deck joint specimen occurred exclusively in the composite material and not in the adhesive layer or interface (Cassity et al. 2002). This deck system has been installed successfully in a number of sites, as shown in Table 1.2 (Keller 2001).

The EZ-Span system consists of pultruded triangular tubes and hand layed-up face sheets. The triangular tubes are made of E-glass braided fabrics embedded in a vinylester resin, while the face sheets are made of E-glass braided fabrics in a vinylester resin (Brown and Zureick 1999). This deck system was initially developed for the Landing Ship Quay/Causeway and the Mobil Offshore Base programs funded by the Defense Advanced Research Projects Administration (DARPA). After laboratory tests, two 10 ft by 20 ft (3 m by 6 m) decks were placed in the Troutville, Virginia weigh station on I-81 to investigate their durability of the deck system. No results from the field implementation have been reported.

Two sandwich construction FRP deck systems were installed in one unique project: the Salem Avenue Bridge on Route 49 in Dayton, Ohio. This bridge provided a test bed for investigating the panel-to-panel connections used in these types of deck systems. The Salem Avenue Bridge is actually a pair of parallel steel girder bridges, each made of five spans of similar length: 129.9 ft, 137.1 ft, 145.0 ft, 137.1 ft and 129.9 ft. The superstructure consists of a deck supported by steel stringers transversely spaced 8-ft 9-in on center (Reising et al. 2004a).

Table 1.2 Summary of road bridges with FRP deck systems constructed between 1997 and 2000 (Keller 2001) – reproduced with permission

Bridge	Year	Type	System
Magazine Ditch Bridge	1997	New hybrid construction, concrete girders	Hardcore
Cecil County Bridge	1997	New all-composite construction	Hardcore
Wilson's Bridge	1998	Repair, steel girders	Hardcore
Bennett's Creek Bridge	1998	New all-composite construction	Hardcore
Muddy Run Bridge	1998	New all-composite construction	Hardcore
Mill Creek Bridge	1999	New hybrid construction, steel girders	Hardcore
Greensbranch Bridge	1999	New all-composite construction	Hardcore
Bentley Creek Bridge	1999	Repair, steel girders	Hardcore
Westbrook Road Bridge	2000	New all-composite construction	Hardcore
Crawford County Bridges	1999	Repair, steel girders	Kansas
Laurel Lick Bridge	1997	New all-composite construction	Superdeck
Wickwire Run Bridge	1997	New hybrid construction, steel girders	Superdeck
Shawnee Creek Bridge	1997	New hybrid construction, steel girders	Superdeck
Laurel Run Bridge	1998	New hybrid construction, steel girders	Superdeck
Salem Avenue Bridge	1999	New hybrid construction, steel girders	Superdeck
Katy Truss Bridge	2000	New hybrid construction, steel girders	Superdeck
Market Street Bridge	2000	New hybrid construction, steel girders	Superdeck
INEEL Bridge	1997	New all-composite construction	DuraSpan
Smith Road Bridge	1997	New all-composite construction	DuraSpan
Darke County Bridge	1999	New hybrid construction, steel girders	DuraSpan
Kings Stormwater Channel Bridge	2000	New hybrid construction, hybrid girders	DuraSpan
Schuyler Helm Lift Bridge	2000	Repair, steel girders	DuraSpan
Warrensburg Bridge	2000	Repair, steel girders	DuraSpan
Bettendorf Bridge	2000	New hybrid construction, concrete girders	DuraSpan
Harford County Bridge	2000	Repair, steel girders	DuraSpan
Troutville weigh station	1999	New all-composite construction	EZ-Span De
Troutville weigh station	1999	New hybrid construction, steel girders	Strongwell I

The Ohio Department of Transportation (ODOT) replaced the old concrete decks of both Salem Avenue bridges with four different FRP deck products: the SuperdeckTM system (referred to hereafter as FRP-1), the Hardcore Composites deck system (FRP-2), a corrugated core deck system fabricated by Kansas Structural Composites Incorporated (FRP-3), and a concrete slab poured on FRP stay-in-place forms and reinforced with FRP top-mat reinforcing bars (FRP-4). ODOT installed FRP-4 deck along the entire length of the one of the two bridges. However, FRP-4 is not a full-composite deck system and will not be discussed further. On the other bridge, ODOT placed all four FRP systems along the length of the bridge, allowing the direct comparison of each system's performance under the same loads (Reising et al. 2004a).

The Superdeck^{TM} panels (FRP-1) were connected as previously shown in Figure 1.7(a). In the FRP-2 system (Hardcore Composites), the hard core formed by multiple wrapped cells was sandwiched by two E-glass fabric face sheets, as shown in Figure 1.2(a). This system

used FRP splice plates as the panel-to-panel connection, as seen in Figure 1.7(d). The FRP-3 system was a corrugated core sandwich system with shear keys for panel-to-panel connections, seen in Figure 1.2(b) and Figure 1.7(d).

The field testing data were recorded during a ten-month period form October 1999 to July 2000. During this period, the largest vertical deck deflection was 0.07 in., occurring on a splice plate connection of the FRP-2 deck system. All other data showed successful shear and moment transfer mechanism in connections between panels from each individual manufacturer. However, ODOT did not specify how to connect panels of different types, which resulted in differential deflections between panels with free edges. The ODOT evaluating team found this to be one reason for cracking in the polymer wearing surface. As part of their final report, the researchers (Reising et al. 2004b) included a number of recommendations for future FRP deck panel construction. The researchers recommend that deck manufacturers should provide thoroughly- developed specifications for the installation (including adhesive application), performance criteria, and field inspection of the deck panels. The researchers also point out that manufacturers should specify quality, workmanship, and dimensional tolerances. In addition, the manufacturer should provide the contractor with specific criteria for product acceptance and rejection.

While the Salem Avenue Bridge project was proceeding in the US, similar work was going on in Sweden, where a group of researchers were working to develop a panel-to-panel connection for the Asset Fiberline system, which originated in Denmark. The group used FEM to analyze both an adhesive connection and a bolted connection, as shown in Figure 1.7 (e) and (f). They used their results to determine critical dimensions and refine concepts. Their results demonstrate the concessions required to adapt bolted connections to composite structures. The bolted connections require a bottom cover plate and a 25% longer lip edge on the deck profile to develop sufficient load capacity; however, this type of connection is weaker than adhesive connections, which require no cover plate. The researchers also noted that designing the bolted connection is much more difficult, “very time-consuming and considerably more expensive to realize”(Zetterberg et al. 2001).

Researchers at Virginia Polytechnic Institute and State University (Virginia Tech) began developing the Strongwell Tube-and-Plate deck system in 1997. Both field and laboratory tests showed that the strength capability of this deck system exceeded what was

mandated by design codes (Coleman 2002; Hayes et al. 2000; Temeles 2001; Zetterberg et al. 2001; Zhou et al. 2005). However, more studies on connection details have to be done to ensure their satisfactory performance in field.

Two panel-to-panel connections suitable for use for the Strongwell Corporation's Extren Tube-and-Plate deck system were developed and tested by Link (2003), as shown in Figure 1.7(g) and (h). One was a bolted connection and the other was an adhesive shear-key joint. Results show that the bolted joints can carry the design loads but are more susceptible to fatigue loads. Because over-sizing the holes was necessary for assembly, relative deflections could not be avoided in the bolted connection. Under cyclic load, the bolts were constantly striking the tub walls near the holes, which created more slope in the connection. Also, the panels were cyclically sliding past one another, and the contacted edge tubes would wear away at each other.

Link's test of adhesively-bonded connection showed inability to carry traffic load. However, it showed far more promise than a bolted connection. The data showed a linear behavior up to failure, and a progressive failure mode. Finally, Link concluded that the capacity of the adhesively-bonded connection was close enough to what would be needed. Therefore, improvements in both connection geometry and manufacturing processes could dramatically increase the strength of the connection to the necessary level (Link 2003). He also presented two redesigned bonded connections which used scarfed joints to eliminate butt joints, as shown in Figure 1.8. The scarfed joint increases bonding area and eliminates the local failure point.

Published research shows that although mechanical connections have the advantage of easy disassembly for repair, adhesively-bonded connections are more efficient in load transfer and fatigue resistance and are easier and cheaper to construct. Thus more research about developing and evaluating a redesigned adhesively-bonded tongue and groove joint will be reported in the later portion of the proposal.

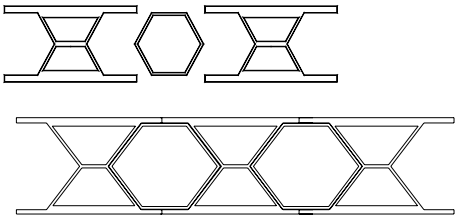

(a) Superdeck by Creative Pultrusions (FRP-1 on Salem Ave. Bridge) (Reising et al. 2004a) - reproduced

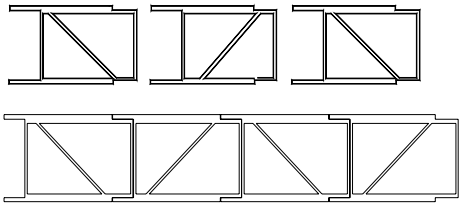

(b) DuraSpan by Martin Marietta Composites (MMC 2002) - reproduced

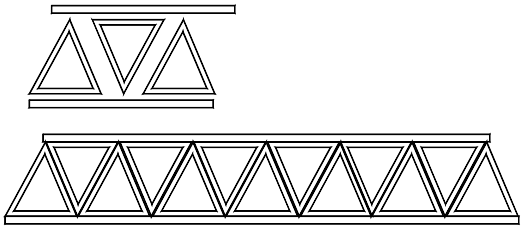

(c) EZ Span system (Brown and Zureick 1999) - reproduced

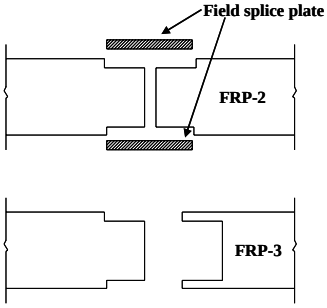

(d) Panel Connections for two sandwich construction FRP deck systems in Salem Ave. Bridge (Reising et al. 2004a) – reproduced

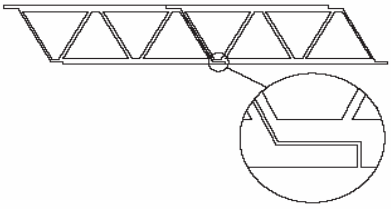

(e) Adhesively bonded connection developed by Zetterberg, et. al. (2001) – used with permission

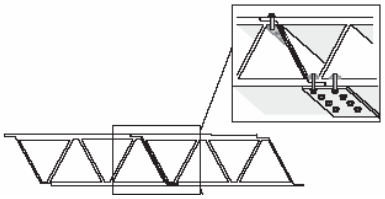

(f) Bolted connection developed by Zetterberg, et. al. (2001) – used with permission

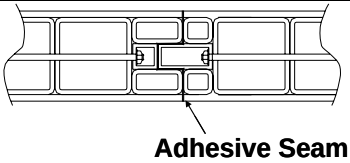

(g) Adhesive bonded shear key connection tested by Link for Strongwell deck system (Link 2003) - reproduced

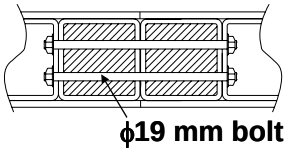

(h) Bolted Connection tested by Link for Strongwell deck system (Link 2003) - reproduced

Figure 1.7 Panel-to-panel connections

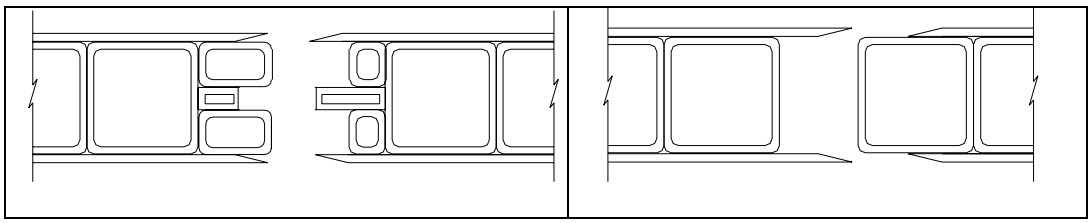

Figure 1.8 Redesigned adhesive bonded connection recommend by Link (2003) - reproduced

1.6.2.3 Deck-to-girder (stringer) connections for FRP deck bridges

The design of reliable and efficient deck-to-girder (stringer) connections is one of the most important topics in FRP deck applications. The literature shows that a number of different deck-to-girder connections have been designed and implemented with varying degrees of success (Keller and Gurtler 2006; Moon and Gillespie 2005; Reising et al. 2004b; Righman et al. 2004). Depending on the requirements of a specific project, the deck-to-girder connections can be a permanent joint which may provide composite action, or a joint with ease of disassembly without the intent of composite action between the deck and its superstructure (stringers or girders). For practical purposes, these connections can be divided into three categories: adhesively-bonded connections, shear-stud connections and mechanical (bolted or clamped) connections.

Some researchers have explored adhesively-bonded connections because of the advantages of easy construction and more uniform stress distribution (Keller and Gurtler 2005; Keller and Gurtler 2006). However, a lack of confidence in the fatigue performance and durability of an adhesive layer applied in the field has left this application still in the research stage. This section will only review shear-stud and mechanical connections.

Shear-stud connections can be used in Superdeck™ (Creative Pultrusions, Inc.), DuraSpan (Martin Marietta Composites) and other systems. The procedure for installing the shear-stud connection on the Superdeck™ system includes: drilling 4-in. diameter holes through the deck over the girder top flange; welding studs onto the girder (field welding is recommended to prevent misalignment between the holes and the studs); constructing form-work around the girder flush to the bottom of the deck; and pumping non-shrink-grout through stud-holes, so that stud-holes and cavities under the panel are filled (Reising et al. 2004b). Figure 1.9(a) shows the additional details in using shear-stud connections.

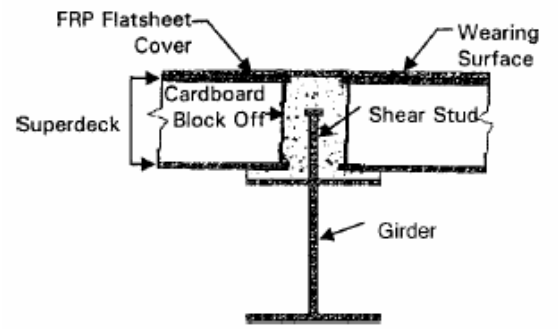

(a) Superdeck™ shear stud connector — (Righman et al. 2004) used with permission from ASCE

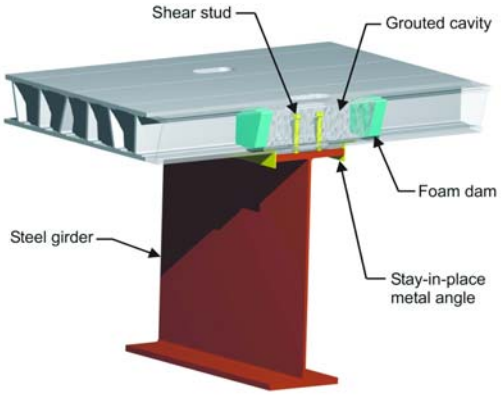

(b) DuraSpan shear stud connector —Martin Marietta Composites (MMC), used with permission

Figure 1.9 Two shear stud type of connections

The DuraSpan system can also use a shear-stud connection in its construction, though differently from with the Superdeck™ system. Specifically, one DuraSpan connection pocket consists of two or three shear studs instead of the one shear stud used in a Superdeck™ connection. Figure 1.9(b) shows the connection details for DuraSpan. Moon and Gillespie (2005) found that a connection consisting of three shear studs with steel spirals aids in grout confinement and is successful after static and fatigue tests (10.5 million cycles represented a 17-year design life).

Shear-stud deck-to-girder connection has the following advantages: ease of installation by utilizing concepts that are widely accepted in infrastructure construction; partial composite action between deck and girders, which can contribute to the stiffness of the superstructure; and good capacity to secure the deck in place and prevent uplift under vertical vehicular loads and horizontal braking force. However, some disadvantages and concerns still exist, including the difficulty of disassembly for repair and low durability of the grout under fatigue loading.

Mechanical connections are usually used when composite action between the deck and its superstructure is not desired. Because of the high modular ratio between the FRP deck and the steel girder, even full composite action contributes negligible stiffness to the girder.

Therefore, in practical applications, there is little benefit to be realized by providing composite action (Righman et al. 2004). Mechanical connections also have the advantages of easy installation, easy replacement, and cost effectiveness.

Mechanical connections usually have two formats, clamped or bolted. A clamp-type connection for use with Kansas Structural Composites, Inc. (KSCI) FRP deck system was reported by Meggers (2000). The connections are only placed at panel-to-panel joints, where each joint contains an FRP tube in which the connection is made. Holes are drilled through the tube, and traditional bolts are used to secure a clamping device installed underneath the top flange of the girder, as shown in Figure 1.10. This assembly effectively prevents uplift of the panels at joints. However, spacing the connections only at the ends of the panels may be insufficient to provide adequate restraint against deck uplift and longitudinal (parallel to the direction of the girder) movement. The clamp device is also fairly labor-intensive, as the connection needs to be installed from underneath the bridge deck.

A bolted connection is another type of mechanical connection used in current FRP bridge deck applications. The Virginia Tech team has tested three different connection methods for use with Strongwell deck systems, as shown in Figure 1.11.

For the Phase I deck, as shown in Figure 1.11(a), traditional bolts (1/2 in. diameter A325 bolt, spaced about 1.5 ft along the supporting girder) are installed inside steel sleeves through matched holes drilled through the entire depth of the deck and the top flange of the girder and seated on the metal sleeve. However, this connection method could induce debonding of the tube-to-plate interface (Temeles 2001). Thus the connection was redesigned for Phase II deck (Figure 1.11(b)). Phase II used 3/4 in. diameter, 2 $^1/_4$ in. long A325 steel bolts to connect the bottom flange of the deck system to the top flange of the support beam (about 5-ft spacing along the supporting girder). Washers were used to prevent local bearing. This solution also proved to be unsatisfactory, because access holes had to be drilled in the sidewalls of the deck to allow installation of the bolts, and these cutouts induced several cracks under fatigue loading (Temeles 2001).

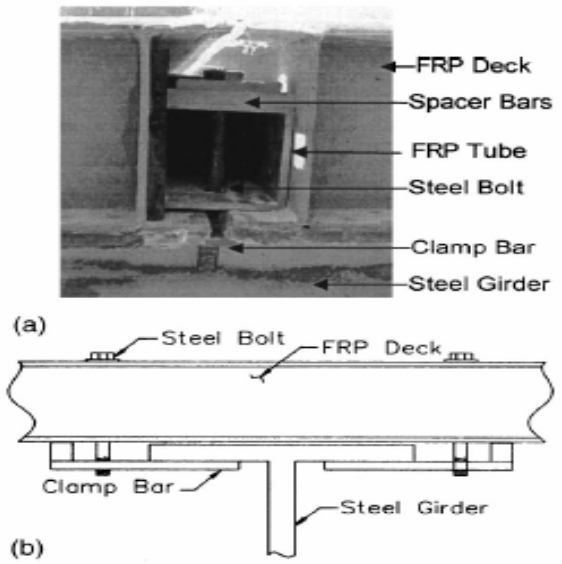

(a) Elevation view; (b) Cross section

Figure 1.10 Mechanical (clamped) connection (Righman et al. 2004) – used with permission from ASCE

In Phase III and IV deck tests, the VT team used a hook bolt (3/4-in. diameter C-1018 steel rod) over the thru-rods to connect the deck to support members (about 4-ft spacing along the supporting girder), as shown in Figure 1.11(c). This design eliminates holes in the deck's top plate and makes the deck more adaptable for use in a bridge structure (Zhou et al. 2005). The bolts are secured using two hex nuts, a flat washer, and a locking washer. This connection method is more difficult to install, but does not result in any discernable damage to the deck system after laboratory and field test. Test results showed that all three connection methods could adequately restrain the deck, as well as prevent uplift and rotation during static and dynamic tests.

The proposed research will investigate and implement a new deck-to-girder connection design without intention of composite action. Detailed results are presented later in the dissertation

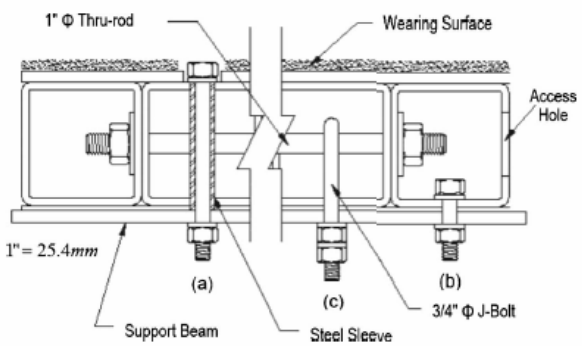

Phase I (a), Phase II (b), and Phases III (c) and IV (c)

Figure 1.11 Mechanical (bolted) connection (Zhou et al. 2005) – used with permission from ASCE

1.7 Review of Development of Design Philosophy for FRP Bridge Deck Systems

Many professional organizations have published codes, standards, test methods and specifications for FRP composites. Table 1.3 summarizes the standards and committees for FRP composites ((MDA) Market Development Alliance 2000).

The American Concrete Institute, and its Committee 440 with ten different subcommittees worked on FRP composites in concrete, covering the state-of-the-art, research, professional and student education, repair, rebar, prestressing, and stay-in-place structural formwork. The technical committee on Structural Composites and Plastics (SCAP) of the American Society of Civil Engineers (ASCE) published a manual on the design and implementation of composites in the early 1980's and is updating this manual to address the many FRP composite products developed over the years. Several ASTM committees are working on consensus test methods for the use of rebars, repair materials, and pultruded structural profiles. The ASTM D30.30.01 (Composites for Civil Engineering) committee addresses FRP composite products used in construction. The American Association of State Highway and Transportation Officials (AASHTO) Bridge Committee established a subcommittee in 1997 called "T-21 Composites". This committee is developing design guidelines for using composites in bridge applications, including FRP reinforced concrete, concrete repair, and vehicular bridge deck panels.

It is apparent that developing standards and specifications for FRP applications in the civil engineering field is an ongoing work. Several international agencies dealing with composites, such as the EUROCOMP, the United States Department of Transportation Federal Highway Administration and the Market Development Alliance, have been conducting the composite structural analysis, either by micromechanics or by finite element analysis. They have been using these results to develop standards and comprehensive design methodologies for structures made of continuous FRP composites. All agree that FRP systems must have high stiffness and strength to ensure proper performance and safety within the expected life of the structure under a set of defined environmental conditions. More specifically, deck systems must be designed to avoid catastrophic failure under impact, collision, fire, etc (GangaRao et al. 1999). The FRP design methods developed by these groups may be summarized into two categories: working-stress design and load-resistance factor design (GangaRao and Siva 2002).

In working stress design philosophy, safety factors are brought into design to account for long-term durability; temperature gradients; moisture and chemical diffusion effects; delamination and edge effects; flammability; and many others. Specifically, appropriate failure criteria incorporating safety margins are used to control the stress and strain level at the laminate level. For example, strain in the fiber direction under all load combinations should not exceed 20% of the minimum guaranteed long-term laminate strain using the maximum strain failure criterion. All appropriate failure checks at the laminate level, shape level, and system level have to be made under tension, compression including buckling, shear, bending, and combined forces. In addition, several checks have to be made at a system level for: (1) allowable bending and shear stresses; (2) deflections including bending and shear effects; (3) local buckling checks; (4) lateral–torsional buckling stress limits; and (5) joints with adhesive bonding and/or mechanical fasteners.

The load-resistance factor design approach is to design a structure to sustain all load actions likely to occur during service with an adequate factor of safety against failure, and to have adequate durability with acceptable failure probability. This approach should consider multiple factors when calculating the probability of failure: the effects of randomness of applied loads, uncertainties in analysis, nonlinear structural responses, approximations in analysis and design, uncertainties in material strength, and process variability. In addition, the design should account for ductile failure by ensuring deck design checks on serviceability limit

states, as well as ultimate limit states, recognizing that coupon/component level failures may be brittle. For example, the design method should identify and quantify the following limit states depending on the availability of FRP coupon and deck test data: (1) service stress, deflection, rotation, vibration, and human response; (2) fatigue; (3) shear, torsion, and a combination thereof; and (4) extreme events. In addition, suggestions have been made to modify internal force effects for varying levels of shape or system level ductility, redundancy, and operational importance. Similarly, strength equations, effective deck width and transverse load distribution factors, and knock-down factors are suggested in terms of shape, size, material type, temperature, aging, and ultraviolet exposure (GangaRao and Siva 2002).

The Federal Highway Administration (FHWA) has suggested the following list of design guidelines (2006) for using FRP materials in bridge applications. Many of these considerations have already been discussed above.

(1) To avoid long term creep, predicted strains under design load shall be less than 20% of the FRP composite's minimum guaranteed ultimate strength. The ultimate strength is based on coupon testing and noted in the approved plans.

(2) An environmental durability factor (knockdown factor) of 0.65 may be applied to the material properties to account for degradation of properties over time.

(3) Because of the material's typical low modulus of elasticity, most designs will be driven by deflection limitations and not strength requirements.

(4) Although the criterion for deflection is somewhat arbitrary, it is typically kept at 1/800 of the supporting span length.

(5) In cases where the deck is expected to fail in a manner other than tension of the laminate, a factor of safety of five should be applied. As reliability factors are obtained for FRP materials, a load and resistance factor design (LRFD) methodology will be developed by AASHTO.

(6) Protect exposed surfaces from ultraviolet (UV) exposure using suitable paint.

(7) If an FRP deck is being installed on a steel superstructure, careful consideration must be given to the method of attachment. Composite action between the FRP and steel is not to be assumed in capacity calculations. However, the connection itself must be detailed to prevent failure when load is inevitably transferred between the two. The

design of the interface should either insure composite action or provide a slip mechanism to prevent it.

(8) FRP can heat up rapidly when exposed to direct sunlight. A dark wearing surface exacerbates the phenomenon. Experience has shown that a thermal gradient will occur between the top and bottom of an FRP deck when surface temperatures change fast but are not able to be conducted through the FRP immediately. This problem is especially likely to occur in early spring or late fall. The design shall assume a 100 °F temperature difference between the top and bottom of the deck and account for any subsequent internal thermal stresses. Since this temperature gradient can lead to an arching action as the top surface expands faster than the bottom, it may also affect the selection of bearing and anchorage details. It is important to note that thermal stresses may be as large as stresses resulting from live loads.

Table 1.3 Summary of Standards Committees for FRP composites

Organization	Committee
American Concrete Institute (ACI)	440 – Composites for Concrete; 440C – State-of-the-art-Report; 440D – Research; 410E – Professional Educations; 440F – Repair; 440G – Student Education; 400H – Reinforced Concrete (rebar); 440I – Prestressed Concrete (tendons); 440J – Structural Stay-in-Place Formwork; 440K – Material Characterization; 400L - Durability
American Society of Civil Engineers (ASCE)	Structural Composites and Plastics
American Society of Testing and Materials (ASTM)	D20.18.01 – FRP Materials for Concrete; D20.18.02 – Pultruded Profiles; D30.30.01 – Composites for Civil Engineering
American Association of State Highway and Transportation officials (AASHTO) Bridge Subcommittee	T-21 - FRP Composites
International Federation of Structural Concrete (FIB)	Task group on FRP
Canadian Society of Civil Engineers (CSCE)	ACMBS – Advanced Composite Materials for Bridges and Structures
Japan Society of Civil Engineers	Research Committee on Concrete Structures with Externally Bonded Continuous Fiber Reinforcing materials
Transportation Research Board	A2C07 – FRP Composites

(9) Each manufacturing method has its own benefits. In general, pultruded sections produce a good quality, consistent product with tight dimensional tolerances; however, prices tend to be slightly higher than for other methods. The more custom methods (VARTM and hand lay-up) allow the depth of the section to be easily changed, and to accommodate a cross slope, inclusion of scuppers, or custom "knockouts". The designer needs to decide if the application necessitates a particular method of fabrication.

(10) Acceptable wearing surfaces will be designated for each particular manufacturer.

(11) A bonded FRP curb may be used if and only if it is protected from impact by bridge rail. Concrete curbs have also been attached to FRP decks.

(12) In a decking application, a joint over the bridge seat can be eliminated by carrying the FRP deck over the abutment stem to terminate on the approach side of the bridge. This allows any joint leakage to weep into the fill rather than onto the seat.

(13) Pourable silicone joint material has performed well and is easily repairable.

1.8 Need for Research

In recent years high-performance fiber reinforced polymer (FRP) composite material has been identified as an excellent candidate for rehabilitating deteriorated bridges. One of the most promising applications of this technology is bridge decking. Since 1996 approximately 83 vehicular bridges in the United States have been constructed or rehabilitated using FRP decks (ACMA 2004) and a number of papers and reports concerning FRP deck development have been published. However an in-depth literature review reveals that a lack of research on the long-term durability, on development of panel-to-panel joints, and on practical design standards for FRP decks.

This research seeks to address some technical needs and questions to advance FRP deck application, including (1) Develop and investigate an effective adhesively bonded tongue-and-groove, panel-to-panel joint; (2) Examine global structural performance of the FRP-deck-on-steel-superstructure bridge both in laboratory and in field; (3) Use finite element method (FEM) and results from step (2) to address two important design issues concerning design of bridges

with FRP decks, namely deck relative deflection and LD to supporting stringers and provide design recommendations. This research has the potential to assist a broad range of engineers who use FRP materials.

CHAPTER 2 DEVELOPMENT AND EVOLUTION OF AN ADHESIVELY-BONDED PANEL-TO-PANEL CONNECTION FOR AN FRP BRIDGE DECK SYSTEM

2.1 Background

Generally, FRP decks are made as wide and as long as is practical to transport. Because of the size limitations, manufacturers typically provide FRP bridge decks in modular panel forms and almost all decks are joined in the field by panel-to-panel connections to create a seamless final installation (Transportation Research Board 2006).

Panel-to-panel connections are designed to efficiently transfer bending moments and shear forces between joined modular panels; to ensure deformation compatibility due to thermal effects; and to simplify on-site installation. Several techniques have been developed for panel-to-panel connections, including adhesively bonded splicing tongue-groove connection and shear key or clip-joint mechanical fixing connection (Zhou and Keller 2005).

Researchers at Virginia Tech began developing the Strongwell Tube-and-Plate deck system in 1997. Both field and laboratory tests showed that the strength of this deck system exceeded what was mandated by design codes (Coleman 2002; Hayes et al. 2000; Temeles 2001; Zhou 2002). Recent research has focused on panel-to-panel connections to ensure their satisfactory performance in field applications. A four-stage research plan was conducted on panel-to-panel connections at Virginia Tech.

The research began with a project conducted by Christopher T. Link (Link 2003) and is referred to as Stage I. Two panel-to-panel connections were developed and tested, as shown in Figure 2.1 (a) and (b). One was a bolted connection and the other was an adhesive shear-key joint. Results showed that the bolted joint could carry the design load, but was susceptible to fatigue damage. The adhesive shear-key connection showed less capacity than bolted connection. However, it showed more promise than a bolted connection because of better fatigue performance and a linear behavior up to failure with a progressive failure mode.

The findings from Stage I research showed that although mechanical connections have the advantage of easy disassembly for repair, adhesively-bonded connections are more efficient in load transfer and fatigue resistance and are easier and cheaper to construct, which

was in agreement with published research (Zetterberg et al. 2001). Thus Stages II through IV research focused on developing and evaluating a redesigned adhesively-bonded tongue and groove joint.

In Stage II, a full-length, simplified adhesively-bonded tongue and groove panel-to-panel connection [Figure 2.1(c)] was tested under a weak-direction (beam) bending configuration. The testing showed some promising aspects: linear behavior up to failure stage; crack initiation after design service load strain was reached; and a factor of safety of 2.4 with respect to the anticipated service strain. Testing results indicated the adhesive bonding was a viable technique in using with panel-to-panel joint for FRP decks. A detailed discussion for Stage II test is presented in Section 2.2. Stage III research was aimed to further optimize this design.

In Stage III, different connection geometries (scarfed vs. butt joint behavior) were investigated. The joining effectiveness of simple butt joint geometry was tested as shown in Figure 2.1(d). Premature cracking was observed in the butt joint area. To eliminate this tendency the joints in Stage III panels were sloped or scarfed, as shown in Figure 2.1(d). Results show that under a four-point bending configuration, FRP samples with a scarfed edge have better performance than those having a butt joint (90°). The critical load and displacement (at crack initiation) increased as scarf angle decreased. But for FRP deck panels, sharper scarf angles (smaller than $^1/_2$ slope) are difficult to manufacture and can be easily damaged during transportation and installation. Therefore, scarf joints with an angle of 27° ($^1/_2$ slope) were used on the test specimens and recommended for future field application.

Two types of adhesively-bonded panel-to-panel connections with scarfed joints were tested in Stage III: one single seam connection and one double seam connection, as shown in Figure 2.1(d). A plate bending setup with three sides simply supported and one side free (which approximates the support condition near an abutment) was used to better represent the on-site situation instead of one-way bending setup in Stage II.

Testing indicated that both types of connections exceeded service load without cracking. Crack initiation in all adhesive joints tested occurred at a load level at least 30% greater than the HL-93 design truck loads as specified in AASHTO LRFD Bridge Design Specifications (AASHTO, 2004). It corresponds to a service tire load of 16 kips, with a dynamic load allowance of 33%, which yields a load of 21.3 kips. The observed failure

occurred not in the adhesive joints, but was localized in the top plate and tube section at a very high load and strain level. Failure loads were at least two times the design service load. No significant advantage or difference in behavior was found using double seam connection (using I-connectors) compared to single seam connection for the deck joints tested. Since the double seam connection involves developing a new, special pultruded shape (I-connector), the single seam connection [Figure 2.1(e)] was used in the Stage IV study: a two-bay mock-up test of the Hawthorne St. Bridge. A detailed discussion for Stage III test is presented in the Section 2.3.

Finally in Stage IV, a full-scale two-bay section of the bridge was constructed and tested in the Structures Laboratory at Virginia Tech. Static, fatigue, and failure tests were conducted on the adhesive panel-to-panel connections to evaluate their performance (details are presented in Section 2.4).

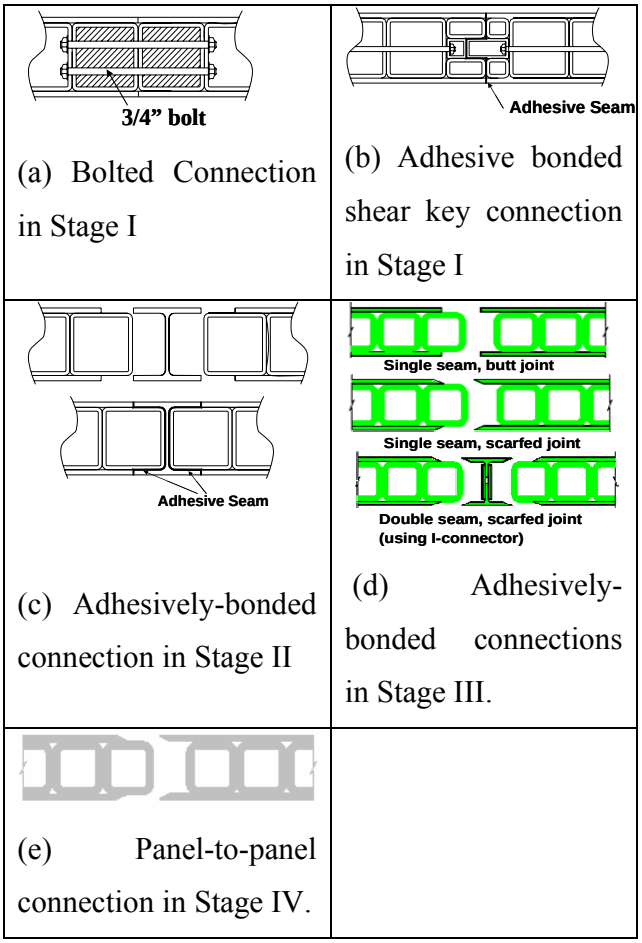

(a) Bolted Connection in Stage I

(b) Adhesive bonded shear key connection in Stage I

(c) Adhesively-bonded connection in Stage II

(d) Adhesively-bonded connections in Stage III.

(e) Panel-to-panel connection in Stage IV.

Figure 2.1 Evolution of panel-to-panel connections at Virginia Tech

2.2 Stage II: Weak-direction (beam) Bending Test

2.2.1 Specimen description

2.2.1.1 Deck panels

The specimens were fabricated with off-the-shelf pultruded Strongwell FRP "EXTREN®" products (Strongwell Inc. 2002): 4 in. x 4 in. x $^1/_4$ in. pultruded square tubes and $^3/_8$ in. pultruded top and bottom plates. The plates and tubes were all from Strongwell's Extren® 500 product line of shapes, which are made of uni-directional and continuous E-glass strand mat fibers, contained in an isophthalic polyester resin. The tubes were first bonded together with an epoxy adhesive and then the top and bottom plates were bonded to the tubes using the same epoxy adhesive. A uniform pressure of 10-14 psi was applied by sealing the deck panel within a vacuum bag to ensure contact until curing was complete.

2.2.1.2 Adhesive bonded panel-to-panel connection

A cross-section of the adhesive connection is shown in Figure 2.2. The connection consisted of two parts: a tongue and a groove. All parts were built using stock Strongwell EXTREN® shapes, arranged as shown. The two dark bold lines in Figure 2.2 represent the adhesive bonds applied to the connection. Bond A is the epoxy resin applied to an I-beam (or I-connector) in order to form the groove shape. Bond B is the adhesive bond that combined the groove and tongue shapes together, using Ashland Pliogrip 7770/300 [Ashland, 2005]. All assembly (vacuum bagging and joining) except Bond B was done by Strongwell and are not discussed here. The procedures for construction Bond B are given below.

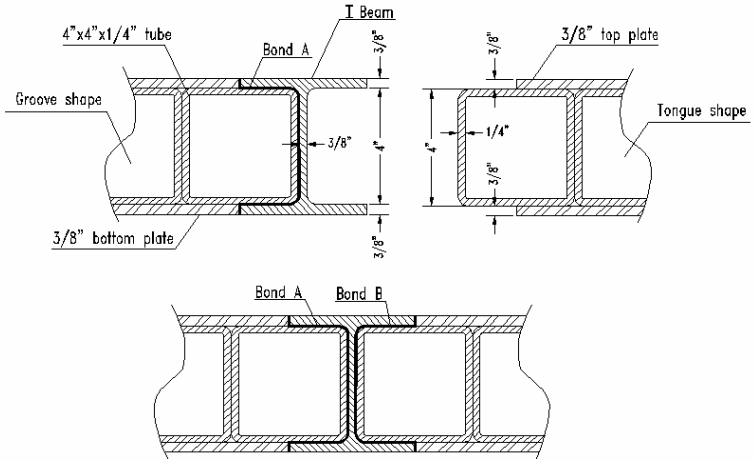

Figure 2.2 Cross Section of Adhesive Connection

An 80-grit sandpaper was used to sand the contact surfaces on both parts to remove all mold release agent from the surface. Typically 0.04 in. (1 mm) of the top surface veil was removed so that traces of fibers could be seen, leaving the surface dull instead of a polished greenish color. Once the sanding was completed, the part with the grooved end was clamped down by two bolts on a flat table. The corresponding part with the tongue end was put on that table with enough room to apply adhesive on both parts. The adhesive was then applied on the contact surfaces using adhesive gun PPA-300A [Cox North American Inc., 2004], as shown in Figure 2.3. Figure 2.4 shows the surfaces where the adhesive was applied and how the adhesive lines were laid out. The panel with the tongue end was pushed into the panel with the groove end. Then they were clamped together using a hydraulic jack; pressure was kept on the two pieces during the curing process. Mold release paper was placed between the deck pieces and the tables along the adhesive seam to prevent accidental bonding between the deck and the table. The bonds were allowed to cure for approximately 24 hours. The specimen was transported from the table to the testing site. Figure 2.5 shows a picture of the setup used to join the panels.

Figure 2.3 Adhesive Gun PPA-300A

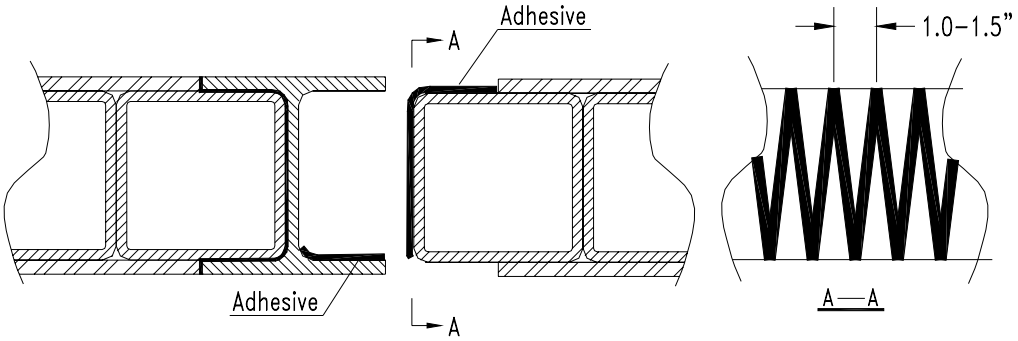

Figure 2.4 Adhesive Arrangement

Figure 2.5 Assembling the Adhesive Connection

2.2.2 Test setup and instrumentation

2.2.2.1 Test setup

All six specimens (referred as Deck #1 to Deck #6) were tested under three-point bending with 6-ft clear span between the supports [Figure 2.6]. The orientation of the connection relative to the supports was rotated ninety degrees, in comparison to the in-site orientation, so that the specimen could be bent in the weak direction and the desired strain along the adhesive seam could be obtained. Because of this fact, testing of the adhesive connection was strain-controlled, rather than load-controlled.

Figure 2.6 Setup of three-point bending test

2.2.2.2 Instrumentation

All six specimens were instrumented with a load cell in the testing frame, six wire pots on the bottom of the deck and one linear variable differential transducer (LVDT) across the bottom adhesive seam. Table 2.1 shows all the instruments used in each specimen during the test. The strain gauge (Measurement Group CEA-06-375UW-350) locations used in the six

decks varied. Decks #1 and #2 used four strain gauges on the bottom of the deck, denoted "SG#1 to #4". Two additional strain gauges were set up on the top of the deck to locate the neutral axis. SG#5 was located above SG#2, and SG#6 was located above SG#4. Deck #3 used more strain gauges (10 strain gauges on the bottom of the deck, denoted "SG#1 to SG#10") in order to collect detailed stress data from the bottom near the adhesive seam. Decks #4 to #6 used six strain gauges on the bottom of the deck, denoted "SG#1 to #6." No strain gauges were set up on the top of Decks #3 to #6. All instrumentation shown in Figure 2.7 (a) to (c) was attached to the bottom of the deck. Since the deck specimen was much stiffer in the direction transverse to that of major bending, a slight variation in the transverse placement of the gauges was not considered to be problematic.

Table 2.1 Instrumentation used in each deck

	Deck #1	Deck #2	Deck #3	Deck #4	Deck #5	Deck #6
wire pot displacement transducer	6	6	6	6	6	6
Strain gauges on the top of the deck	2	2	0	0	0	0
Strain gauges on the bottom of the deck	4	4	10	6	6	6
LVDTs	1	1	1	1	1	1
Load Cell	1	1	1	1	1	1

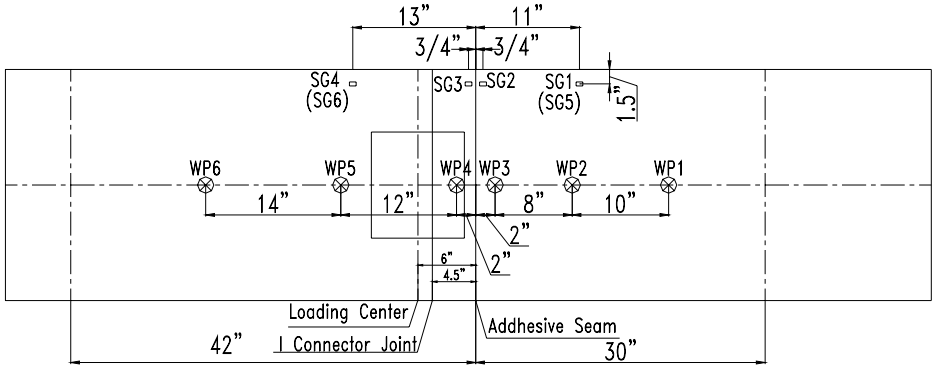

(a): Deck #1 and #2

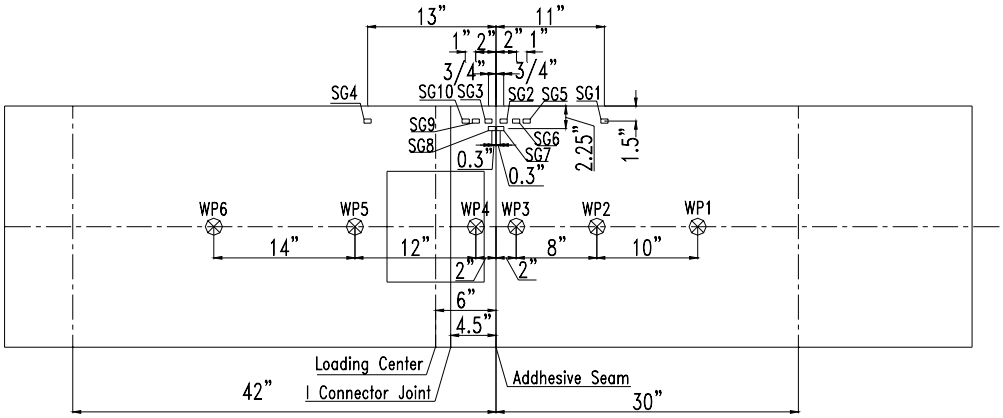

(b): Deck #3

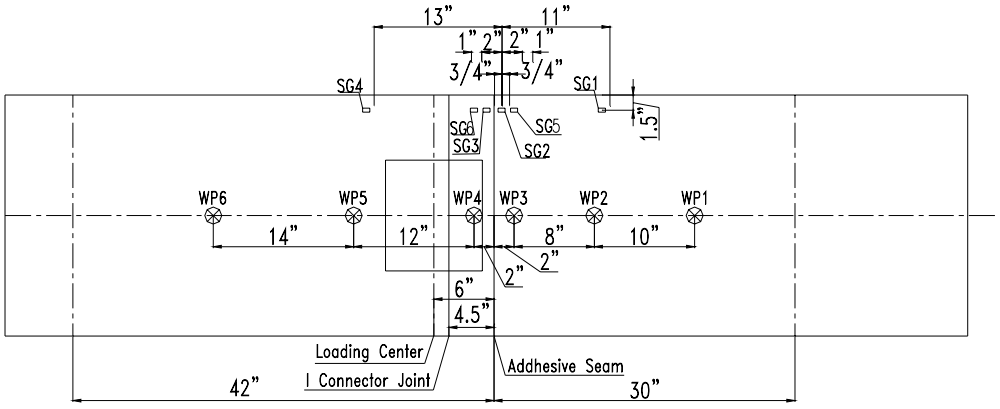

(c): Deck #4~#6

Figure 2.7 Instrumentation for six deck specimens

2.2.3 Experimental procedure and results

2.2.3.1 Review of tests by Coleman

Testing of the adhesive joints under a weak-direction (beam) bending configuration was strain-controlled; the service strain was from Coleman's research. The strain data with normalized values and nomenclature presented in Table 2.2 is retained from Coleman's thesis (Coleman 2002). The "F" indicates the gauges that were on the external face of the deck, the "E" or "W" indicates which span (east or west, respectively) the gauges were located in, and the "T" indicates the orientation of the gauges with respect to the span direction of the tubes (transverse). All strains listed in Table 2.2 are transverse strains recorded directly under the load patch during single span tests in the lab. These strains were normalized to both a 26 kips (HS-25) and 20.8 kips (HS-20) patch load, and then averaged. HS-20 is specified in the 17th Edition of AASHTO's Standard Specifications for Highway Bridges (AASHTO 2002). HS-25 is not defined in the AASHTO specifications, but it is commonly used by some state transportation departments to design their highway bridges. An HS-25 design truck is the same as an HS-20 truck, except that all loads are increased by 25%.

Although the average strain from the field test of 341 με (normalized values for HS-20) is much smaller, the average strain of 501 με based on lab testing seen in the HS-20 column was used as a conservative service strain for this testing. Each specimen was loaded to this service strain. If the adhesively bonded connection had no initiation of crack below service strain, the connection was judged to be safe under service load. Each specimen was also loaded until failure and an ultimate factor of safety (ultimate strain with respect to the service strain) was calculated to evaluate the performance of the adhesive connection.

Table 2.2 Strain Values from Previous Research –Reproduced with permission (Coleman 2002)

Stiffness Test							
Test #	Rep.	Load	Active Patch	Gauge	Strain Value	Normalized Values	
						(26k) (HS-25)	(20.8k) (HS-20)
2	1	24.3	E	F_E_T	620	663	531
	2	24.1	E	F_E_T	624	673	539
	3	24.2	E	F_E_T	614	660	528
	4	23.6	E	F_E_T	581	640	512
	5	24	E	F_E_T	611	662	530
	6	24.4	E	F_E_T	601	640	512
3	1	23.6	W	F_W_T	510	562	449
	2	26.5	W	F_W_T	518	508	407
Average:					**585**	**626**	**501**
Field Tests							
5 (9 27.01)	1	22.15	E	F_E_T	349	410	328
5 (9 27.01)	2	22.15	E	F_E_T	368	432	346
5 (9 27.01)	3	22.15	E	F_E_T	362	425	340
5 (9 27.01)	4	22.15	E	F_E_T	368	432	346
5 (9 27.01)	5	22.15	E	F_E_T	371	435	348
Average:					363	427	341

2.2.3.2 Service load tests

In service load tests, each specimen was loaded slowly to around 501 με three times. The test was controlled by whichever strain gauge read the highest value (since there was some variation as to where the maximum strain was located). This gauge was generally SG#3. Each deck was then loaded until its collapse. For all tests, the instrumentation was zeroed before the loading ram was extended to touch the deck. A special loading patch, which consisted of a quarter tire filled with silicone rubber, was used to mimic the cushioning effect of a pneumatic tire. This was done to minimize local stress concentrations of a standard rectangular steel patch (Zhou 2002).

All six specimens exhibited approximately linear behavior up to service load (0 to 501 με). Every specimen deflected linearly, emitted very little noise, and supported the service load without any indication of cracking or other behavior indicative of structural deterioration. Figure 2.8 is a representative plot of load versus maximum strain recorded during the test and illustrates this linear behavior.

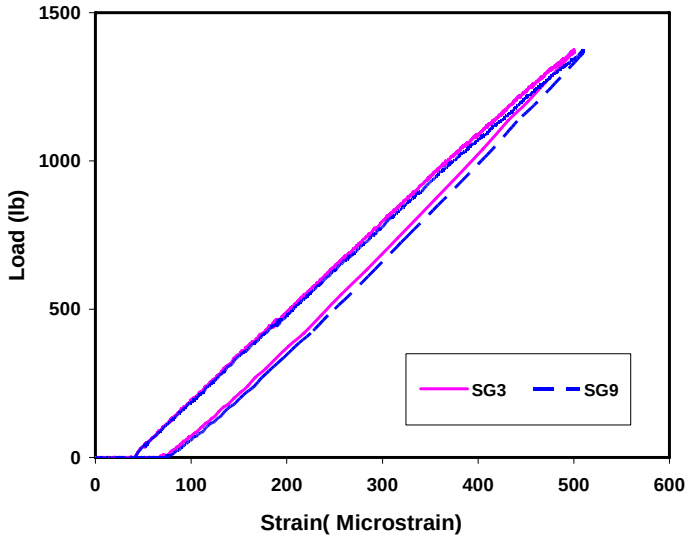

Figure 2.8 Representative plots of load vs. strain in service load test (Deck #3)

In all specimens except Deck #3, SG#3 reported the maximum strain values measured during testing. In Deck #3, SG#9 recorded the maximum strain value, but this value is only 10 με larger than the corresponding value recorded by SG#3, as shown in Figure 2.8. In Figure 2.8, strain values shift as the loading values still equal zero. The reason is that the weight of the loading ram acted on the deck before the loading ram began to compress the load cell and thus the load cell showed load values.

2.2.3.3 Crack Initiation and Failure Tests

After being tested at service load level (0 to 501 με), each specimen was then loaded until failure. Audio indications helped to capture the appearance of initial cracks in the connection during test. A sudden popping sound was heard and a sudden drop in strain values was simultaneously observed by the monitoring computer at the time of the first crack. However, no crack could be seen with the naked eye. In all the tests, initial cracking was noticed by these two means. Data analysis after the test also provided evidence of crack initiation. The evidence of cracking in Deck #1 (Figure 2.9) is typical of what was seen in all the specimens: a sudden drop of strain with a slight decrease of load. The data from the LVDT also showed the first crack point. As seen in Figure 2.10, a small disturbance of displacement with a sudden drop of strain values shows the first crack point of Deck #1.

After crack initiation, all decks were continuously loaded to 200 με above the strain at first crack point then unloaded and reloaded until failure (shown in Figure 2.9). Data indicated no significant stiffness loss occurred after crack initiation until the deck approached ultimate failure. As seen in Figure 2.9, there was no significant slope change in the load vs. strain plots after the first crack, until near the ultimate failure. The comparison among the six specimens during the failure testing is presented in Table 2.3.

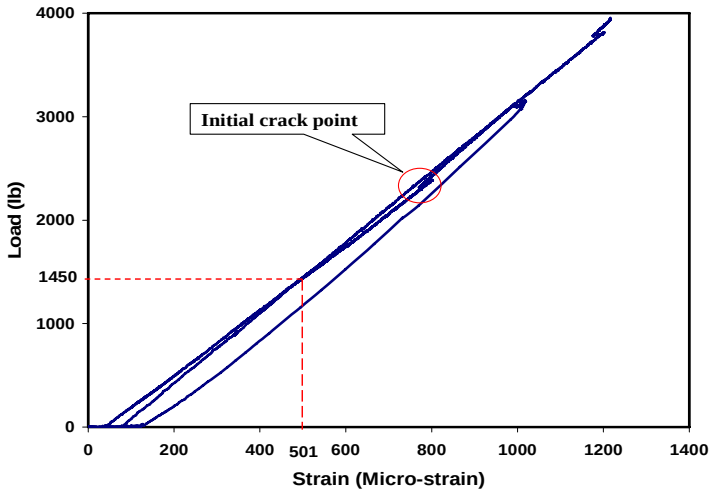

Figure 2.9 Representative plots of load vs. strain in failure test (Deck #1)

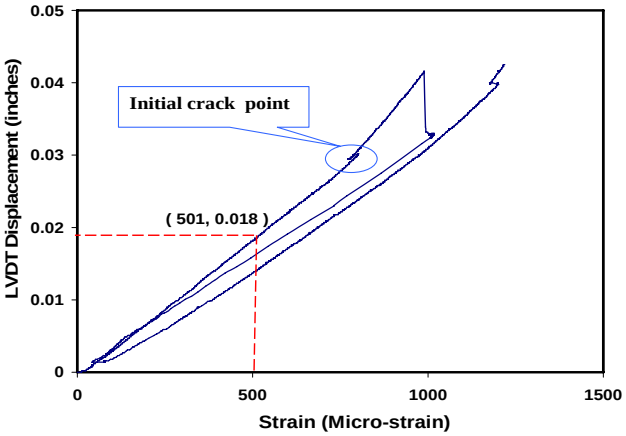

Figure 2.10 Representative plots of LVDT vs. SG#3 Strain in failure test (Deck #1)

Table 2.3 shows both the maximum strain sustained before cracking initiated and the maximum strain the specimen sustained at any point during the failure testing. The initiation of

crack occurred at load levels varying from 121% to 260% above the target strain. Deck #5 was able to sustain the highest strain level before crack initiation (1300με), followed by Deck #1 (802με). Deck #6 was by far the weakest of the six, supporting 607 με before crack initiated.

Table 2.3 Behavior Comparison during Failure Stage

	Deck #1	Deck #2	Deck #3	Deck #4	Deck #5	Deck #6	Average
Strain at Initial Crack (με)	802 (SG#3)	683 (SG#3)	671 (SG#9)	791 (SG#3)	1300 (SG#3)	607 (SG#3)	809
Stain at Ultimate Failure (με)	1240 (SG#3)	1020 (SG#3)	1370 (SG#9)	1250 (SG#3)	1510 (SG#3)	850 (SG#3)	1210
Failure location	Bond A	Bond B	Bond B	Bond A	Bond A	Bond A	
Failure type	Progressive	Brittle	Brittle	Brittle	Brittle	Brittle	

This variability in performance may be a direct result of the bond quality. Understandably, the amount of adhesive used to make the joint and the quality of its application have a large influence on the performance of the joint. Since the bottom side of the seam is in tension, any undulation or anomaly in the adhesive can serve as an initiator of a crack. Deck #6 was the first specimen fabricated. Due to lack of experience and human error, not enough adhesive was applied, and the excess adhesive was not squeezed out from the bottom side of the seam. A black "line" can be seen along the joint where the adhesive receded and formed a depression along the seam, approximately as deep as half the depth of the bottom plate. The recess on Deck #6 is essentially a built-in crack former. The deck capacities reflected these differences, with Deck #6 being the weakest one.

The failure modes were different. As seen in Table 2.3, four specimens (Decks #1, #4, #5 and #6) failed at Bond A, which is a factory made epoxy resin connection. Two decks, #2 and #3 failed at Bond B, which is a polyurethane adhesive connection. Two kinds of failure types were observed in this test. Progressive failure only happened on Deck #1, and all other specimens were brittle failure.

Figure 2.11 shows a progressive failure of Deck #1. The crack initiation started at the bottom butt joint of Bond A. After crack initiation, the stresses were redistributed and the connection continued to resist load. It seemed that adhesive bonding was stronger than the

bottom plate of the tube near the seam. Final failure mode was a tensile failure in the bottom plate of the tube, rather than adhesive or adhesive interface failure, which showed the success of this adhesive joint.

All other specimens showed brittle failures in the failure test. The crack initiation started inside the seam, at either Bond A or Bond B. No crack could be seen along the seam with the naked eye, but a sudden popping sound and a sudden drop in strain values could be observed at the time of crack initiation. After crack initiation, the stresses were redistributed and the connection continued to accept load until another crack formed. While cracks developed inside the seam, popping and creaking noises were audible, but no cracks could be seen with the naked eye. When the load reached ultimate, a sudden popping sound was heard and the specimen totally separated, as seen in Figure 2.12

Figure 2.11 Progressive failure of Deck #1

Figure 2.12 The groove shape after brittle failure

Another noteworthy characteristic of these brittle failures was the partial "fuzzy" nature of the bonded surfaces (as seen in Figure 2.13), characteristic of a combination of cohesive failure (within the composite tube) and adhesive failure (within the adhesive layer or at the interface of the adhesive and the tubes). This indicated an unsuccessful bonding process: the adhesive did not fully penetrate the surface of the connected tubes. The failure was actually occurring partially within the tube wall and partially within the adhesive layer.

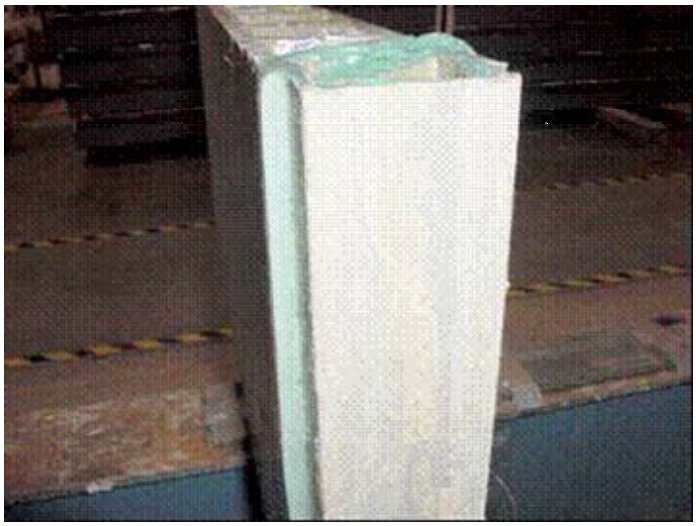

Figure 2.13 The bonded face after brittle failure

2.2.4 Summary of Stage II Testing

Based on the test results discussed above, this adhesive connection does have some promising aspects: such as linear behavior up to failure stage, no initiation of crack below service strain, and an ultimate factor of safety of 2.4 with respect to the target service strain (501 με, AASHTO Standard Specification HS-20 design load). Moreover, from a manufacturing and contractor perspective, the adhesive connection has the advantages of easier and faster manufacture and construction, which can reduce project costs. In conclusion, the adhesive connection holds a very promising future in the FRP deck system assembly.

However, there is one issue indicated by the results that must be addressed before the adhesive connection can be successfully implemented. The sudden brittle failure character of this adhesive connection does show a negative aspect of this connection. This may due to the different bending orientation of the connection in testing in comparison with the in-situ orientation. For more accurate stress distribution and failure mode prediction, adhesive joints should be tested in arrangements that more accurately approximate the support conditions in actual bridges.

By studying the test results, some recommendations can be made: (1) more care should be taken in the procedure of surface preparation in order to prevent adhesive failure within the adhesive layer or at the interface between the adhesive and the tubes; (2) some re-design should be done to improve the performance under service load. One method is changing the butt joint to a stepped or scarfed joint, which would allow more uniform load transfer. Another method is increasing contact areas to apply adhesive, which would help transfer more shear forces in the connection; (3) in future tests, the adhesive seam orientation should be perpendicular to the support line and tested under a plate (two-way) bending configuration. This would help investigate the real stress distribution and failure mode.

2.3 Stage III: Plate Bending Test

2.3.1 Specimen description

2.3.1.1 Deck panels

Stage III panels were fabricated from the 6 in. x 6 in. x 3/8 in. pultruded square tubes and the 3/8 in. pultruded top and bottom plates, standard EXTREN® structural shapes and plate manufactured by Strongwell Corp. of Bristol, VA. This configuration will be used in the Hawthorne St. Bridge rehabilitation.

The tubes and plates were made of E-glass mats (continuous) and roving embedded in an isophthalic polyester resin. The assembly procedures were discussed in Section 2.2.l.

Two sets of FRP deck panels were shop-fabricated by Strongwell Corp. of Bristol, VA and transported to Virginia Tech. Each set of panels included three pieces: 4x6 ft, 2x6 ft, and 3x6 ft. At the Virginia Tech Structures Laboratory, each set of panels was jointed using full-length, adhesively-bonded, tongue and groove, panel-to-panel joints to form two 9x6 ft specimens. One specimen used single-seam scarfed connection [Figure 2.14(b)] and the other one used double-seam (using I-connector) scarfed connections [Figure 2.14(c)].

2.3.2 Study on connection geometry: scarfed vs. butt joint behavior

To achieve better fatigue performance and uniform load transfer across the panel-to-panel connection, adhesive bonding is preferred over conventional mechanical fastening (bolts, rivets etc) (Zetterberg et al. 2001). However, the performance of adhesive bonding depends upon surface preparation, the amount of adhesive applied, as well as joint geometry.

The joining effectiveness of simple butt joint geometry was tested as shown in Figure 2.14(a). Premature cracking was observed in the butt joint area. To eliminate this tendency the joints in Stage III panels were sloped or scarfed, as shown in Figure 2.14(b) and (c). Figure Figure 2.15(a) shows the testing setup used to determine the best slope angle. Each specimen includes two 1.5 in. x 16 in. x 3/8 in. plates. The bottom plate was cut into 15, 30, and 45 degree scarf angle, and 90 degree butt angle. Six replicates of each angle were made for testing. All the plates were sanded and washed using acetone to insure proper boding of the polyurethane adhesive. The Ashland Pliogrip 7770/300 (Ashland Pliogrip 7770 cartridge

adhesive systems work sheet, Ashland 2005), two-part polyurethane adhesive was then applied on the bonding surfaces with a special pneumatic gun, PPA-300A from Cox North American Inc. (Technical data, Cox North American Inc., 2004). Clamps were used to create pressure until the adhesive hardened.

Figure 2.15(b) shows that under a four-point bending configuration, FRP samples with a scarfed edge have better performance than those having a butt joint (90°). The maximum load and displacement (at crack initiation) increased as scarf angle decreased. But for FRP deck panels, sharper scarf angles (smaller than 27°) are difficult to manufacture and can be easily damaged during transportation and installation. Therefore, scarf joints with an angle of 27° were used for future application. The study is part of National Science Foundation (NSF) and Research Experience for Undergraduates (REU) Summer Undergraduate Research Program (SURP). Details of the testing can be found in "Design and Testing of Adhesively Bonded FRP Deck Joints" (Soto J et al. 2004).

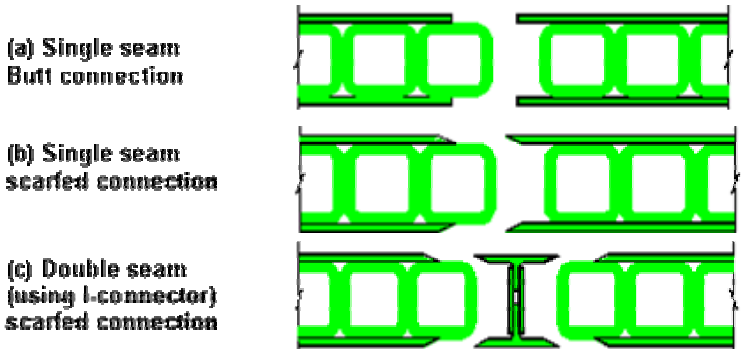

Figure 2.14 Implementation of scarf geometry for panel-panel connections

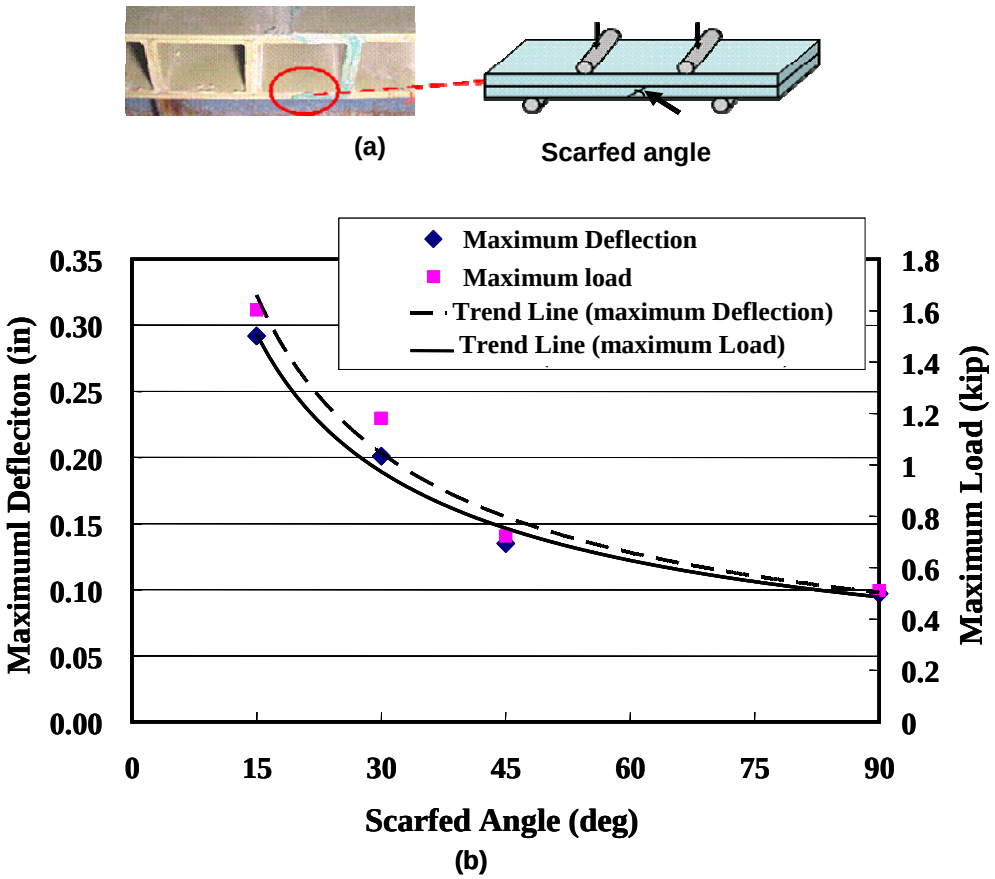

Figure 2.15 Critical load and displacement increased as scarf angle decreased, under 4-point bend test.

2.3.3 Construction for adhesively-bonded panel-to-panel connections

The contact surfaces on both mating deck panels were first sanded to get rid of all mold release agent on the surface of the tubes and plate sections. The level of sanding was determined subjectively by observation. The mating surfaces were sanded until they appeared dull to the human eye (no shine or polish remaining from the mold release agent used during pultrusion process and some fiber exposed). Once the sanding was completed, the grooved deck panel was clamped down by two bolts on a flat steel work surface. The tongue deck panel was aligned and positioned so that it could be pushed to fit. Then the mating surfaces were thoroughly washed with acetone to remove any dirt particles that could hinder the quality of the adhesive bond. The Ashland Pliogrip 7770/300 (Ashland Pliogrip 7770 cartridge adhesive systems work sheet, Ashland 2005), two-part polyurethane adhesive was then sufficiently

applied on the bonding surfaces with a special pneumatic gun, PPA-300A from Cox North American Inc. (Technical data, Cox North American Inc., 2004), as shown in Figure 2.3. Figure 2.16 shows the surfaces where the adhesive was applied and how the adhesive lines were laid out. This layout pattern allowed air between adhesive lines to evacuate and prevented air voids inside the bond lines. After the application of adhesive, the mating deck panels were pushed together. The combined parts were then clamped together until the adhesive hardened. Figure 2.17 shows the adhesively- bonded joints after curing. This figure also shows that plenty of adhesive was squeezed out from the top, bottom and side sides, indicating sufficient adhesive application

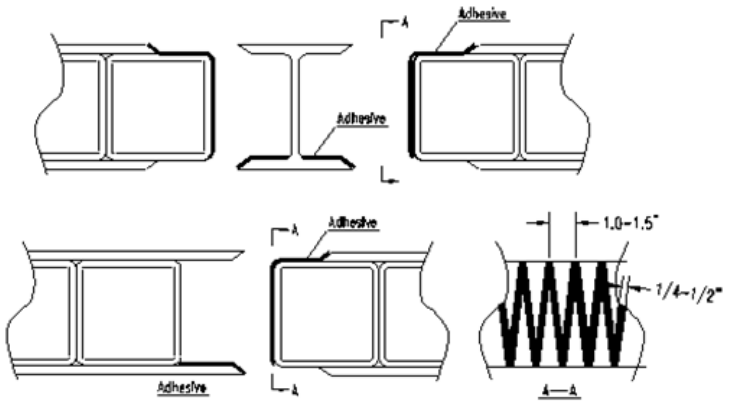

Figure 2.16 Adhesive layout

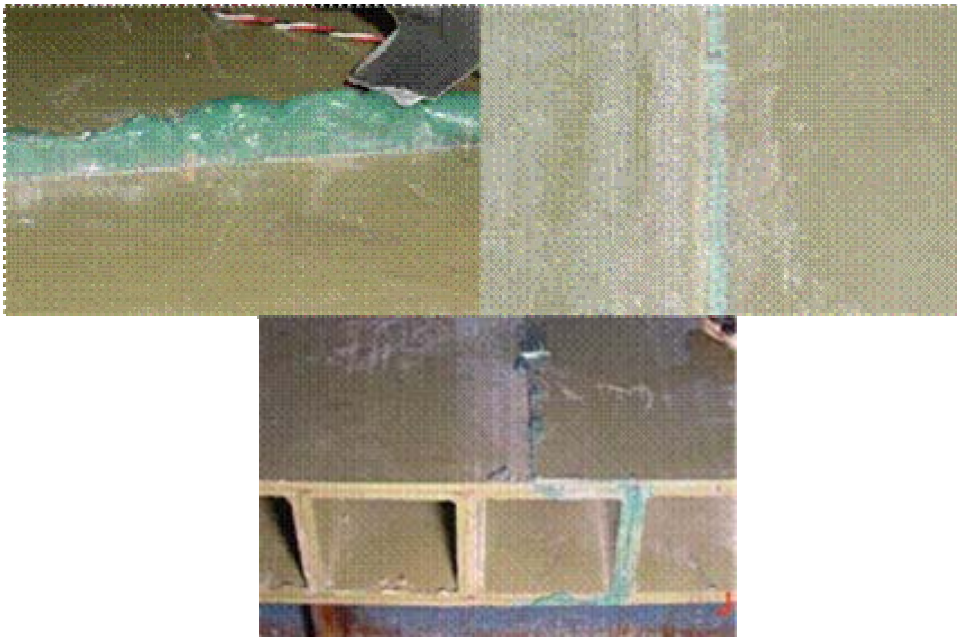

Figure 2.17 Adhesively-bonded joints after curing

2.3.4 Test setup and instrumentation

After joining the deck sections, the panels were tested to evaluate the performance of the two joint designs. There were two objectives for the testing program. First, the decks were tested under a service tire patch load to evaluate the performance of the two joints at service load levels. Second, the panels were loaded until failure to determine and compare the strength and failure modes of the two joints.

2.3.4.1 Test setup

All testing was conducted in the Structures Laboratory on the campus of Virginia Tech. Figure 2.18(a) shows a photo of deck panel testing. A plate bending configuration with three sides simply supported and one side free (which approximates the support condition near an abutment) was used. The supports under the two long sides represented the support of stringers with a clear span of 4 ft and the short side support represented the abutment for the terminal end of a deck panel. Bearing pads were used between deck panels and steel supporting girders. Each deck panel was loaded near the adhesive seams with a quasi-static load (see Figure 2.19 for load positions). A special loading patch, which consisted of a quarter tire filled

with silicone rubber [Figure 2.18(b)], mimiced the cushioning effect of a pneumatic tire. This was done to minimize local stress concentrations that are inherent to more stiff loading systems.

(a) (b)

Figure 2.18 Test setup and tire loading patch.

2.3.4.2 Instrumentation

Two types of sensors (strain gauges (Measurement Group CEA-06-375UW-350) and wire pots) were mounted on the specimens to capture their response under load, as shown in Figure 2.19. Strain gauges were attached at the bottom of the deck, 0.5 in. away from the seam. Due to the orthotropic property of FRP material and the two-way plate bending characteristic of plate, two strain gauges were set at each side of an adhesive seam. One was parallel to the seam and the other perpendicular. These measured the strain changes close to the seam under load. Four wire pots were used to record the displacement contour under the loading patch.

The vertical loads applied on to the deck were measured using a 200 kips load cell placed between the hydraulic actuator and the bearing block, fixed on the load frame. Also a data acquisition system was connected to monitor and record the sensor output during testing.

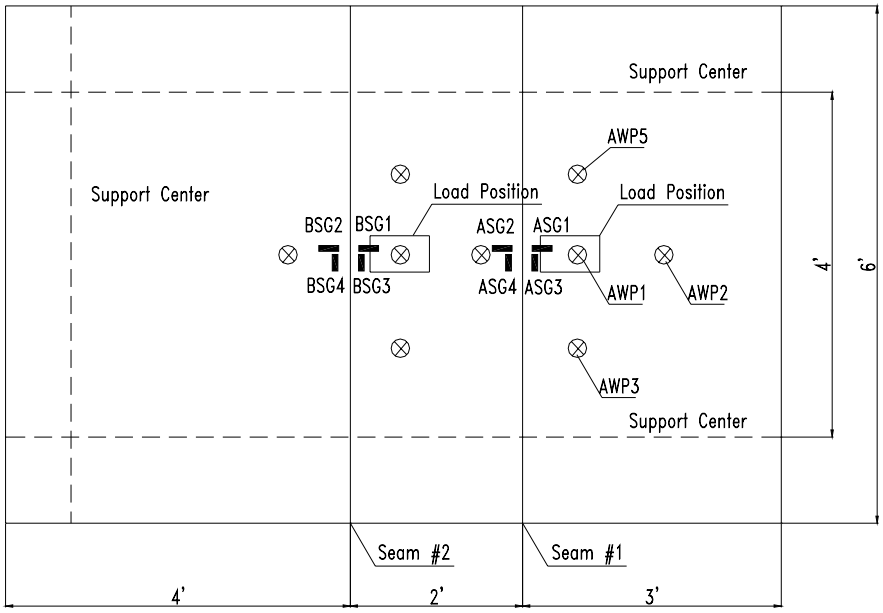

(a) Specimen #1 (Single-Seam Connection) Instrumentation Key.

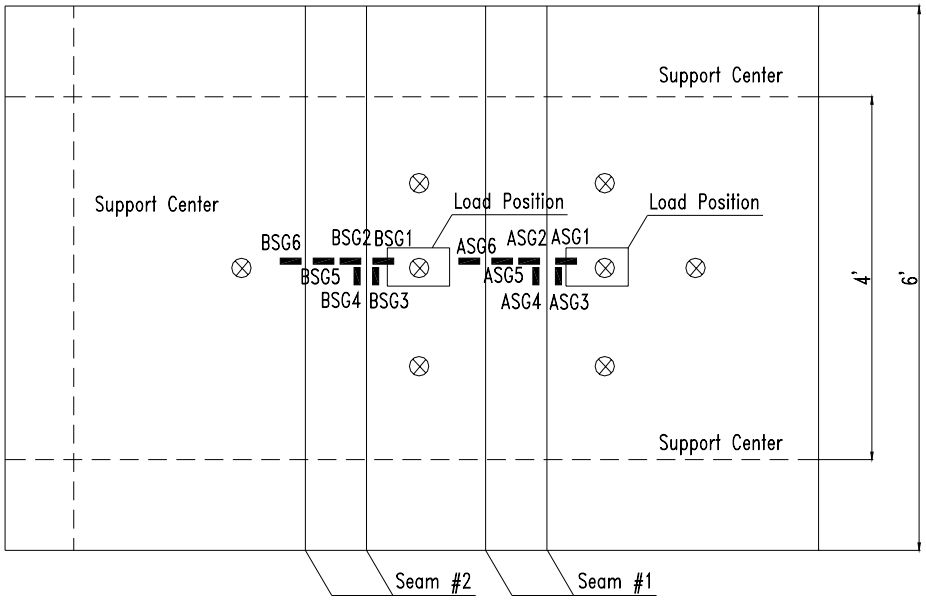

(b) Specimen #2 (Double-Seam Connection) Instrumentation Key.

Figure 2.19 Instrumentation key for two specimens

2.3.5 Experimental procedure and results

The AASHTO LRFD Bridge Design Specifications (AASHTO 2004) HL-93 design truck loads were used to evaluate the deck structure. For the local effects of a wheel at or near an adhesive joint, a tire patch load was used. Based on AASSTO LRFD, this is a load of 16 kips with a dynamic load allowance of 33%. This yields a service tire patch load (serviceability limit state) of 21.3 kips. Therefore, a load limit of 22 kips was chosen because it was slightly higher than the required 21.3 kips. The factored wheel load (strength limit state) corresponding to an HL-93 truck is 21.3 kips increased by a 1.75 load factor, which yields an ultimate design load of 37.2 kips.

2.3.5.1 Service load test

During the service load tests, behavior of the adhesive joints up to 22 kips was observed. Test results showed that both joint configurations were able to resist the service tire patch load without any indication of cracking. A summary of strain and deflection data corresponding to HL-93 loading is furnished in Table 2.4. A complete presentation of test results under design service load is given in Appendix A.1.

Table 2.4 Strain and deflection data of service load test

Specimen Type		Load (kips)	Maximum longitudinal strain (με)	Maximum transverse strain (με)	Deck deflection (in)	Span/ Deflection
Deck # 1 (single seam connection)	First Seam	22.0	700	141	0.121	395
	Second Seam	22.2	490	244	0.127	378
Deck# 2 (double seam connection)	First Seam	22.0	905	404	0.144	334
	Second Seam	22.1	826	557	0.186	258

The maximum longitudinal (along the tube direction) strains reported in Table 2.4 were always strain readings from gauges ASG3 and BSG3, which were close to the loading patch (see gauge locations in Figure 2.19). The maximum transverse strain is 557 με, which is

a little higher than the 501 με used as control service strain in Stage II testing. This may be due to the fact that the 501 με comes from HS-20 load (20.8 kips), however, 22 kips was used in this test. All load-versus-strain and load-versus-deflection behavior was linear elastic throughout the test. The maximum deck deflection was recorded by the wire port under the tire patch during Deck #2, second seam test, which was 0.186 in. under a 22 kips service load. This indicates an L/258 response; none of the deflections could meet the desired deflection index of less than L/800, which is the recommended limit of live load deflection for steel, aluminum and concrete construction by AASHTO LRFD Bridge Design Specifications (AASHTO 2004). It should be noted that this limit is not intended for application to FRP composite bridge decks. However, no appropriate design limit is presently available. Composite bridges constructed for demonstration projects have been designed based on a range of L/425 to L/1,000 (Demitz et al. 2003). Deflection limit for FRP deck bridges will be further discussed in Section 4.4.1.

2.3.5.2 Crack Initiation

After service load tests, the specimens were loaded until the first crack was detected and then unloaded. The onset of the first crack was detected audibly (by hearing cracking sounds) and visually (by observing a slight strain change near the joint and a deflection change across the joint). The cracks themselves were not externally visible at crack initiation. Load, strain, and deflection data were continuously recorded during testing using a data acquisition system. Figure 2.20 shows a representative load vs. strain behavior. In this figure the first crack initiated at about 1347 με and 42 kips. After the crack initiated, the deck panel was unloaded for inspection. The critical values corresponding to the first crack initiation for the different deck joints tested are summarized in Table 2.5. Note that each seam was loaded to at least 29% more than the AASHTO design service load before cracking. A complete presentation of test results at the moment of crack initiation is given in Appendix A.2.

Table 2.5 Data of initial crack test

Specimen Type	Test Location	First Crack initiated at		
		Load (kips)/ % of service load (21.3 kips)	Maximum strain (με)	Deflection (in.)
Deck # 1 (single seam connection)	First Seam	28 / 129%	920	0.127
	Second Seam	42 / 196%	1347	0.166
Deck# 2 (double seam with I-connector	First Seam	30 / 143%	1150	0.167
	Second Seam	37 / 172%	1280	0.226

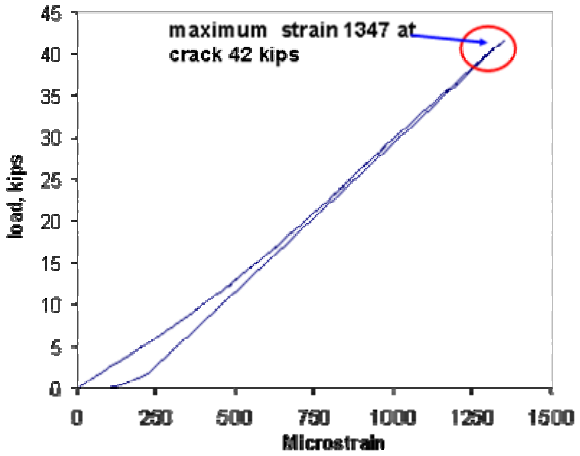

Figure 2.20 Typical load versus strain behavior until initiation of crack.

2.3.5.3 Failure Test

Subsequent to the tests to first cracking, the deck panels were tested to failure adjacent to each of the four joints. During testing to failure, initiation of failure was identified with loud cracking noises and significant strain drop. A representative load vs. deflection plot is shown in Figure 2.21. In this figure the failure was at about 104 kips and a sudden load drop could be seen. Visible cracking and failure of the top plate was also observed, as shown in Figure 2.22. There was no evidence of cracking at any of the adhesive seams even after failure. Results from the tests to failure are summarized in Table 2.6. Each seam resisted at least triple the AASHTO design load (21.3 kips) before failure. A complete presentation of test results at ultimate failure is given in Appendix A.3.

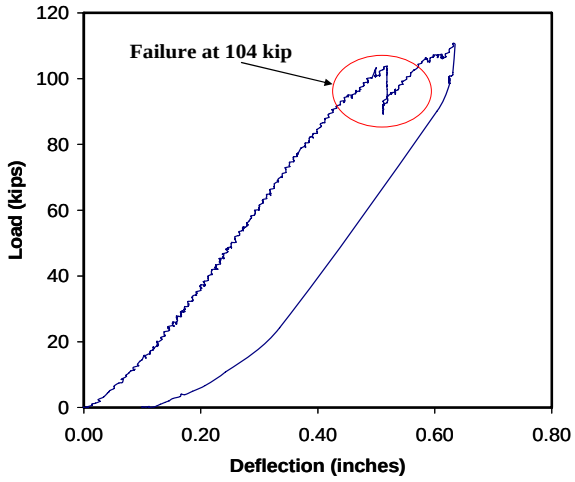

Figure 2.21 Representative load versus deflection until failure (Deck #2, second seam)

Table 2.6 Data of failure test

Specimen Type	Test Location	Failure At			
		Load (kips)/ % of service load (21.3 kips)	Load (kips)/ % of ultimate design load (37.2 kips)	Strain (με)	Deflection (in.)
Deck # 1 (single seam connection)	First Seam	80/ 377%	80 / 216%	3340	0.322
	Second Seam	92 / 433%	92 / 248%	3740	0.520
Deck# 2 (double seam with I-connector	First Seam	95 / 444%	95 / 254%	3460	0.323
	Second Seam	104 / 487%	104 / 279%	3600	0.519

Figure 2.22 An undamaged seam on the bottom of the deck and local damage at the load patch.

2.3.6 Summary of Stage III Testing

FRP samples with a scarfed edge were shown to have better performance than those having a butt joint (90°). The critical load and displacement (at crack initiation) increased as scarf angle decreased. But for FRP deck panels, sharper scarf angles (smaller than $^1/_2$ slop) are difficult to manufacture and can be easily damaged during transportation and installation. Therefore, scarf joints with an angle of 27° were used on future test specimens.

Testing indicates that both connection types exceeded service load without cracking. The load level corresponding to crack initiation in all the adhesive joints tested was at least 30% greater than the HL-93 design truck loads, which is specified in the AASHTO LRFD Bridge Design Specification (a service tire load of 16 kips with a dynamic load allowance of 33%, which yields a load of 21.3 kips). The measured strains near adhesively bonded joints at crack initiation are all above the service strain of 501 με discussed in Stage II testing.

The observed failure mode was not in the adhesive joints, but rather it was a localized failure of top plate and tube section (flange) at a very high load and strain level. Failure occurred at loads at least three times higher than the service load. There was no visible crack at any adhesive, suggesting that the adhesive joints are safe for the intended application.

No significant advantage or difference in behavior was found using double seam connection (using I-connectors) compared to single seam connection for the deck joints during testing. Since the double seam connection involved developing a new, special pultruded shape (I connector), the simpler single seam connection was used in the Stage IV study: a two-bay mock-up test of the Hawthorne St. Bridge.

Some recommendations can be made from this study: (1) quality control on the accuracy of panel dimensions of the mating parts has an impact on the ease of installation and quality of the adhesive panel-to-panel joints. Better manufacturing quality and tighter tolerances are believed to be crucial for improving the adhesively-bonded panel-to-panel joints; (2) a well-defined protocol should be developed to guide adhesive construction. It should quantitatively detail every step in the bonding process. The steps consist of surface preparation, adhesive lay-out pattern, amount of adhesive applied, and proper curing.

2.4 Stage IV:Full-scale Mock-up Test

2.4.1 Purpose and Scope

In order to evaluate the structural behavior and constructability of the proposed panel-to-panel connection, a 33 ft by 22 ft FRP deck supported by a two-bay mock-up of the Hawthorne St. Bridge superstructure was built in the Structures and Materials Laboratory at Virginia Tech. Following construction and testing of the two-bay mock-up the proposed deck system was installed in the Hawthorne St. Bridge. Conclusions and Recommendations resulting from the installation and a subsequent live load test (performed during May, 2007) are reported in Chapter 3.

The constructability and performance of an adhesively-bonded, panel-to-panel connection is reported herein. The objectives of part of the investigation were four-fold: (1) investigate connection behavior under simulated pseudo-static service load; (2) examine flexural strength and failure mode of connections and deck; (3) explore fatigue behavior during cyclic wheel loading and residual strength after fatigue loading; and (4) develop installation protocol of panel-to-panel connection in Hawthorne St. Bridge.

2.4.2 FRP Bridge Deck System

The FRP Deck System developed for the Hawthorne St. Bridge was based on previous research projects conducted at Virginia Tech, and was fabricated from standard EXTREN® structural shapes and plate manufactured by Strongwell Corp. of Bristol, VA. These components are made of E-glass roving and continuous strand mat embedded in polyester resin. The typical cross section of a deck panel is shown in Figure 2.23. The off-the-shelf components include: 6 in. x 6 in. x 3/8 in. pultruded EXTREN® tubes, 3/8 in. pultruded EXTREN® top and bottom plates as well as 1 in. diameter steel thru-rods. The tubes and top and bottom plate are adhesively bonded to form FRP bridge deck panels. The steel thru-rods are used to provide binding forces when the deck panels are curing. Bonding is accomplished in a vacuum bag to produce uniform pressure and continuous bonding.

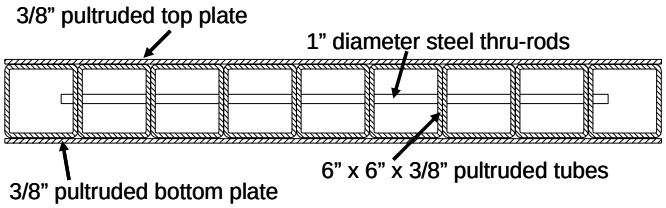

Figure 2.23 Cross section of the Strongwell FRP Deck System

The material properties of Strongwell's deck components are listed in Table 2.7 (tube and plates). The given material properties are taking from Extren Design Manual (Strongwell Inc. 2002), which are minimum ultimate coupon properties.

Table 2.7 Material Properties of Strongwell's Deck Components

Mechanical Properties	Top/Bottom Plate	Tube
Ultimate flexural stress, LW[1] (ksi)	30	30
Ultimate flexural stress, CW[2] (ksi)	18	10
Flexural modulus of elasticity, LW[1] (ksi)	2000	1595
Flexural modulus of elasticity, CW[2] (ksi)	1400	800
Estimated ultimate strain[3], LW[1] (με)	15000	18800
Estimated ultimate strain[3], CW[2] (με)	12800	12500

1: LW – lengthwise (longitudinal); 2 CW – crosswise (transverse);
3: Ultimate strain approximated by dividing the ultimate stress by the corresponding elastic moduli

Figure 2.24 shows a plan view of the deck panels, panel-to-panel connections, and supporting steel superstructure used in the two-bay mock-up. The FRP deck specimen consisted of five individual modular deck panels that were jointed together using three adhesive panel-to-panel connections (Seam #1 through #3) and one dowel joint. The dowel joint was developed as an expansion joint for future applications, and will not be discussed here. Each individual panel was 22 by 7.5 ft, with the exception of the two end panels which measured 22 by 5.5 ft, and 22 by 5 ft. These individual panels were connected to form a full width 22 ft panel that was about 33 ft long in the direction of traffic.

The FRP deck specimen was connected to stringers by deck-to-stringer connections; these connections were not intended to develop composite action. Neoprene rubber pads ($^1/_4$ in.

thick) were used to cover all contact areas between the deck panels and the steel superstructures.

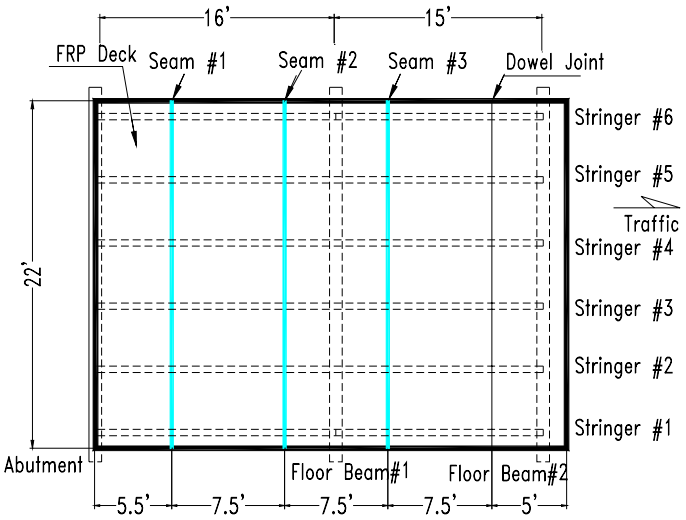

Figure 2.24 FRP deck panels and joints of the Hawthorne St. Bridge mock-up.

2.4.3 Construction of Adhesively-bonded Panel-to-panel Connections

The accuracy of panel dimensions of the mating parts has a significant impact on the ease of installation and quality of the adhesive panel-to-panel connections. Therefore, the first step was to dry-fit every panel-to-panel connection to ensure the best fit. Specifically, the scarfed edges should match and side walls of the tube bonding surface should match as well [Figure 2.25(a)]. The gap distance between two bonding surfaces should be controlled to less than 0.1 in. to ensure adhesive can fill the entire gap without voids.

During dry-fitting of three panel-to-panel connections, it was found that the sweep of the tubes was not well controlled during pultrusion. Figure 2.25(b) shows the curved panels resulting from the use of curved tubes. Each panel had a pre-existent sweep with a midway deflection of about 0.5 in. [Figure 2.25(c)]. The worst case was Seam #1 with two opposite curvatures at the side walls of the tube bonding surface. Although Seam #2 and #3 also had similar curvatures, mating tubes were bent in the same direction. The deck panels were autopsied after testing was completed to further investigate the bonding quality. Figure 2.25(d) shows that the gap distance between two bonding tube surfaces of Seam #1 was about 1 in. The

gap distances of Seam #2 and #3 were less than 0.1 in. and all scarfed edges matched well. Figure 2.25(e) shows the bonding quality of Seam #2.

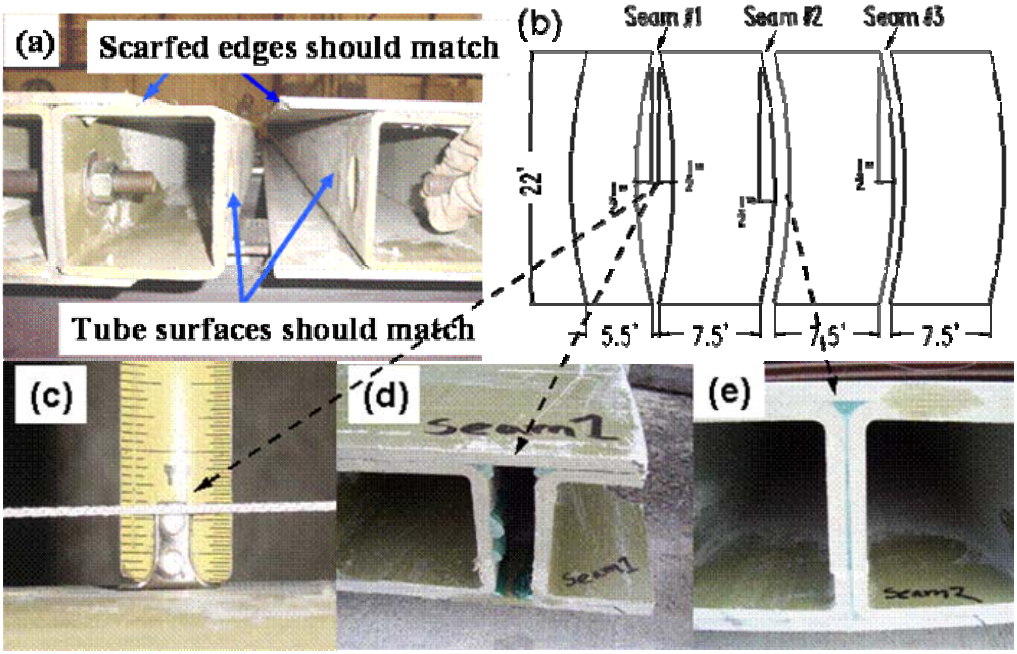

Figure 2.25 Fitting of the adhesively-bonded panel-to-panel connection.

Quality control procedures were adopted to prevent such out-of-straightness of panels. The manufacturer improved the panel quality by using stricter quality control procedures during pultrusion and bonding of tubes. The quality of the panels used in the actual bridge was much improved (described later in this report). The gap distance reported above for Seam #2 and Seam #3 were typical of what was seen in the field.

The fabrication protocol developed for construction of the adhesively-bonded panel-to-panel connections included:

(1) Sanding the bonding surfaces to remove the non-stick film remaining from pultrusion. This typically involved removing about 0.04 in (1 mm) from the top surface so that traces of fibers could be visible; then the surface looked dull instead of a polished greenish color.

(2) Bolting down the deck panel with the grooved end (the right side of the connection in Figure 2.25(a)) to the stringers with deck-to-stringer connectors.

(3) Flushing of all the bonding surfaces with acetone to remove any loose dirt that could hinder the bonding quality. Note that the surface must be allowed to dry before adhesive application.

(4) Trial application of adhesive on flat surface to make sure the correct mixing proportions of the adhesive.

(5) Appling structural urethane adhesive on the bonding surfaces with a special pneumatic gun from a bulk dispensing unit, shown in Figure 2.26(a). The adhesive layout pattern will be discussed later in this section.

(6) Aligning the tongue-end panel (the left side of the connection in Figure 2.25(a)) so that the tongue fits in the groove.

(7) Joining deck panels by equal jacking pressure from six hydraulic jacks with a manifold system, shown in Figure 2.26(b). Enough pressure must be applied to close the joint and ensure that adequate adhesive squeezes out.

(8) Maintaining the jack pressure for about 12 hours, until the adhesive cures.

(9) Bolting down the deck panel to the stringers with deck-to-stringer connectors.

(10) Going through steps (3) through (9) for another adhesive connection.

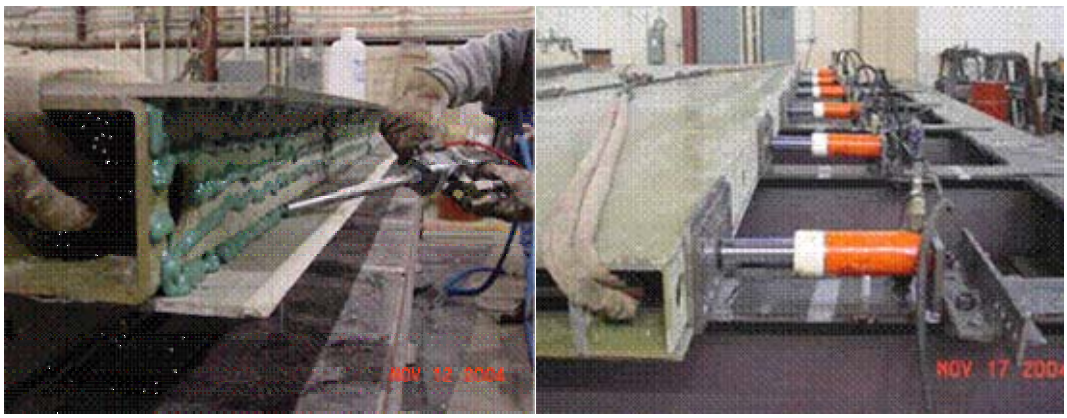

(a) Adhesive application (b) Jacking system

Figure 2.26 Adhesive construction for panel-to-panel connection.

The performance of adhesive bonding is not only dependent on the matching condition of mating parts, surface preparation, and joint geometry as discussed above, but also the amount of adhesive applied. Adequate adhesive squeeze out is a sign that adequate

adhesive was applied and is recommended as the quality control check-point in field construction. Increasing amounts of adhesive were applied to the three seams in order to compare performance of seams with different amounts of adhesive (Seam #3 had the most and Seam #1 had the least). Seam #3 was thought to be the best joint with the best fit and sufficient adhesive squeeze out. Figure 2.27 shows Seam #3 after adhesive was applied and adequate adhesive squeezed out from the top, side and bottom of the joint. Although Seams #1 and #2 performed well during static tests (discussed in a later section), the amount of adhesive used for Seam #3 was selected as enough to ensure adequate strength and life of the panel-to-panel connection.

(a) Side view (b) Bottom view

Figure 2.27 Adhesive squeezing out from joints during adhesive construction.

The Pliogrip 8000/6660 two-component, structural urethane adhesive system from Ashland Chemicals Inc. was used in this application for its superior adhesion property, UV resistance and proper glass transition temperature. Figure 2.28 shows how the adhesive beads were applied on the tongue and groove parts. Each bead had a width of between 0.4 to 0.6 in. and a thickness of between $^{1}/_{4}$ to $^{1}/_{2}$ in. One bead of adhesive was applied on each scarfed edge. The amount of adhesive applied per connection was about 3.8 gallons of Pliogrip 8000 and 1.7 gallons of Pliogrip 6660.

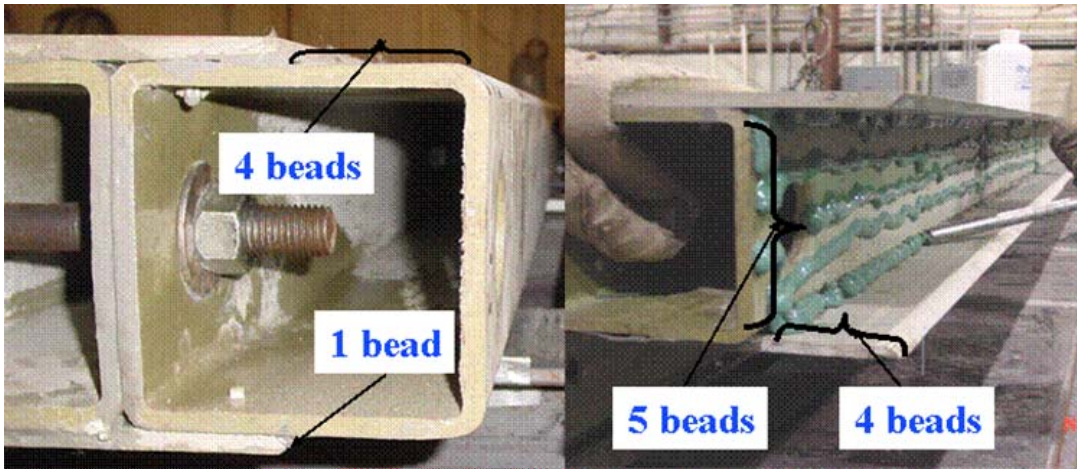

(a)Adhesive on tongue part (b) Adhesive on groove part

Figure 2.28 Adhesive layout pattern.

The available working time for the adhesive is 45 minutes at 73°F and 35 minutes at 99°F (Ashland 2003). Application of adhesive and joining of deck panels took approximately 25 minutes and was performed at an ambient temperature of 75°F.

2.4.4 TEST SETUP AND INSTRUMENTATION

2.4.4.1 Test Setup

The steel frame mock-up of the Hawthorne St. Bridge superstructure consisted of two bays, which were 16 ft and 15 ft in length in the direction of traffic. Figure 2.29(a) and (b) shows a framing plan and an overview of the steel superstructure. Each bay had six wide-flange W14x34 stringers, having a transverse spacing of 4 ft on-center. Diaphragm members, consisting of C10x15.3 steel sections, were bolted to connector plates, which were in turn welded to the stringers. Two W14x120 floor beams were supported by four pedestals that simulated the hangers in the through-truss bridge. All steel member sizes and dimensions mimic the actual ones in the Hawthorne St. Bridge superstructure. Neoprene pads were used between floor beams and pedestals to avoid direct contact of steel and to allow some movement at floor beam ends. Stringers and floor beams were joined together using moment resisting connections. Figure 2.29(c) shows the detail of the abutment side. A W21x132 beam

was used to simulate the concrete abutment in situ, and five end diaphragms (C10x30) were flush with the top stringer to avoid free edge bending of the FRP deck. All stringers at the abutment rested on the bearings anchored to the abutment.

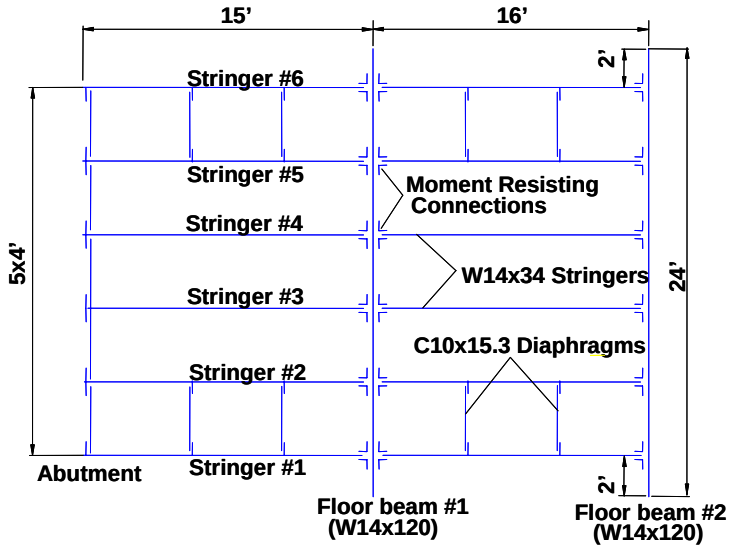

(a) Framing plan of the steel superstructure

(b) Assembly of the steel superstructure

(c) Abutment detail

Figure 2.29 Steel superstructure of the Hawthorne St. Bridge mock-up.

Although the rehabilitated bridge will still be posted to 20 tons, a higher load level (HL-93 design truck loads as specified in AASHTO LRFD Bridge Design Specifications) was used for evaluating the performance of the adhesive panel-to-panel connections. The purpose was to gain some insight into the applicability of this deck system to the typical highway

bridge deck which is designed for the HL-93 design truck. This yields a service tire load of 16 kips with a dynamic load allowance of 33%, which yields a load of 21.3 kips. Therefore, a load limit of 22 kips was chosen because it was slightly higher than the required 21.3 kips.

Five Load Cases used for service load tests are shown in Figure 2.30. These service load cases were used throughout the laboratory mock-up test, not only for the performance of the panel-to-panel connections but also for the global structural performance of the FRP-deck-on-steel-superstructure system as discussed in Chapter 3. All Load Cases followed HL-93 truck weights and dimensions to apply the worst-case load scenario to the FRP deck and superstructure. Load Cases 1 to 4 were single truck cases. Load Cases 1, 2 and 4 were the critical cases for flexure of the FRP deck transverse to the traffic, with a wheel located at mid-span between two stringers. Load Case 3 represented a truck straddling Stringer 3. Load Case 5 is the symmetric case, with double trucks representing the full lane Load Case. Since no instrumentation was installed between Stringer #3 and #4, and Stringer #4 and #5 (shown in Figure 2.38), only Load Case 1, 4, and 5 were used to evaluate the three adhesively bonded panel-to-panel connections since each of these case had one wheel located at mid-span of two stringers. Load Case 1 to 5 were used to investigate the global behavior of the supporting steel superstructure and are discussed in detail in Chapter 3. In the traffic direction, the loading patches with 22 kips load were centered over on the connections.

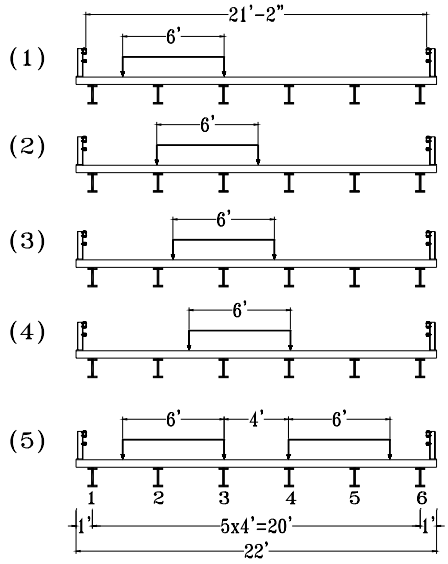

Figure 2.30 Load Cases for service load test.

For single truck cases (cases 1 to 4), a 200-kip hydraulic actuator was used to apply load. An 8 ft long, 22 in. tall spreader beam (I-shaped) was utilized to apply the load at mid-span. The double truck service load test (case 5) was simulated by two single-truck setups, as shown in Figure 2.31. Load was transferred to the FRP deck by the two spreader beams and four special tire patches [Figure 2.32]. The tire patch consisted of a quarter tires internally reinforced with silicone rubber and used to mimic the cushioning effect of a pneumatic tire. This was done to minimize the local stress concentrations of a standard rectangular steel patch because of the relative local flexibility of the FRP composite cellular decks, as compared to the steel plate (Zhou et al. 2005). In service load test, each truck wheel was simulated by one tire patch due to limited tire patches available.

Figure 2.31 Experimental Setup for service load test (Load Case 5) on Seam #3

Figure 2.32 Special tire patches used to mimic the cushioning effect of a pneumatic tire

A number of strength and fatigue tests were performed on the adhesively bonded panel-to-panel connections and on the FRP deck, as shown in Figure 2.33. Two strength tests were conducted on the panel-to-panel connections (at mid-span between Stringers #4 and #5 on Seams #2 and #3). The strength tests did not use a spreader beam to distribute load as in the service load test, the load was applied in two tire patches to the deck between two adjacent stringers using the hydraulic actuator(as shown in Figure 2.34). Two tire patches were used to better simulate a truck wheel, which was different from the service load test. A number of steel plates were inserted in between the loading ram and the tire patches to ensure a nearly uniform distribution of load from the actuator to the two tire patches.

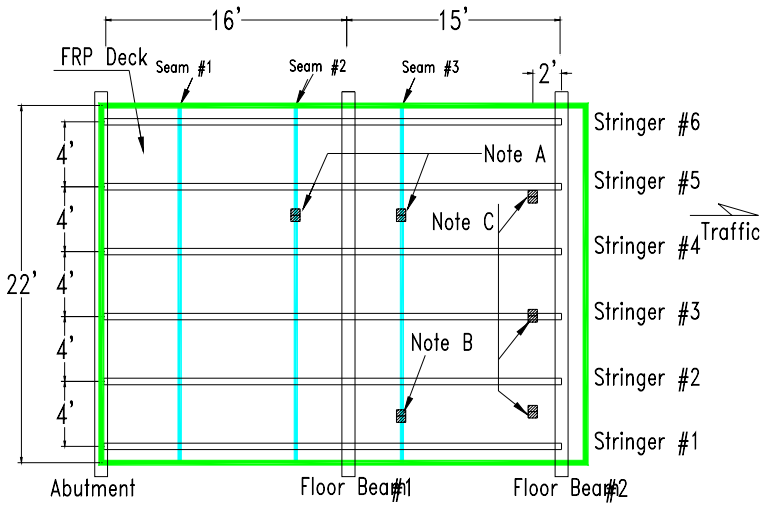

Figure 2.33 Strength and fatigue tests locations

Figure 2.34 Experimental setup for strength tests

Strength tests were also conducted on as-received (continuous) deck at a location 20 in. away from Floor Beam #2 (shown in Figure 2.33). This created a benchmark for evaluating the strength and failure mode at adhesively-bonded panel-to-panel connections. Figure 2.35 shows three different Load Cases. These cases were designed to study which one is the worst case and what is the corresponding failure mode. Load Case A was the critical case for flexure of the FRP deck transverse to traffic, with a pair of tire patches located at mid-span between Stringers #1 and #2. Load Case B is a pair of tire patches straddling Stringer #3, which is the critical case for compression. Load Case C is a pair of tire patches sitting just at the edge of Stringer #5, which is the critical case for punching shear. The same setup (Figure 2.36) and procedure as strength tests on the panel-to-panel connections were used. A pair of tire patches were used to simulate one wheel load.

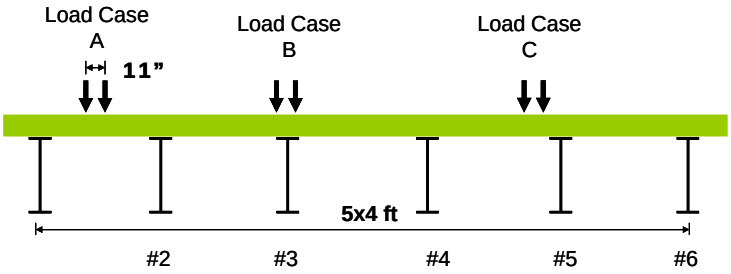

Figure 2.35 Load Cases for strength tests on as-received deck.

Figure 2.36 Experimental Setup for strength tests on as-received deck

One fatigue test was performed at mid-span between Stringers #1 and #2 on Seam #3 (shown in Figure 2.33). For fatigue tests, load was applied using a servo-controlled hydraulic actuator mounted on the same load frame (shown in Figure 2.37). Because of concern about stability of the actuator and load patch assembly, a neoprene rubber patch was used instead of a tire patch to transfer load from the actuator to the top surface of the deck on top of the adhesive joint. The neoprene rubber pad can also prevent the steel plate connected to the actuator from locally damaging the deck and joint during testing. The base neoprene rubber pad was 18 in. by 9 in. and. The base neoprene rubber pad is a little smaller than the “tire contact area” of 20 in. by 10 in. defined in AASHTO LRFD Specifications (2004). The fatigue test was followed by a residual strength test at the same location.

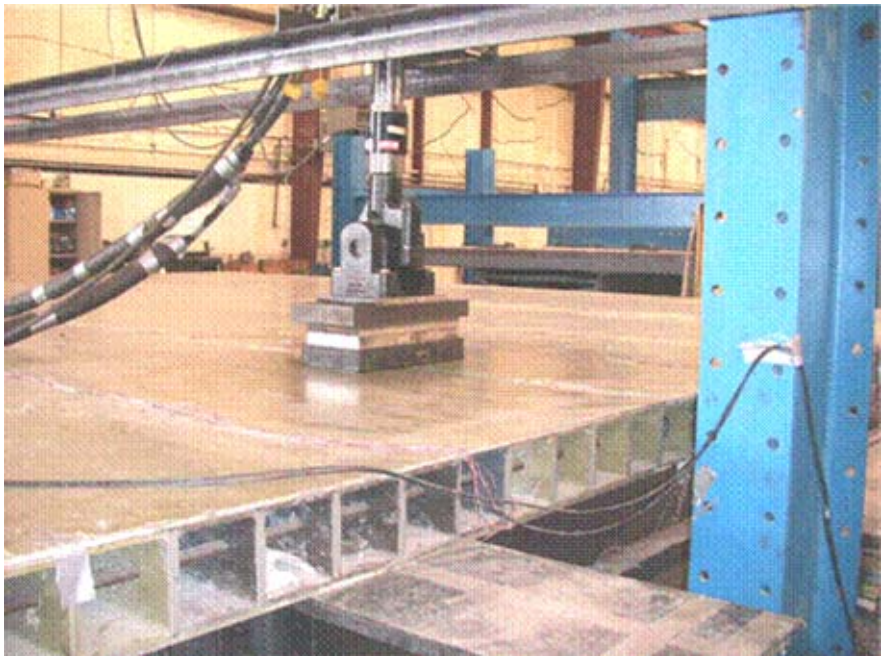

Figure 2.37 Experimental setup for fatigue test.

2.4.4.2 Instrumentation

The schematic of the instrumentation plan used to investigate the performance of adhesively-bonded joints is shown in Figure 2.38. The stringers and floor-beams are referred to as “Stringer #1” through “Stringer #6” and “Floor Beam #1” and “Floor Beam #2.” For consistency throughout the discussion, all references to “longitudinal” and “transverse” are given with respect to the bridge deck orientation; thus, “longitudinal” implies parallel to the pultruded tube direction of the FRP deck system, and the “transverse” direction refers to the traffic flow direction (perpendicular to the tube axis).

As shown in Figure 2.38, at the bottom surface of the deck, two strain gauges (Measurement Group CEA-06-375UW-350) and two wire pots (displacement transducers) were used to measure transverse strains and displacements, respectively, at both sides of the joint. Another strain gauge was placed to measure longitudinal strain at the side of the adhesive joint adjacent to the load. A specially-designed crack detection gauge [shown in Figure 2.38] was installed across each joint to monitor crack opening, if any. This instrumentation pattern was repeated for each loading location while testing near a joint. Three strain gauges were mounted on top of the deck, close to the seam and right on top of Stringers 1–3, to measure the

longitudinal strains in the negative moment region, as shown in Figure 2.38. Load, deflection, and strain were continuously recorded during testing using a high-speed data acquisition system.

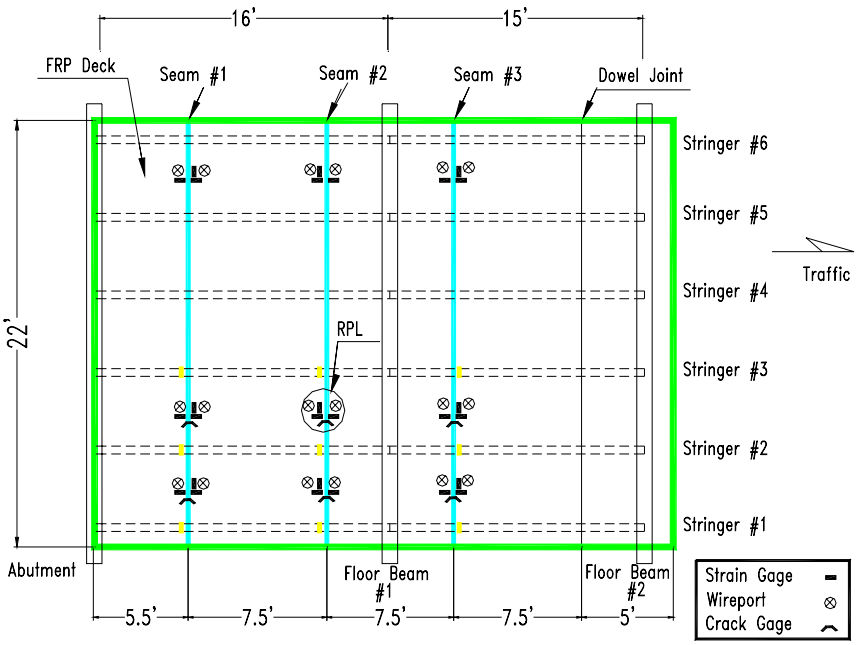

Figure 2.38 Instrumentation for three adhesively-bonded panel-to-panel connections

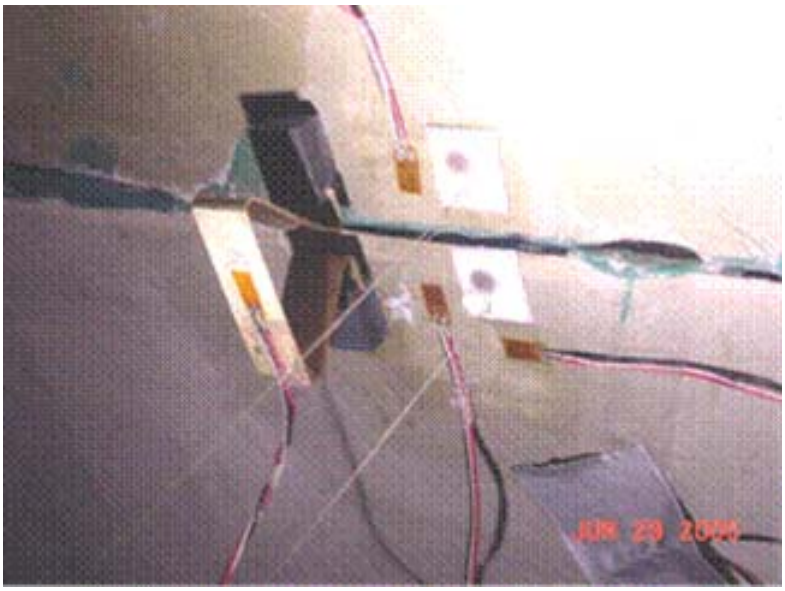

Figure 2.39 Instrumentations at one adhesive joint below the deck.

For strength tests on as-received deck, two strain gauges were mounted to the bottom side of the FRP deck, mid-way between Stringers #1 and #2, as indicated in Figure 2.40. Gauges were oriented in both the longitudinal and transverse directions to measure flexure strains from Load Case A. Five wire pots were used to measure the vertical deflection of the FRP deck at critical locations. One was located mid-way between Stringers #1 and #2, and two were applied at the bottom of the FRP deck near two tips of the top flanges of Stringers #3 and #4. Six wire pots were mounted to the bottom face of the bottom flange of the six stringers to measure the overall stringer deflections.

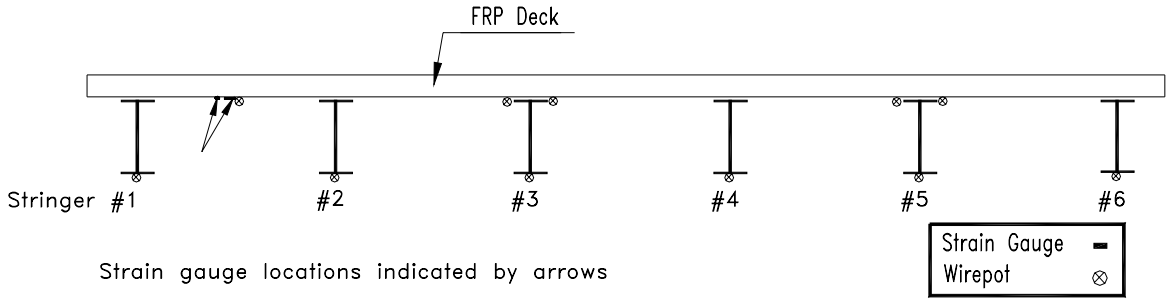

Figure 2.40 Location of instrumentation for failure tests on as-received deck

2.4.5 Results and Discussion

2.4.5.1 Service Load Test

The purpose of these tests was to observe the behavior and assess the serviceability and performance of the adhesively-bonded, panel-to-panel joint up to a wheel load of 22 kips (a 44 kips axle load).

The representative longitudinal and transverse strain, span deflection and crack gauge responses at one location, location RPL (representative plot location, shown in Figure 2.38) for Seam #2 under Load Case 4 are shown in Figure 2.41. The load vs. strain and load vs. deflection behaviors were observed to be linear elastic up to the design service load. The overall deflection at the mid-span of the deck was 0.343 in., as shown in Figure 2.41(a), and the relative deflection at this point with respect to supporting stringers was 0.074 in. at the design service load, which indicated an L/649 response. The proposed FRP deck system is thought to provide acceptable span/deflection ratios and details will be discussed in Chapter 4.

At location RPL under Load Case 4, the longitudinal strain on the bottom plate right under the load patch was 1090 με (Figure 2.41 (b)), which is only 6% of the estimated ultimate strain of the bottom plate (Table 2.7). The strain gauge on the top plate of the deck over Stringer # 3 was in tension (130 με) as shown in Figure 2.41(c), indicating that this gauge was in the negative moment region of the continuously-supported deck. Transverse strain at the side of the seam closest to the loading patch was 490 με (Figure 2.41(d)) at the design service load, which was about 45% of the longitudinal strain at this load. However, transverse strain at the other side of the seam was -290 με (Figure 2.41 (e)) at the design service load, which was in compression; this indicated that this region experienced double curvature due to an applied load at one side of the seam. This finding is also further confirmed in the field test (reported in Section 3.3.3.4.3). The linear response of crack gauge indicates that no crack was initiated up to design service load, as shown in Figure 2.41 (f).

For all loading cases, deflection and longitudinal strain were reasonably consistent (Table 2.8). This consistency of measured responses from both continuous deck sections and adhesive joints indicated no crack initiation inside the adhesively-bonded, panel-to-panel connections. However, transverse strains were found to be sensitive to the exact location of both the gauge and the applied loads, and were more difficult to interpret (see Table 2.8). This is due to the fact that the cellular deck experiences double curvature when a load moving across the instrumented area, which also agrees with published findings (Coogler et al. 2005; Turner et al. 2004; Wan et al. 2005). Due to their variability, such measurements are less suitable for performance assessment and will not be used in strength and fatigue performance evaluation.

All the adhesive connections were able to resist the service tire patch load without any indication of cracking. Table 2.8 summarizes data of service load tests performed on Seams #1 to #3. In each of these tests, Load Cases 1, 4 and 5 were followed.

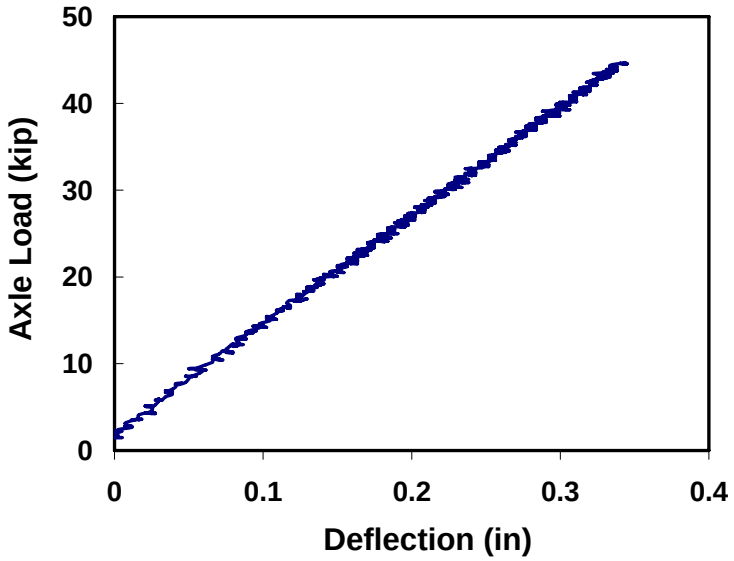

(a) Load vs. deck overall deflection

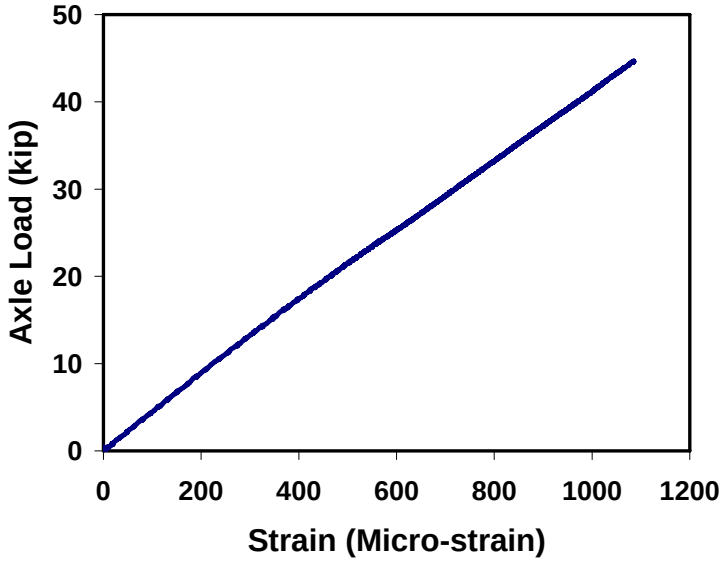

(b) Longitudinal strain (at the bottom plate right under the load patch) vs. load

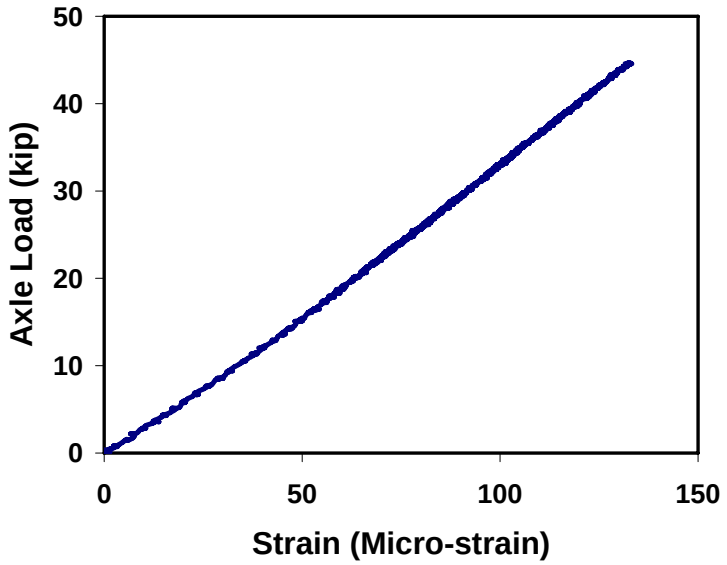

(c) Longitudinal strain (on top of the deck over Stringer #3) vs. load

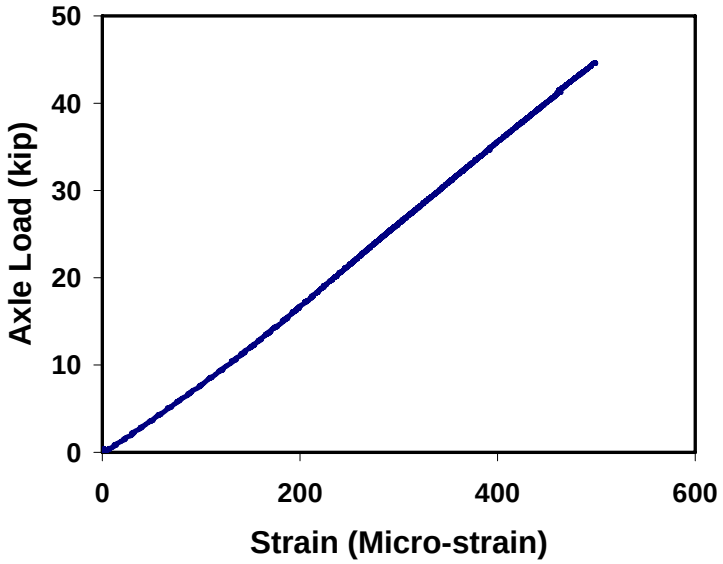

(d) Transverse strain (close to the loading patch) vs. load

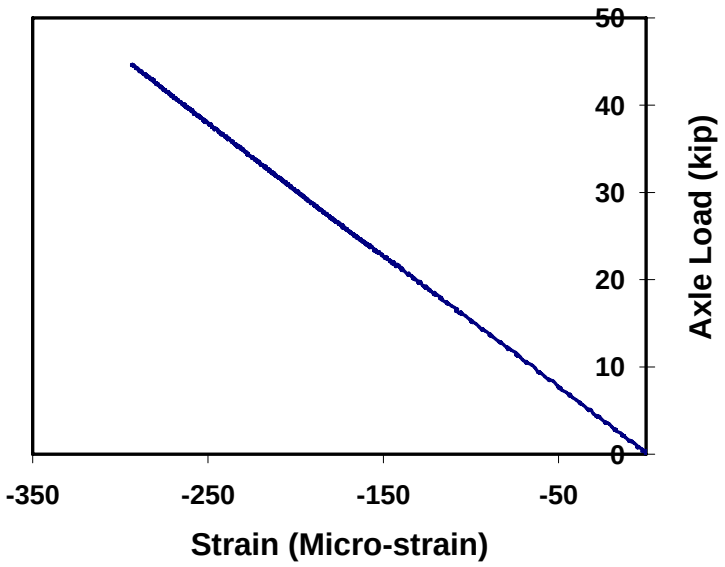

(e) Transverse strain (away from the loading patch) vs. load

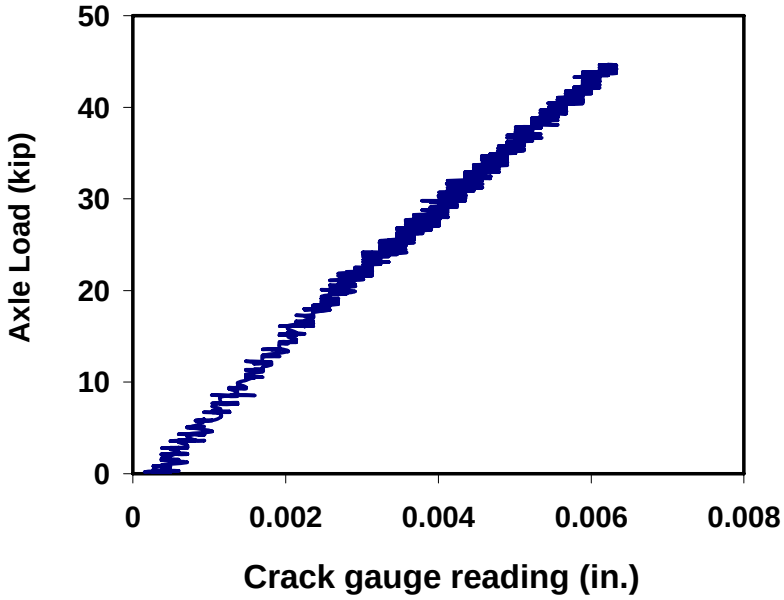

(f) Load vs. crack gauge reading

Figure 2.41 Representative plots in service load tests

Table 2.8 Data from Service Load Tests

	Load case	Maximum longitudinal strain (με)	Transverse Strain (close to loading) (με)	Transverse Strain (away from loading) (με)	Mid-span deflection Overall/relative[1] (in)	Deflection index (span length/relative deflection)
Seam #1	1	839	-205	-516	0.275 / 0.081	596
	4	549	-171	-450	0.246 / 0.089	537
	5	852	-204	-505	0.234 / 0.061	785
Seam #2	1	804	210	-130	0.280 / 0.067	714
	4	1085	490	-290	0.343 / 0.074	649
	5	802	588	-190	0.347 / 0.071	679
Seam #3	1	680	150	-591	0.266 / 0.082	583
	4	535	167	-635	0.318 / 0.062	770
	5	688	130	-577	0.370 / 0.072	663
Average		759	128	-431	0.297 / 0.073	664

Note: 1. Relative deflection is defined as deck deflections under the tire patches with respect to the supporting stringers.

2.4.5.2 Strength test on the as-received deck

Three strength tests were conducted to evaluate the overall safety factors of the as-received deck and to investigate the failure mode and failure load at different locations. This also created a benchmark for evaluating the strength and failure mode at adhesively-bonded panel-to-panel connections. All testing data from strength tests on the as-received deck are included in Table 2.9. Test results show that Case A (flexure of the FRP deck transverse to traffic) is the critical case, Other Load Cases had larger safety factors, calculated as failure load at crack initiation divided by the design service load of 21.3 kips (HL-93 design truck loads as discussed earlier). The results from Case A will be discussed below, which was the critical case with the lowest failure load at crack initiation.

Figure 2.42(a) shows mid-span deflection versus load and Figure 2.42(b) shows load versus mid-span maximum strain (which is always longitudinal strain) in this strength test. During the loading up to 94 kips, both the deflection and strain data indicate fairly linear and consistent response. The local deformation on top of the deck near the tire patch could be easily perceived by visual inspection because of high compressive strain levels in the contact area. Slight cracking noises were first heard at about 94 kips; load, strain and deflection drops could also be observed at this load (Figure 2.42), which will be referred to as the “crack

initiation" load. Then the deck was continuously loaded up to 96 kips, with increasing cracking sounds. Because visible cracks on the top plate of the deck could be easily observed at the load of 96 kips, the deck was unloaded and two rubber patches were removed to inspect the failure mode. After the load was removed, the deck went back to almost its initial position. No further cycles were performed because of significant failure in the top plate and the tops of the tubes.

Other cases (B and C) followed the same procedures and had higher loads at crack initiation compared to Case A. Therefore, other cases do not control and will not be discussed in detail here. Table 2.9 summarizes data of three strength tests. A complete presentation of test results of all cases at crack initiation is given in Appendix B.1. Note that the safety factor is calculated as the failure load at crack initiation divided by the design service load (21.3 kips); For case A, deck relative deflection is defined as deck deflections under the tire patches with respect to the supporting stringers. For case B and C, deck relative deflection is defined as the average deck deflection at two sides of the stringer with respect to the stringer under loading patch. The failure modes of these strength tests will be discussed in section 2.4.5.5.

Table 2.9 Strength Tests on As-Received Deck

Load case	Load at crack initiation (kips)	Maximum longitudinal strain at bottom surface of deck (με)	Deck relative deflection (in.)	Safety factor
A	94	3950	0.515	4.4
B	148	N/A	0.222	6.9
C	158	N/A	0.517	7.4

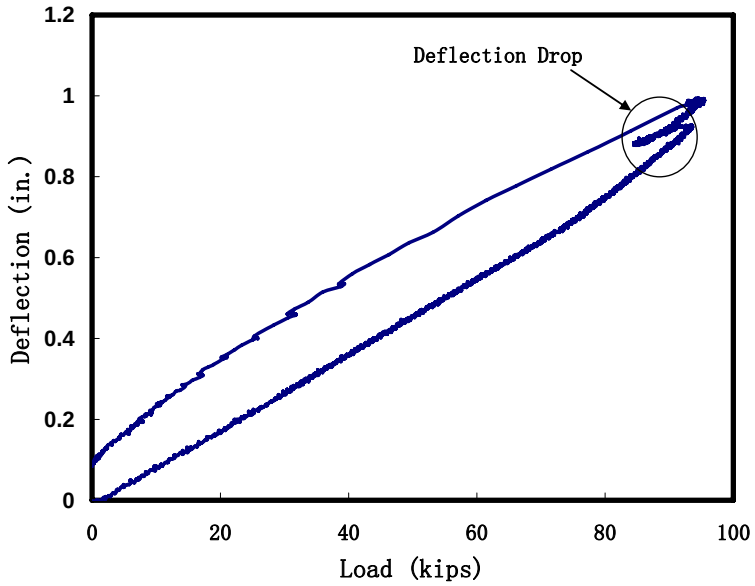

(a) Load versus mid-span deflection

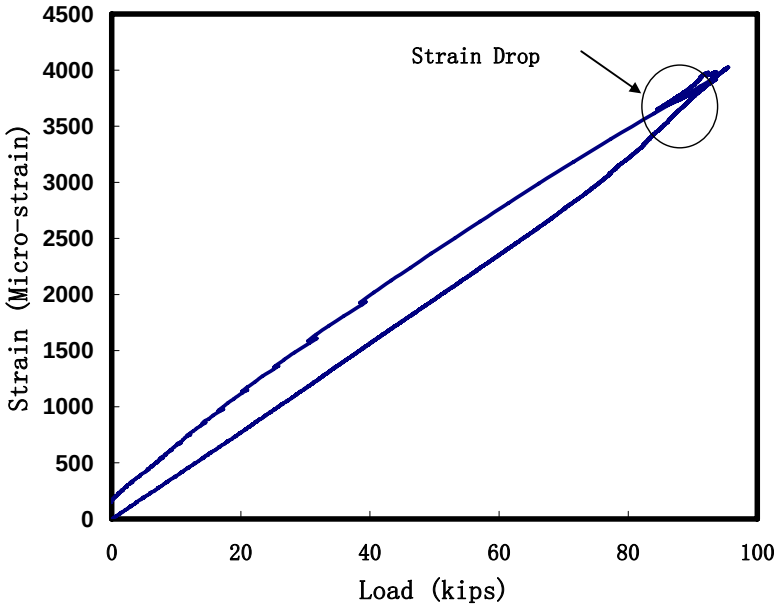

(b) Load versus mid-span longitudinal strain

Figure 2.42 Mid-span longitudinal strain and deflection versus load in as-received deck strength test at mid-span between Stringer #1 and #2

2.4.5.3 Strength Test on the panel-to-panel connections

Two strength tests were conducted at mid-span between Stringers #4 and #5 on Seams #2 and #3. These tests were designed to evaluate the quality of the adhesive joints and investigate the failure mode. The strength test included several static load cycles of increasing intensity. Load was increased at 25 kips increments until failure was detected. The results from the last one of these cycles in the strength test at mid-span between Stringers #4 and #5 on Seam #2 will be discussed below.

Load versus mid-span deflection and load versus mid-span maximum strain (which is always longitudinal strain) during the last load cycles are shown in Figure 2.43. In order of progression, the load cycle up to 75 kips preceded the load cycle up to 100 kips. For the cycle up to 100 kips, both the deflection and strain data indicate fairly linear and consistent response. The local deformation on top of the deck near the tire patch could be easily perceived by visual inspection because of high compressive strain levels in the contact area. Slight cracking noises were first heard at about 93 kips; small strain and deflection drops could also be observed at this load, which will be referred to as the "crack initiation" load. Then the deck was continuously loaded up to 96 kips, with increasing cracking sounds. Because visible cracks on the top plate of the deck could be easily observed at the load of 96 kips, the deck was unloaded and two rubber patches were removed to inspect the failure mode. No further cycles were performed because of significant failure in the top plate and the tops of the tubes.

The average first failure load for the two joints (Table 2.10) was 100 kips, which is close to the first failure load of the critical case A found in the strength test of the as-received deck (Table 2.9). This indicates the adhesive joint will not influence the strength of the deck. A complete presentation of test results at crack initiation is given in Appendix B.2. The failure modes of these two strength tests are discussed in section 2.4.5.5.

Table 2.10 Strength Tests Results on the panel-to-panel connections

Location	Load at initiation of crack (kips)	Mid-span relative deflection (in.)	Safety Factor
Seam #2	93	0.441	4.4
Seam #3	107	0.457	5.0
Average	100	0.449	4.7

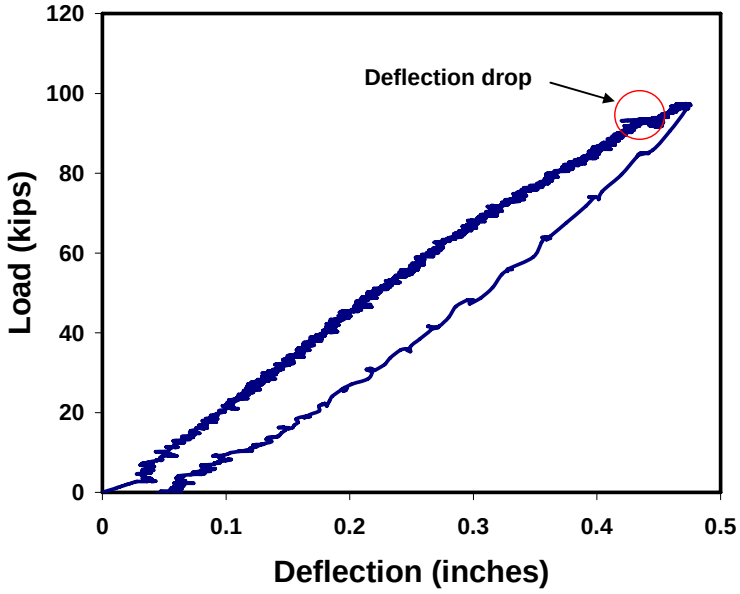

(a) Load versus mid-span deflection

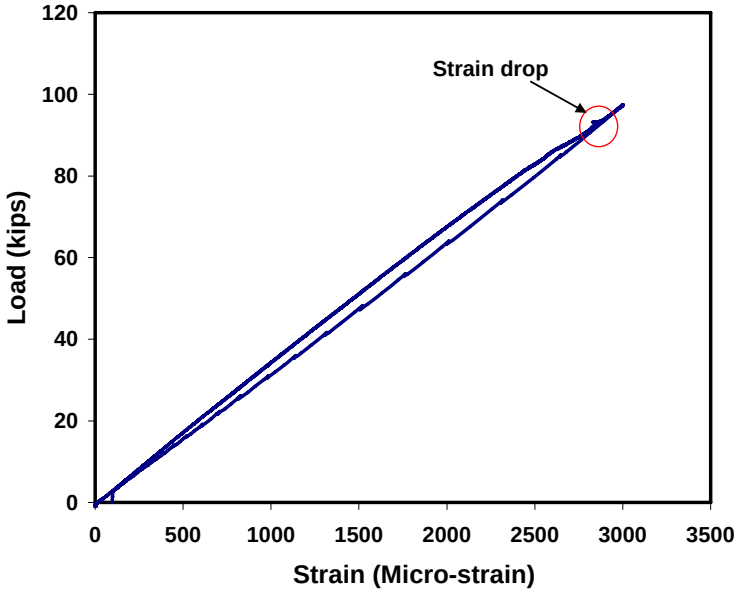

(b) Load versus mid-span longitudinal strain

Figure 2.43 Mid-span longitudinal strain and deflection versus load in strength test performed at mid-span between Stringer #4 and #5 on Seam #2.

2.4.5.4 Fatigue Performance and Residual Strength

At mid-span between Stringers #1 and #2 on Seam #3, the deck was subjected to fatigue loading for 3,000,000 cycles, then tested to failure under a static loading. It should be note that the number of cycles (3 million) is not indicative of the service life of the Hawthorne Street Bridge. This bridge will be still posted to 20 tons after rehabilitation; therefore, no heavy vehicles such as HS-93 design trucks will legally cross the bridge during the bridge's service life. Three million cycles are chosen because this number is well excess the service life of the Hawthorne Street Bridge and also fits within the available time and resources to complete the test.

The fatigue test was conducted in load control at a minimum/maximum load ratio of R=0.1, with a maximum load of 22 kips and a minimum load of 2 kips. The deck cycled through a maximum overall deflection range of about 0.19 in. at the load point and through a maximum bottom plate longitudinal strain (along the tube direction) of about 600 με underneath the loading patch. These two values are a little smaller than the average overall deflection of 0.297 in. and average maximum longitudinal strain of 759 με in service load tests on the seams (Table 2.8). This is understandable since the neoprene rubber pad (18 in. by 9 in.) used in the fatigue test has larger contact area than the tire patch (9 in. by 9 in.) used in the service load tests on the joints. The fatigue cycles were interrupted periodically for static service load tests, and the deck panel was inspected for signs of deterioration at this time as well.

The maximum deflection and strain measurements at the service load (22 kips) taken during each static test can be seen in Figure 2.44(a) and (b), respectively. The results from maximum deflection and strain measurements taken during the static tests after 1,100,000, 2,000,000, and 3,000,000 cycles are shown in Figure 2.45(a) and Figure 2.45(b), respectively. The deflection and strain responses remained fairly constant for all of the static service load tests, and the deck demonstrated no apparent loss in stiffness near the adhesive joint.

Figure 2.46(a) shows the crack gauge measurements taken during the static test after 3,000,000 cycles. It behaved linearly and showed no crack was initiated after 3,000,000 cycles. Figure 2.46(b) shows the deflection measurements at two sides of the adhesive joints taken during the static test after 3,000,000 cycles. Similar deflections at two sides of the adhesive joints also demonstrated that no crack was initiated inside the joint.

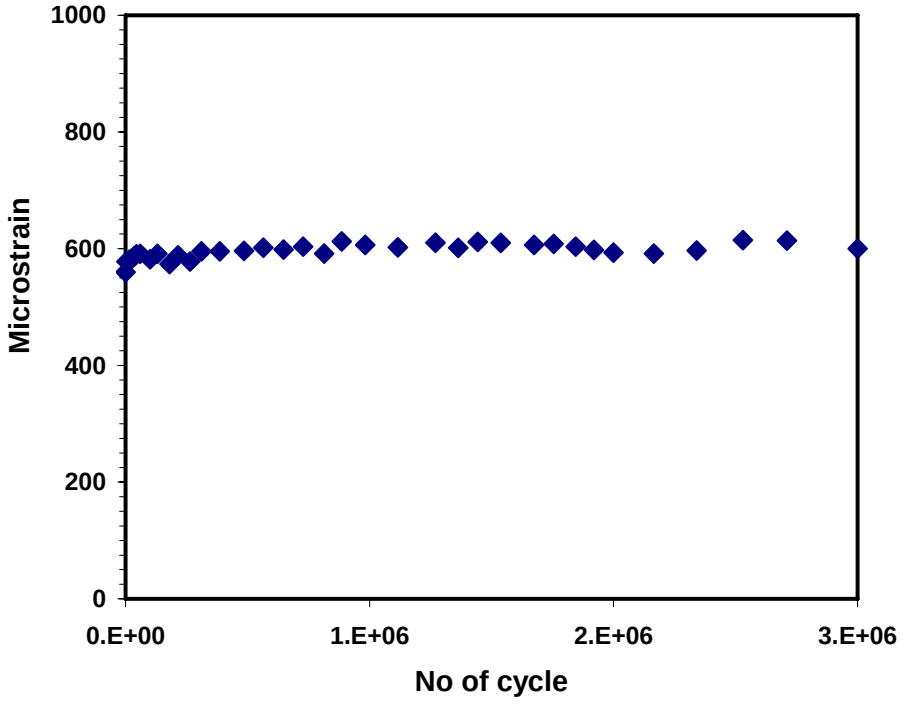

(a) Strain

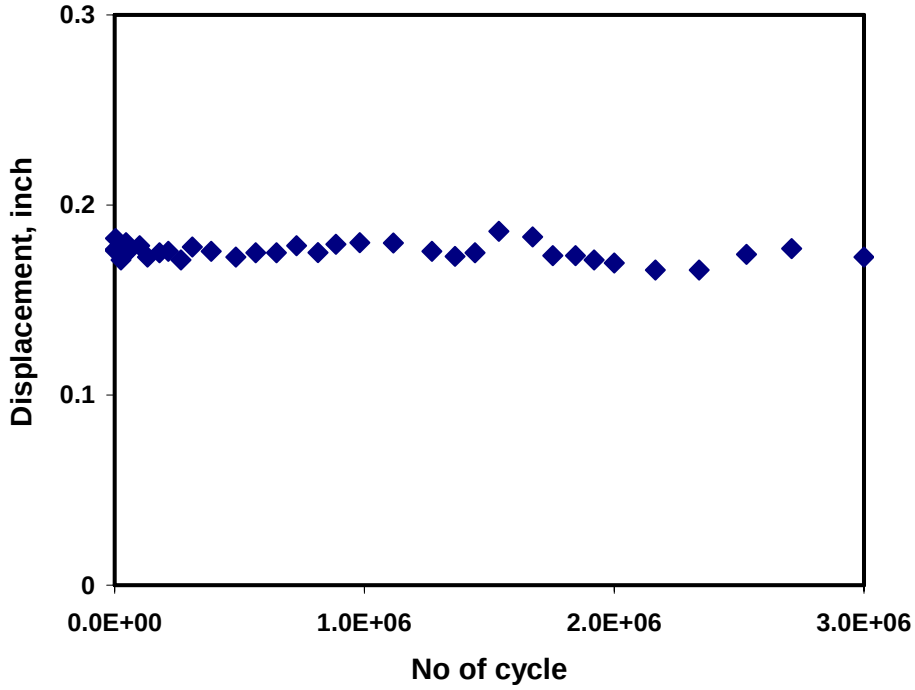

(b) Deflection

Figure 2.44 Maximum strain and deflection at service load after interrupted fatigue loading.

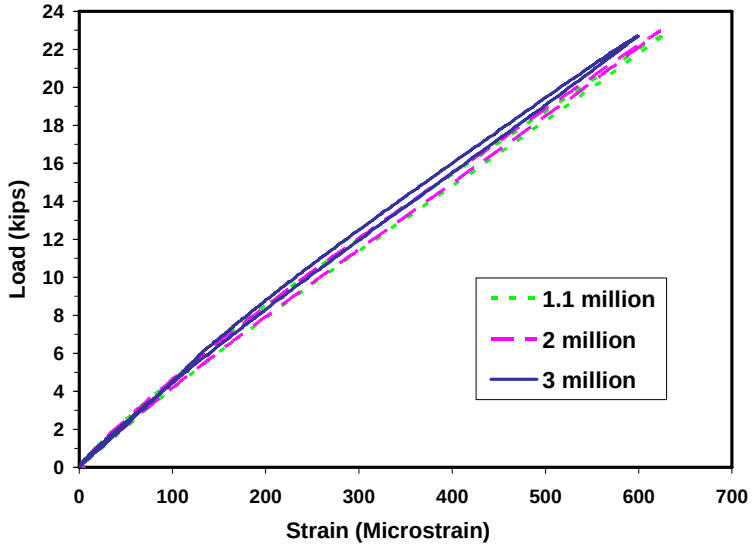

(a) Load vs. strain

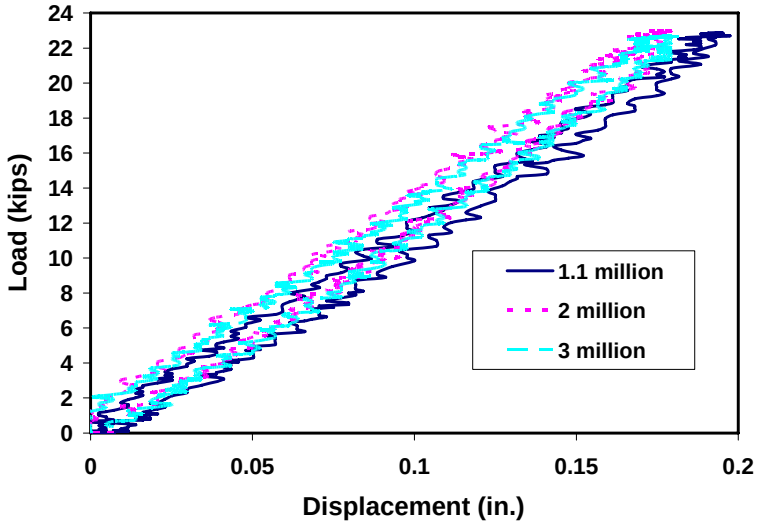

(b) Load vs. deflection

Figure 2.45 Deck load vs. strain and deflection from interrupted fatigue cycling.

Inspection of the deck at the time of each static service load test also revealed no visible signs of damage to the plate or adhesive bonding due to fatigue loading. In addition, a careful inspection the area of deck-to-stringer connections near loading patch was conducted after 3,000,000 cycles, and no damage to the deck panel and no slack in the connection were observed.

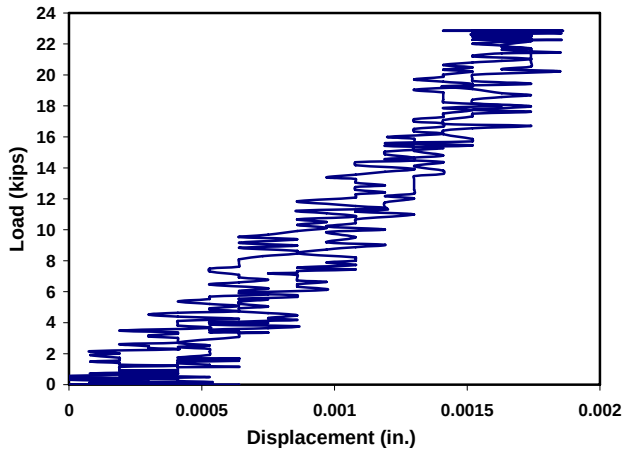

(a) Load vs. crack gauge reading

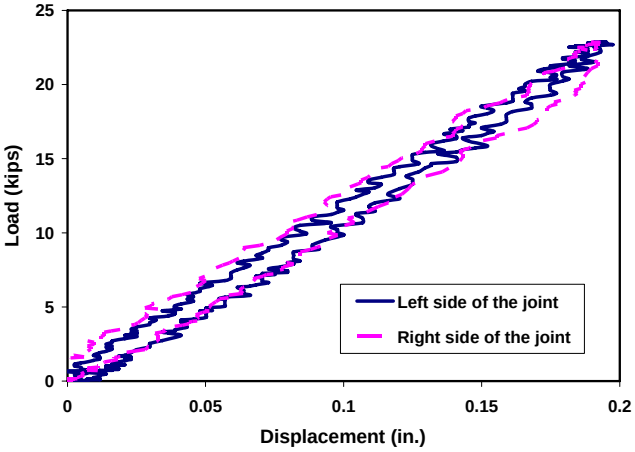

(b) Load vs. deflection at two sides of the adhesive joint

Figure 2.46 Crack gauge and deflection results after 3,000,000 cycles

The fatigue test was followed by a residual strength test at the same location. Figure 2.47(a) shows the load versus deflection plot and Figure 2.47(b) shows the load versus crack gauge plot. Both responses showed fairly linear-elastic behavior up to the crack initiation of the adhesive joint after 3,000,000 fatigue cycles. The first failure (crack initiation in the joint) occurred at 94 kips. At the crack initiation point, both plots showed a significant drop due to stiffness loss caused by cracking in the adhesive joint. Figure 2.47(b) also shows a clear crack propagation stage after crack initiation. Data from all strength tests are summarized in Table 2.11. The critical loads at initiation of crack after fatigue and without fatigue shown in Table

2.11 indicate no significant loss in strength after fatigue. The critical loads for adhesively bonded joints after fatigue and without fatigue are close to the first failure load of the critical case A found in strength test of as-received deck. This indicates the adhesive joint will not influence the strength of the deck.

The residual strength mode of failure observed on the fatigued seam is typical of those observed in the two strength tests discussed above. This observation, when combined with the observed retention of stiffness after fatigue loading, demonstrates the good durability of the adhesive joint under repetitive loadings.

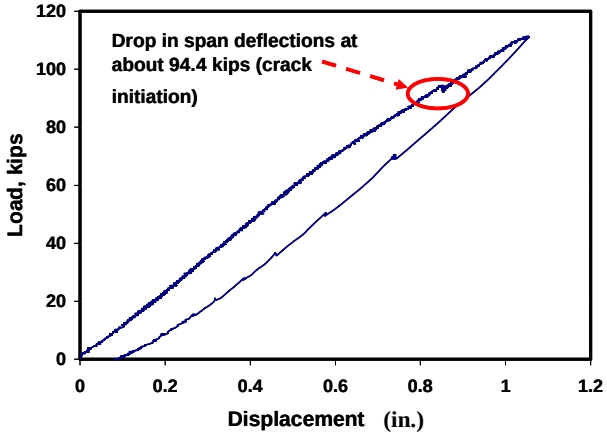

(a) Load versus deflection

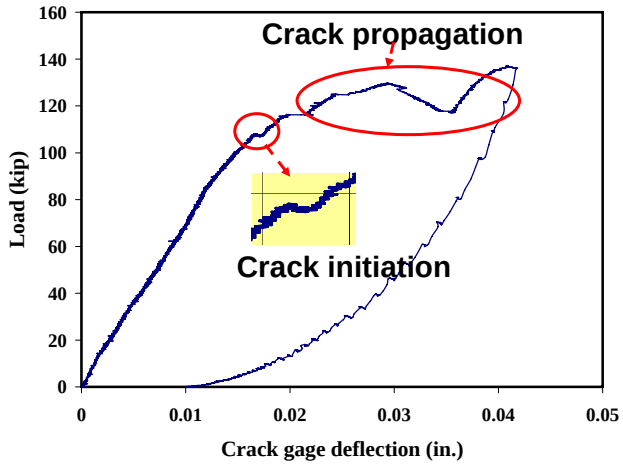

(b) Load versus crack gauge reading

Figure 2.47 Crack gauge and deck deflection results in residual strength test after 3,000,000 cycles

Table 2.11 Strength Tests Results

Location		Load at initiation of crack (kips)	Mid-span relative deflection (in.)	Safety factor
Without fatigue	Seam #2	93	0.441	4.4
	Seam #3	107	0.457	5.0
As received deck	Case A	94	0.476	4.4
	Case B	148	0.220	6.9
	Case C	158	0.516	7.4
After fatigue	Seam #3	94	0.403	4.4

2.4.5.5 Failure Modes

The failure modes observed in three strength tests on as-received FRP deck were consistent. Failure areas were highly localized and right under the tire patches, as seen in Figure 2.48. Failure modes were flexural failure of the top plate and top flange of the tube. Three cracks could be seen in Figure 2.48 (a) to (c). Two cracks were developed along two webs of the tube under the loading tire patch, and one crack was at about the center of the span between two webs of the tube. Figure 2.48(d) shows a side view of the top surface flexural failure; no crack was observed on the tube webs. Also, no visible cracks were observed at the bottom surfaces of the deck after the top surfaces failed in all three tests. From the above observations, it can be concluded that the top plate and the top flange of the tube failed through weak-axis bending, with cracking parallel to the tube webs.

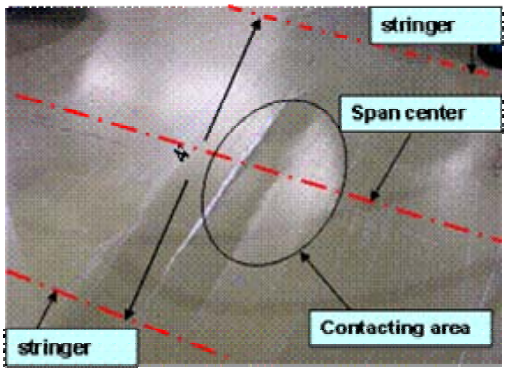

(a) Failure mode of Load Case A

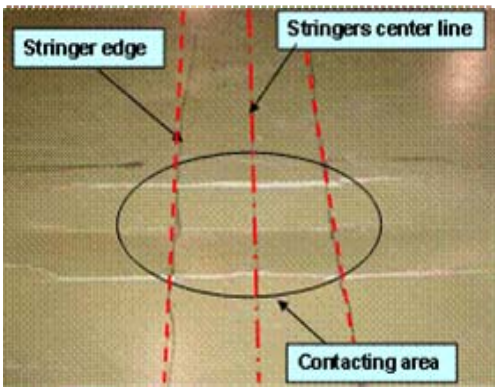

(b) Failure mode of Load Case B

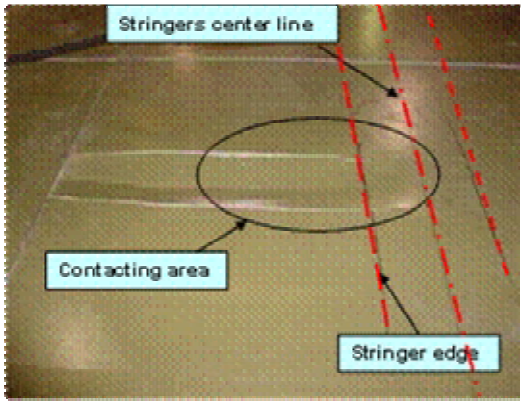

(c) Failure mode of Load Case C

(d) Side view of the flexural failure of top surface

Figure 2.48 Failure mode in as-received strength tests

The failure mode observed on the seam that was fatigued to 3,000,000 cycles and then tested to failure is very consistent with that observed on two adhesive seams tested to failure without being fatigued. For all seams in the ultimate test, the failure areas were highly localized and right under the tire patches, as seen in Figure 2.49(a). Failure mode was flexural failure of the top plate and top flange of the tube. Three cracks could be seen [Figure 2.49(b)]. Two cracks developed along two webs of the tube under the loading tire patch, and one crack was at about the center of the 6 in. span between two webs of the tube. Figure 2.49(c) shows a side view of the top surface flexural failure; no crack was observed on the tube webs. Also, no visible crack was observed at the bottom side of the deck near the adhesive joint after the top surface failed. From these results, it was concluded that the top plate and the top flange of the tube failed in weak-axis bending, with cracking parallel to the tube webs.

Another important observation from Figure 2.49(b) is that although the fracture at mid-span of two webs of the tube was near the adhesively-bonded line, no failure was observed

in the adhesive layer or in the joint interface. This suggests the adhesive layer and adhesive-substrate interface are stronger than the FRP components and that adhesive bonding is a viable technique for the panel-to-panel connections in FRP bridge deck system. In addition, the tests demonstrated a local failure rather than a total collapse, which would provide plenty of time for evacuation and maybe considered as another advantage of this FRP deck system.

The failure mode observed on the seam is consistent with the failure mode in strength tests of as-received decks, which demonstrate that adhesive bonded joints will not influence the failure mode of the deck.

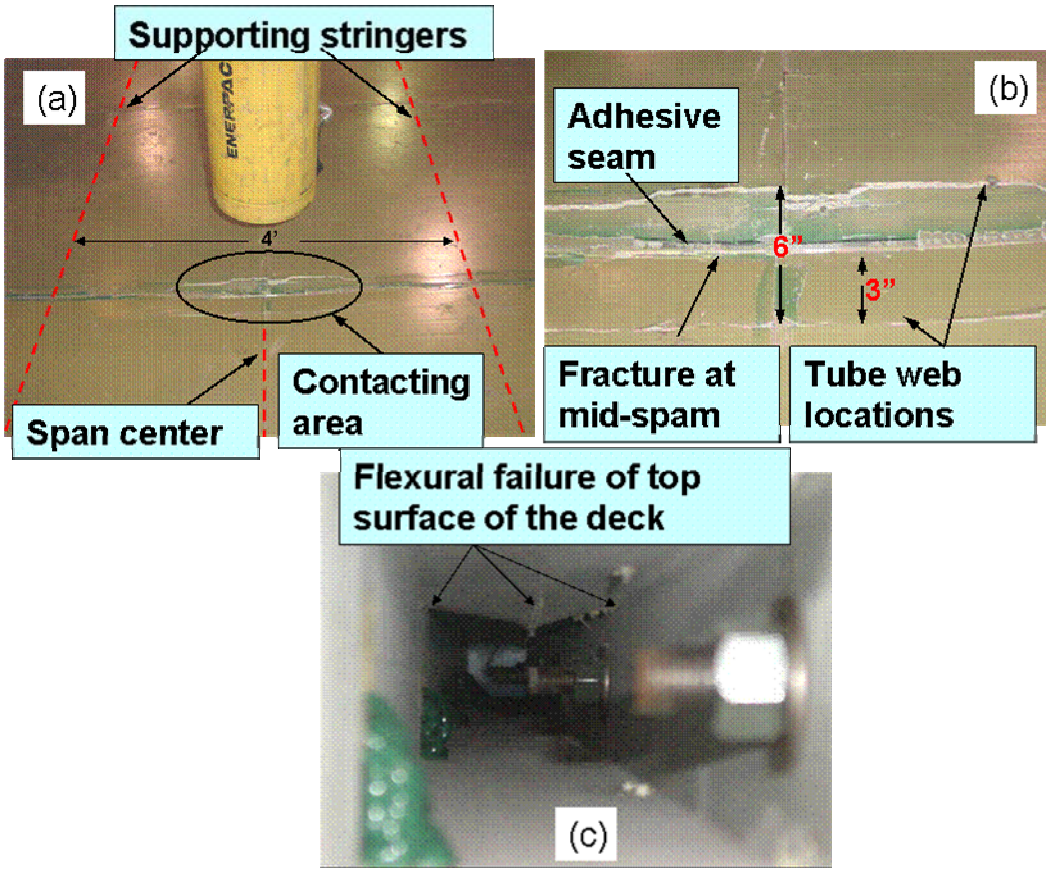

Figure 2.49 Failure mode in strength test after fatigue (a) Highly localized surface failure (b) Failure detail on top surface of the deck (c) Side view of the flexural failure of top surface

2.4.6 Bridge Installation

The FRP bridge deck installation was started at the Hawthorne St. Bridge on August 29th, 2006. Figure 2.50 shows the adhesive bonding process of the panel-to-panel connections during deck installation. The accuracy of panel dimensions of the mating parts was well controlled and installation protocols were strictly followed during the field installation. A controlled live load field test has been conducted on the bridge after rehabilitation and the response of the adhesively bonded panel-to-panel connection is monitored and reported in Section 3.3.3.4.

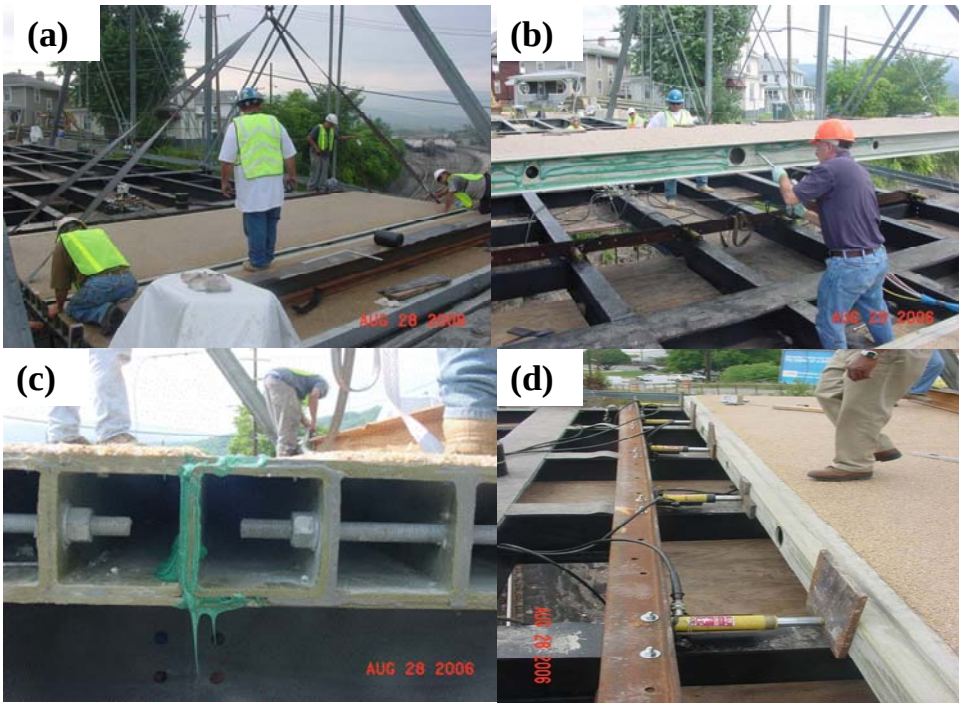

Figure 2.50 Field installation of the FRP bridge deck (a) Dry fit (b) Adhesive application (c) Seam curing (d) Jacking system

2.4.7 Summary of Stage IV Test

The following conclusions can be drawn from the static and fatigue tests conducted on the adhesively-bonded, panel-to-panel connections of an FRP bridge deck system.

1. All the adhesive joints were able to resist the design service load without any indication of cracking.

2. The strain and displacement showed linear elastic behavior up to design service load. The test results revealed an average deflection of span/664, which is slightly larger than the span/800 criteria in the AASHTO LRFD Bridge Design Specifications (2004). It should be noted that this limit is not intended for application to FRP composite bridge decks. However, no appropriate design limit is presently available.

3. The proposed full-length, adhesively-bonded tongue and groove panel-to-panel joints can meet the necessary strength performance criteria. No failure was observed in the adhesive layer or in the joint interface, which indicates the adhesive layer and adhesive-substrate interface are stronger than the FRP components. Thus adhesive bonding will not control the design strength of this FRP deck system.

4. The average first failure load was 100 kips in the strength tests on the adhesive joints, about five times the design service load of 22 kips. This value is close to the first failure load found in strength tests of as-received decks and indicates the adhesive joint will not influence the strength of the deck.

5. The failure in the top plate and the top flange of the tube was caused by weak-axis bending, with cracking parallel to the tube webs. This is also consistent with the failure mode in strength tests of as-received decks.

6. No significant change in stiffness or strength of the deck after 3,000,000 cycles of a fatigue load at a minimum/maximum load ratio of R=0.1, with the maximum load of 22 kips and the minimum load of 2 kips. This demonstrated the durability of the adhesive joint under repetitive loading.

The full scale model of two bays of the five-bay Hawthorne St Bridge provided valuable insights into the constructability of the adhesive panel-to-panel connections. The resulting field joint fabrication protocol was developed and used during fabrication of the deck joints in the field. The fabrication of the actual deck joints went smoothly and therefore validates the use of the developed protocol on other FRP deck installations.

Furthermore, based on the test results obtained during the laboratory testing of the two bay model, it was concluded that this adhesive bonding technique has the necessary serviceability and strength characteristics to be used in other similar bridge deck replacements. The testing program addressed the performance of the proposed bridge deck system under repeated (cyclic) loads. No discernable loss in strength or stiffness was observed. However,

since the testing only subjected the deck to one source of degradation (repeated loads), future research should focus on the performance of the Strongwell FRP deck system when subjected to varying moisture and temperature environments.

CHAPTER 3 GLOBAL STRUCTURAL PERFORMANCE OF THE HAWTHORNE ST. BRIDGE

3.1 Laboratory Full-Scale Mock-up Test

3.1.1 Objective of Testing Program

A series of tests were conducted on the two-span mock-up of the Hawthorne St. Bridge (as discussed earlier in Section 2.4) to investigate several topics related to the global structural performance of the FRP-deck-on-steel-stringer system under service load, including: (1) structural behavior; (2) transverse load distribution factor; and (3) degree of composite action.

3.1.2 Specimen Description

The same Strongwell FRP deck system as presented in Section 2.4.2 are used, thus a description will not be repeated here. Five individual panels were connected using adhesively-bonded tongue-and-groove, scarf-edged panel-to-panel connections to form a full width 22 ft specimen that was about 33 ft long in the direction of traffic. The FRP deck specimen was connected to stringers by deck-to-stringer connections to form a two-bay mock-up structure representative of the Hawthorne St. Bridge. These connections were not intended to develop composite action.

3.1.3 Test setup and Instrumentation

3.1.3.1 Test setup

The same test setup used for evaluating the structural performance of the adhesively bonded panel-to-panel connections was used in this test. The detailed description can be found in Section 2.4.4.1.

3.1.3.2 Instrumentation

Figure 3.1 gives an overview of the instrumentation plan for evaluating structural performance of the FRP-deck-on-steel-stringer systems in the Hawthorne St. Bridge mock-up test. The stringers and floor beams are referred to as "Stringer #1" to "Stringer #6" and "Floor Beam #1" to "Floor Beam #2," respectively. For consistency throughout the discussion, all references to "longitudinal" and "transverse" are given with respect to the bridge deck orientation; thus, "longitudinal" implies parallel to the pultruded tube direction of the FRP deck system, and the "transverse" direction refers to the traffic flow direction (perpendicular to the tube axis). All instrumentation was installed at locations A and B. Location A is located 7 ft - 8 in. from the abutment, where the maximum moment of the first span occurs. Location B is at the center of the second span.

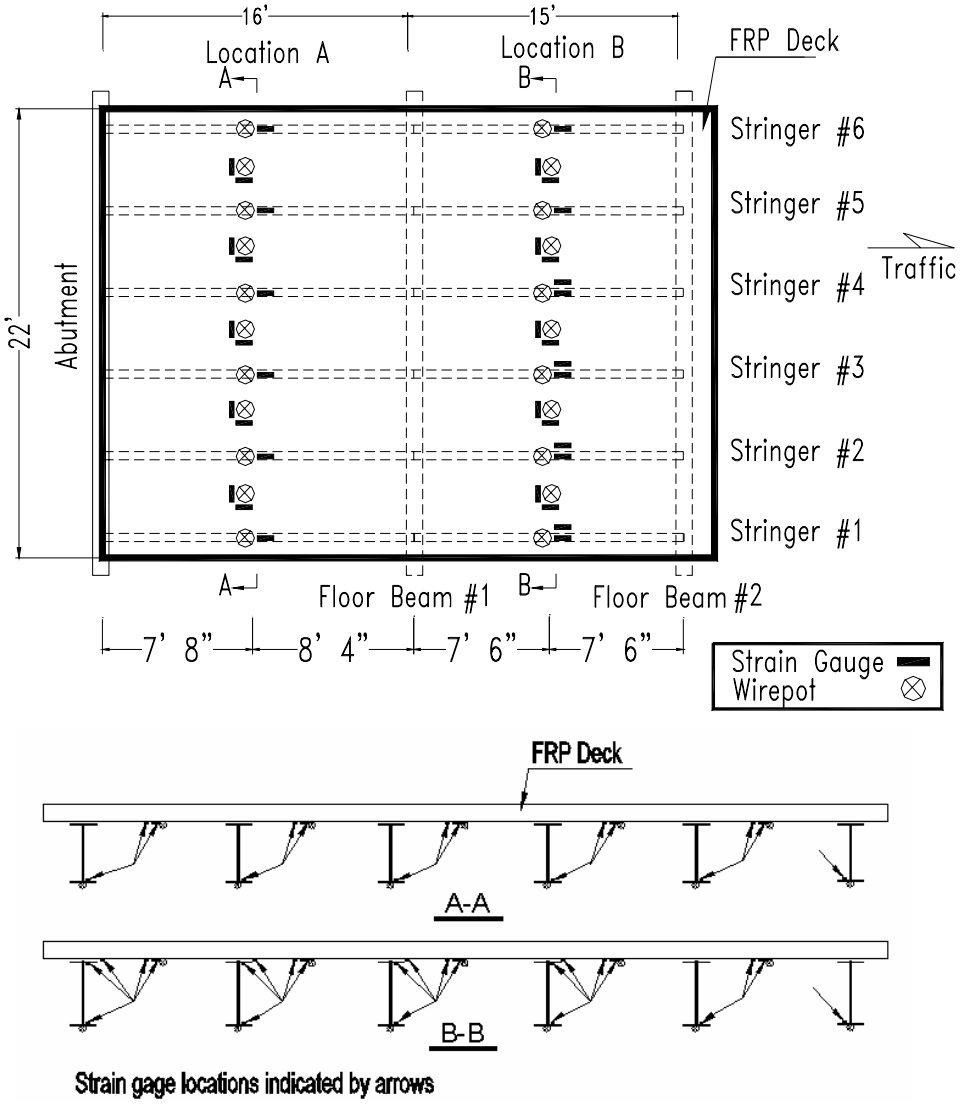

Figure 3.1 Location of instrumentation for global performance of FRP deck systems.

Strain gauges (Measurement Group CEA-06-375UW-350) were mounted on the top face of the bottom flange, 0.5 in. from the web for each stringer at all locations. At location B, strain gauges were also applied to the bottom face of the top flange of Stringers #1 to #4, 0.5 in. from the web; and to the bottom face of the FRP deck, 0.5 in. from the flange tip of Stringers #1 to #4. Gauges at these locations were oriented in the transverse direction. Additionally, strain gauges were applied to the bottom side of the FRP deck, midway between the instrumented stringers at all locations, as indicated in Figure 3.1. Gauges at these locations were oriented in both the longitudinal and transverse directions. Wire pots were used to

measure the vertical deflection of the FRP deck at these locations. Six wire pots were connected to the bottom face of the bottom flange of the six stringers at each location (A or B) to measure the overall stringer deflections.

The vertical load applied to the deck was measured using a 200 kips capacity load cell placed between the hydraulic actuator and bearing block fixed on the load frame. Load, deflection, and strains were continuously recorded during testing using a high-speed data acquisition system.

3.1.4 Experimental Procedure and Results

Five Load Cases, corresponding to the axle orientations given in Figure 2.30, were performed at Locations A and B. These service load cases were used throughout the laboratory mock-up test, not only for evaluating the global structural performance of the FRP-deck-on-steel-superstructure system, but also for evaluating the performance of the panel-to-panel connections as discussed earlier in Chapter 2. Service load was 21.3 kips, the AASHTO LRFD HL-93 design wheel load with dynamic load allowance included. Each Load Case was repeated three times. Load deflection and strain were continuously recorded during testing using a high-speed data acquisition system. All testing data were separately reduced and analyzed. The data obtained during three repetitions of each Load Case were observed to be repeatable and consistent. The deflections and strains on the stringers were used to give an indication of the overall behavior of the bridge, including the degree of composite action (if any) and transverse load distribution between stringers. The deflections and strains on the FRP deck were used to evaluate the global performance of the deck under service load.

3.1.4.1 Global behavior of the FRP bridge deck system

The load vs. stringer deflections showed linear elastic behavior up to design service load during all the Load Cases (a representative plot is shown in Figure 3.2). Figure 3.3(a) and (b) give recorded stringer deflections under design service load at Locations A and B, during Load Case 1 through 5. The maximum deflections of the end-span and second span during Load Case 5 (representing two full lanes) were 0.36 in., 0.52 in., respectively. A complete presentation of recorded stringer and deck deflections under design service load are included in Appendix C.

The load versus strain behavior was also linear elastic up to design service load (a representative plot shown in Figure 3.4). A complete presentation of recorded stringer and deck strains under design service load are included in Appendix C. Figure 3.5(a) and (b) show the maximum longitudinal and transverse strain at the bottom surface of the deck (right under the loading patch) at Locations A and B during Load Cases 1 through 5. The maximum recorded longitudinal strain was 875 με at Location B during Load Case 4. The maximum recorded transverse strain was 650 με at Location B during Load Case 2. Transverse strains were always smaller than longitudinal strains at the same location.

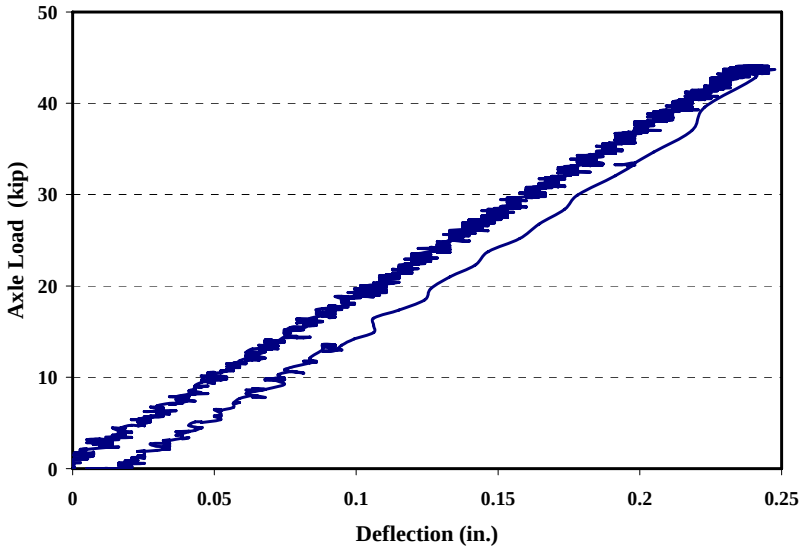

Figure 3.2 A representative load vs. stringer deflection plot
(Location A, Load Case 1, Stringer #3)

Table 3.1 summarizes the deck deflection data at Location A and B during Load Cases 1, 2, 4 and 5. Load Case 3 is not listed because in this case the truck was straddling Stringer #3 and the load patch was not at the mid-span of two stringers. The maximum absolute deflection (overall deflection reference to the floor) at the mid-span of the deck was 0.40 in. and occurred at Location B during Load Case 5. The maximum relative deflection (deck mid-span absolute deflection minus the average deflection of two adjacent supporting stringers) was 0.105 in. at Location B during Load Case 4. The 4-ft stringer spacing indicates an L/457 response at design load. None of the deflection indices listed in Table 3.1 could meet

the desired deflection index of less than L/800, which is the recommended limit of live load deflection for steel, aluminum and concrete construction by AASHTO LRFD Bridge Design Specifications (AASHTO 2004). It should be noted that this limit is not intended for application to FRP composite bridge decks. However, no appropriate design limit is presently available. Composite bridges constructed for demonstration projects have been designed based on a deflection limit range of L/425 to L/1,000 (Demitz et al. 2003). The applicability of the L/800 deflection limit to FRP decks is discussed in detail in Section 4.4.1.

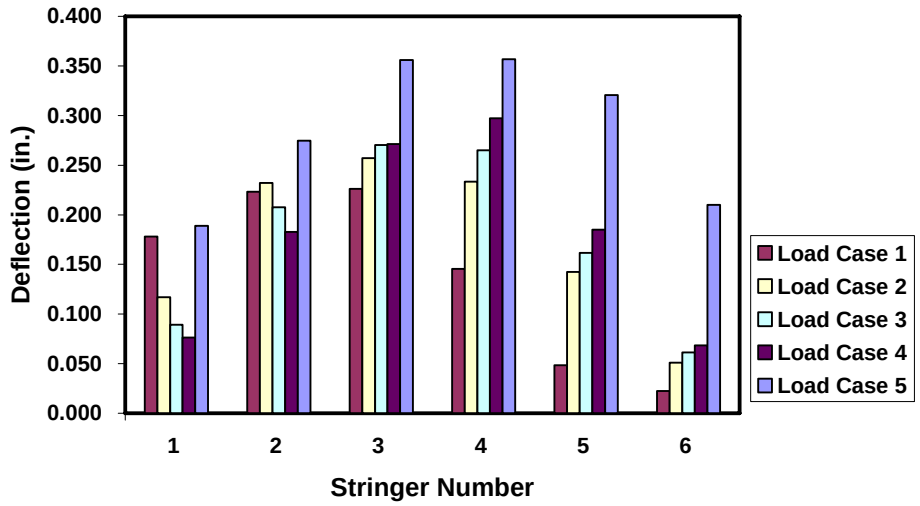

(a) Location A

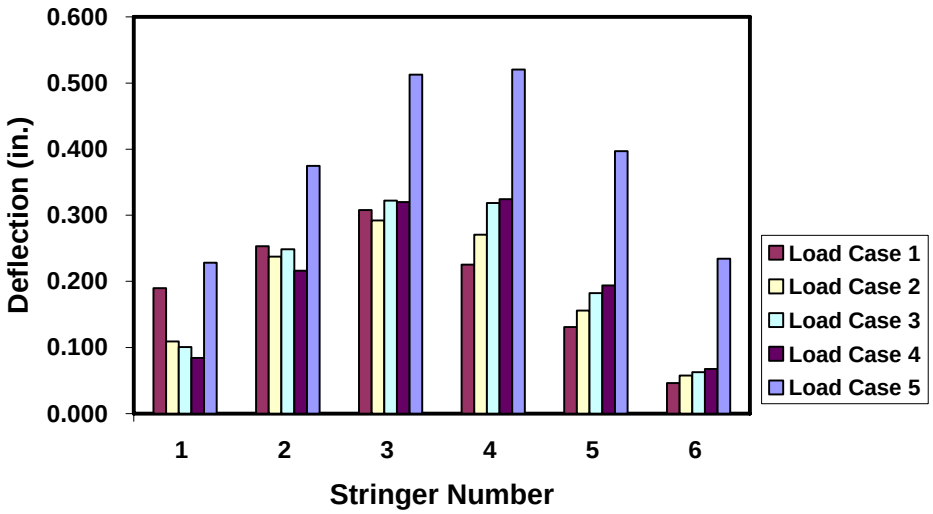

(a) Location B

Figure 3.3 Deflection distribution on stringers at Locations A and B during Load Cases 1 through 5

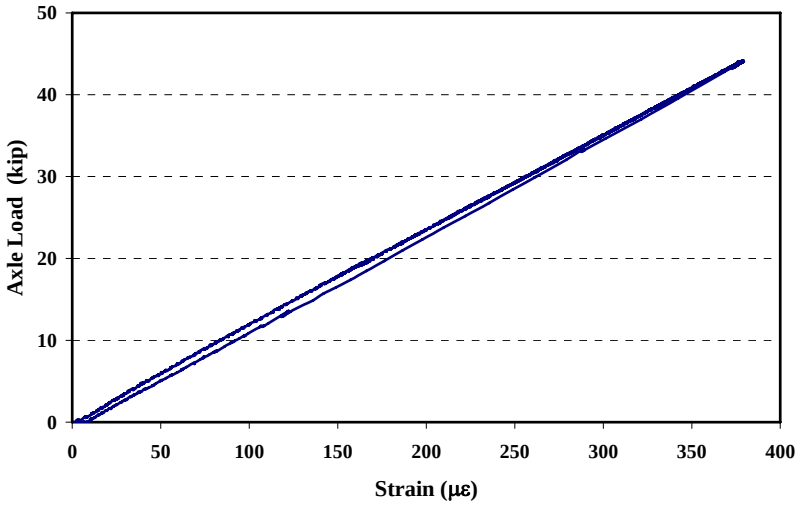

Figure 3.4 A representative plot of load vs. stringer strain
(Location A, Load Case 1, Stringer #1)

Table 3.1 Data of Service Load Test

	Load Case	Maximum deck deflection location	Mid-span deck deflection (in.)	Mid-span relative deck deflection (in.)	Deflection index (relative deflection/deck span)
Location A	1	Mid-span between Stringer #1 and #2	0.288	0.087	554
	2	Mid-span between Stringer #3 and #4	0.341	0.095	503
	4	Mid-span between Stringer #2 and #3	0.312	0.085	568
	5	Mid-span between Stringer #1 and #2	0.359	0.094	512
Location B	1	Mid-span between Stringer #1 and #2	0.321	0.100	481
	2	Mid-span between Stringer #3 and #4	0.386	0.092	525
	4	Mid-span between Stringer #2 and #3	0.382	0.105	457
	5	Mid-span between Stringer #5 and #6	0.403	0.102	471

Note: Load Case 3 is not listed because the load patch was not at the mid-span of two stringers.

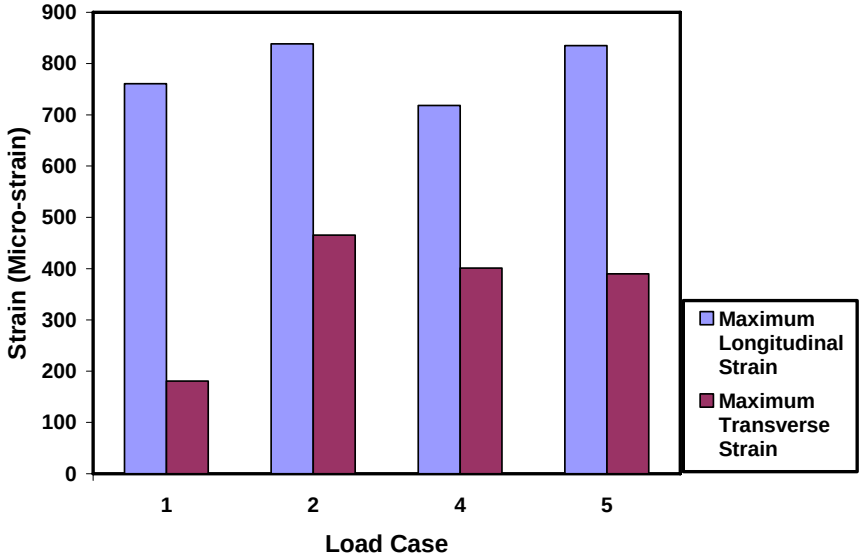

(a) Location A (Load Case 3 not included since no strain gauges located directly under loading patch)

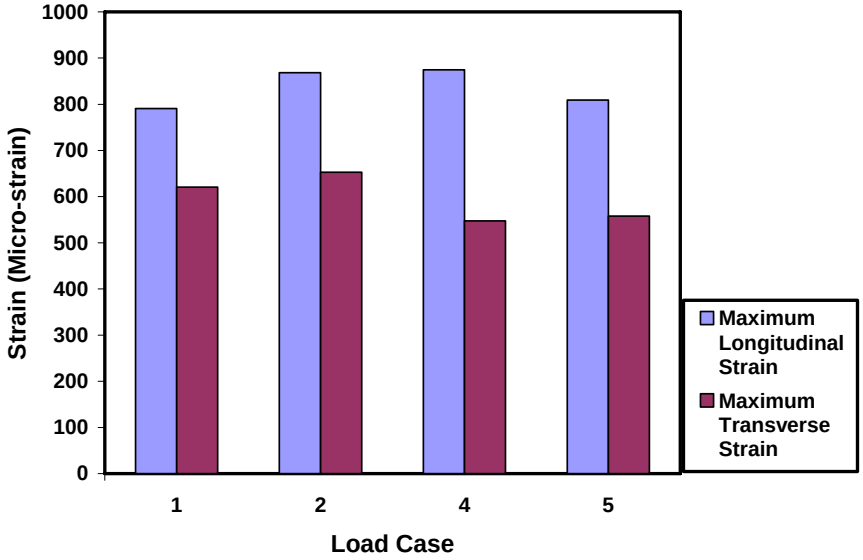

(b) Location B (Load Case 3 not included since no strain gauges located directly under loading patch)

Figure 3.5 Maximum longitudinal and transverse strain at the bottom of the deck under loading patch at Locations A and B during Load Cases 1 to 5.

3.1.4.2 Lateral Load Distribution Factors

The lateral load distribution factor (DF) is a measure of the fraction of load resisted by a stringer within the bridge. This factor is given as a fraction of the design load and is an

important design tool used to determine the maximum expected load each supporting stringer must be able to resist.

DFs observed during lab tests were calculated from the recorded strains on the stringers by assuming that the response of the bridge was elastic under service load. The distribution factor, DF was calculated as the ratio of the strain in a given stringer to the total strain of all the stringers.

$$DF_{stringer,j} = \frac{Strain_{stringer,j}}{\sum_{stringers} Strain} \qquad \text{Eq. 3.1}$$

A complete presentation of recorded stringer strains under design service load for all load cases are included in Appendix C. Calculated DFs from laboratory measurements for the mock-up structure are shown in Table 3.2. The slightly asymmetric distribution factors under Load Case 5 (the symmetrical loading case) may be due to an imbalance of the load transferring to load patches under a single actuator.

Table 3.2 Calculated Distribution Factors

Location	Load Case	Stringer number					
		Exterior	Interior				Exterior
		1	2	3	4	5	6
A	1	0.19	0.27	0.42	0.10	0.02	0.00
	2	0.08	0.32	0.34	0.19	0.04	0.05
	3	0.04	0.29	0.34	0.26	0.06	0.01
	4	0.02	0.24	0.35	0.30	0.08	0.01
	5	0.21	0.34	**0.47**	0.41	0.29	0.27
B	1	0.27	0.26	0.32	0.12	0.02	0.00
	2	0.11	0.28	0.32	0.23	0.05	0.00
	3	0.07	0.25	0.31	0.29	0.07	0.01
	4	0.04	0.20	0.31	0.33	0.10	0.02
	5	**0.27**	0.29	0.44	0.42	0.31	0.27

Note: Bold values are the control DFs for exterior and interior stringers.

From this table, it can be observed that the distribution factors for the double truck case are generally greater than those of the single truck; which indicates that the double truck loading is critical for both the interior and exterior stringers.

The lateral distribution factors calculated based on the testing data show that the deck provided sufficient stiffness to distribute axle load to the stringers. A comparison of the distribution factors from lab tests to that from AASHTO LRFD (AASHTO 2004) and Standard specifications (AASHTO 2002) was done to gain some insight into the applicability of current provisions to FRP deck design. Equations specified by both AASHTO bridge design specifications for LDF calculation are included in Table 4.9, thus not presented here.

No appropriate provision from either AASHTO bridge design specifications is available for calculating distribution factors of an FRP deck on steel stringers. For simplification the FRP-deck-on-steel-stringer system was assumed to behave similarly to two types of decks contained as categories in both AASHTO specifications: (1) a 4000 psi compressive strength, reinforced concrete deck of similar thickness supported by steel stringers; (2) a glue laminated wood deck of similar thickness on steel stringers. This allowed for a generic comparison of the AASHTO code predictions to test results without using higher level models (such as grillage or finite element analysis).

Note that definitions differ somewhat between the AASHTO standard and the LRFD specifications. The stringer distribution factor (GDF) defined by the Standard specification is classified as the percentage of a wheel line (half of a truck load) resisted by the most heavily loaded stringer within the bridge. For the LRFD specification, the distribution factor (g) is defined as the percentage of a lane load (total truck load) resisted by the most heavily loaded stringer. The two definitions can be related as shown in Eq 3.2. In this research, DFs are defined as per LRFD specification. The DFs calculated from Standard specification was divided by two to compare with those from LRFD specification.

$$g = \frac{1}{2} GDF \qquad \text{Eq 3.2}$$

For completeness, the lever rule was used to calculate DFs. This yields an upper bound on the DFs. In addition, an equal distribution between stringers is provided to gain some insight of the relative stiffness of the FRP deck system and to provide a lower bound. Summaries of lateral load distribution factors for interior stringers are provided in Table 3.3. Due to the relatively low modulus of the FRP deck, only short deck overhangs are typically used in FRP deck applications (12 in. overhang in this project). Therefore, the DFs for exterior

stringers are generally smaller than those for interior stringers, which do not control the design and thus are not discussed here. Comparison of the lateral load distribution factors at Location A and B is shown in Figure 3.6.

Table 3.3 Summaries of DFs for interior stringers

Location	Load Case	Test Results	Std. Spec		LRFD Spec.		Lever rule	Equal Dist.
			RC	Timber	RC	Timber		
A	One Lane	0.42	0.34	0.46	0.41	0.46	0.50	0.33
		% difference	-19	10	-2	10	19	-21
	Two Lane	**0.47**	0.36	0.44	0.47	0.44	0.50	0.33
		% difference	-23	-6	0	-6	6	-30
B	One Lane	0.32	0.34	0.46	0.40	0.46	0.50	0.33
		% difference	6	44	25	44	56	3
	Two Lane	**0.44**	0.36	0.44	0.46	0.44	0.50	0.33
		% difference	-18	0	5	0	14	-25

From these comparisons, it can be observed that both AASHTO lateral load distribution factors for the category of glued laminated wood panels on steel stringers showed good agreement with tested results. Design value of DFs for interior stringers is 0.44 (same from both specifications) is 6% smaller than critical tested value of 0.47 at Location A and the same as critical tested value of 0.44 at Location B. This indicates that the FRP deck can provide longitudinal stiffness similar to a laminated timber deck.

AASHTO LRFD distribution factor for a similar concrete deck also showed good agreement with the critical tested data for interior stringers (the same when comparing predicted 0.47 with tested 0.47). However, the FRP deck has no composite action with supporting stringers in this FRP deck application, the calculation of AASHTO LRFD distribution factor of a concrete deck is based on the assumption of composite action between stringers and decks. It can be concluded that AASHTO LRFD distribution factor for a similar concrete deck is not applicable in this case.

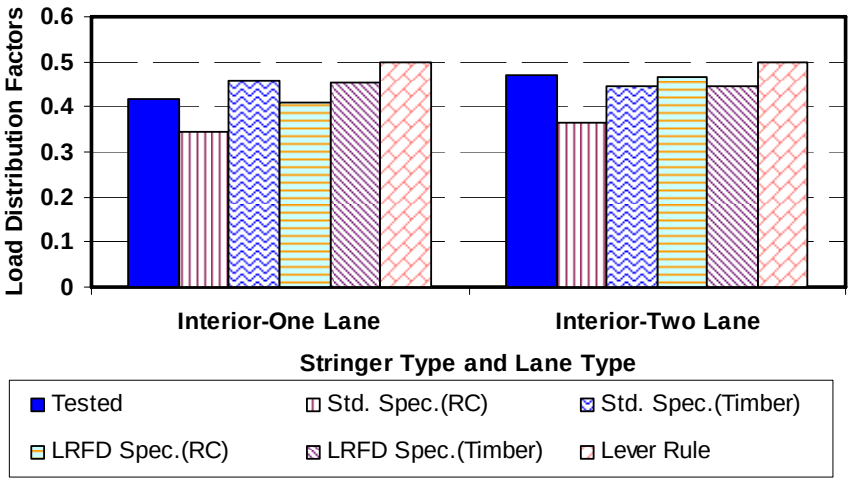

(a) Location A

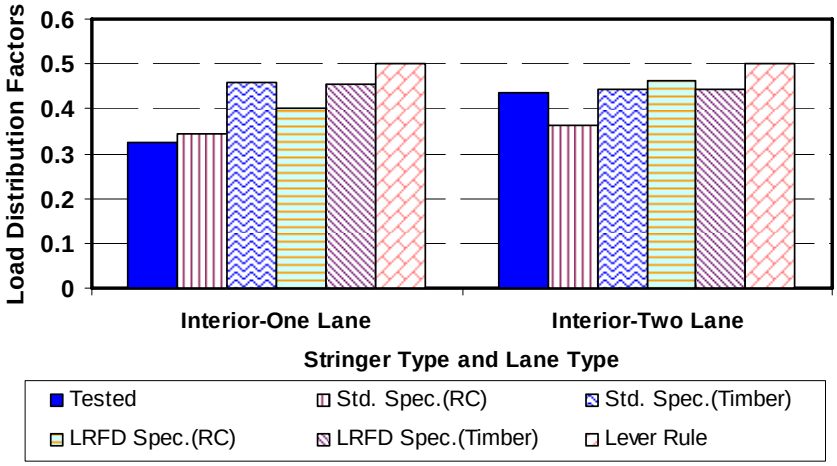

(b) Location B

Figure 3.6 Load distribution factors at Locations A and B

AASHTO Standard Specification for a similar concrete deck gave poor predications (23% smaller when comparing predicted 0.36 with tested 0.47 for interior stringers) and was thought inappropriate to predict the load distribution factors for this type of FRP deck system.

At both Location A and B, the lever rule seems to be a reasonable and appropriately conservative method to predict DFs. Design value of DFs for interior stringers is 0.5 using lever rule is 6% larger than critical tested value of 0.47 at Location A and 14% larger than critical tested value of 0.44 at Location B.

The preceding discussion indicates that the FRP deck has a lower longitudinal (perpendicular to traffic direction) flexural stiffness as compared to a similar depth concrete deck, which results in larger DFs for the FRP deck. The FRP deck can provide longitudinal stiffness similar to a laminated timber deck. Both AASHTO lateral load distribution factors for the category of glued laminated wood panels on steel stringers can give good estimations in design purposes. Also as a simplified method, the appropriately conservative design DFs may be found using the lever rule by assuming no load transfer across an interior stringer (deck is hinged at each stringer).

3.1.4.3 Degree of composite action of the FRP-on-steel-stringer system

In the Hawthorne St. Bridge the existing deck was not designed to act compositely with the steel stringers, hence the deck-to-stringer connection proposed for use is not intended to develop composite action. The forces the deck-to-stringer connection must resist are from braking of vehicles on the bridge deck and from uplift.

The preliminary design, created by VDOT, attaches the panels using a bolt through the bottom flange of the deck with a clip to the side of the steel stringer top flange. One nut, bearing plate and steel sleeve is welded together as a connector. Then the connector is pushed along the tube to drop into the hole pre-drilled through the bottom plate and the bottom face sheet of the tube. Finally a 3/4 in. bolt is screwed into the matched nut of the connector from underneath the deck system. The bolted connection was spaced at 24 in. along the traffic direction for each stringer. A schematic and photograph of the deck-to-girder connection is shown in Figure 3.7.

One method to prove composite or non-composite action of the FRP-on-steel-stringer system is to locate the neutral axis of the stringers. Since the bridge remained in the elastic range under service loads, the strain in the stringer would change from compression to tension at or near the neutral axis of the stringer with little composite action. At Location B, Stringer #1 to #4 were instrumented with strain gauges on the top of the bottom flanges and bottom of the top flanges as indicated in Figure 3.1. The purpose of this instrumentation was to locate the position of the neutral axis.

With the assumption that the strain in the stringer remains linear (plan sections remain plane), the neutral axis was calculated based on the strain readings for each stringer. Figure 3.8 shows the calculated location of the neutral axis for Stringers #1 to 4 during Load Case 5, based on the strain measurements (included in Appendix C). It is clear that the neutral axes were still located near mid-depth of the stringers, indicating that little or no composite action was attained, which fulfilled the design intention.

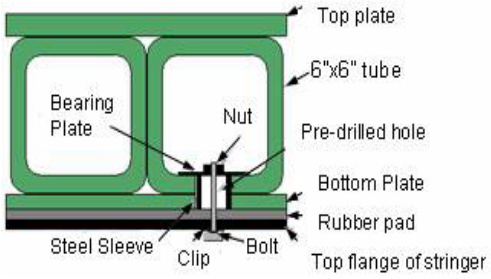

(a) Schematic figure

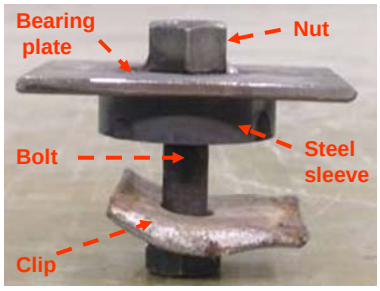

(b) Connector with bolt and clip

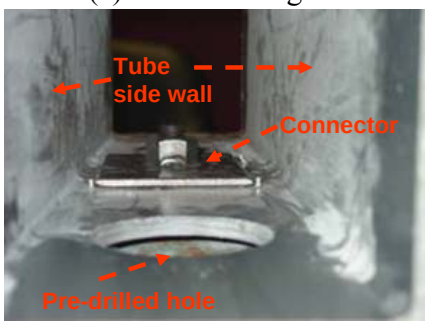

(c) Place connector into pre-drilled hole

(d) Assembly of deck-to-stringer connection

Figure 3.7 Deck-to Girder connection.

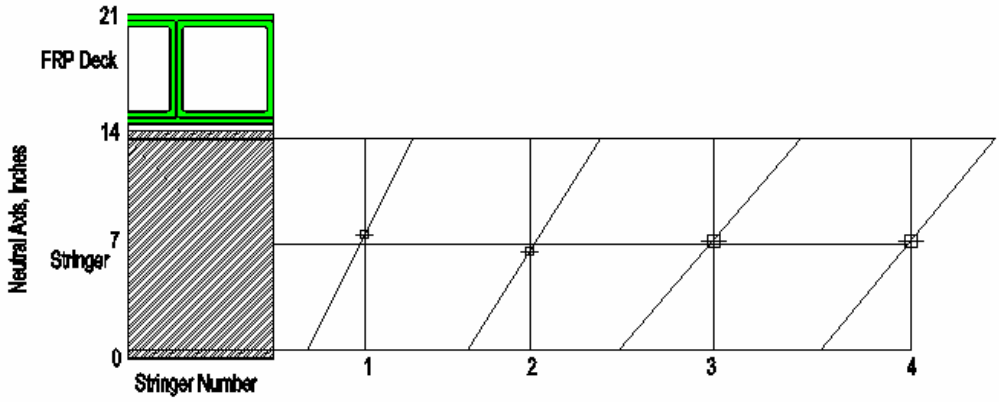

Figure 3.8 Location of neutral axis for Stringers 1 to 4 during Load Case 5

3.2 Field Test

3.2.1 Bridge Rehabilitation

The Strongwell FRP deck system was used to rehabilitate a historic bridge (Hawthorne St. Bridge) in Covington, Virginia during the spring and summer of 2006. The rehabilitation project included a number of steps listed below. Due to the advantage of FRP deck's low self-weight, the installation of the FRP panels only took one week to finish although the total construction lasted about three months.

1. Remove entire existing concrete deck and sidewalk, vehicular railing and pedestrian railing for subsequent re-installation.
2. Construct new abutment seat and backwall and add abutment footing toe walls.
3. Replace the bridge superstructure with a new deck/beam/girder system [Figure 3.9(a)];
4. Perform all structure repairs, clean and paint existing and replacement members.
5. Install the FRP deck panels [Figure 3.9(b)];
6. Install vehicular post and railing and re-install existing pedestrian railing.
7. Replace approach and install the sidewalk.

3.2.2 FRP Deck System

The same panel geometry and material properties of Strongwell FRP deck as presented in Section 2.4.2 were used in the bridge rehabilitation.

Figure 3.10 shows a plan view of deck panels, panel-to-panel connections, and supporting steel superstructure. The FRP deck consists of eleven individual modular deck panels that are jointed together using ten adhesive panel-to-panel connections (Seam #1 through #10). Each individual panel is 22 ft by 7.5 ft, with the exception of the two end panels which are 22 ft by 5.5 ft in plan. These individual panels are connected to form a full width 22 ft panel that was about 78.5 ft long in the direction of traffic.

The individual deck panels were pre-fabricated in the manufacturer's shop and transported to the field before construction started. The tubes and top and bottom plate are adhesively bonded to form FRP bridge deck panels. The steel thru-rods are used to provide binding forces when the deck panels are curing. Bonding is accomplished in a vacuum bag to produce uniform pressure and continuous bonding.

The manufacturer improved the panel quality by using stricter quality control procedures during pultrusion and bonding of tubes. The gap distance for all seams in the actual bridge was within 0.1 in. The bonding surfaces of the tongue-and-groove connection were also sanded in shop to remove the non-stick film remaining from pultrusion. A polymer concrete wearing surface was applied on top of the FRP deck during shop fabrication except the slots on top of the tongue-and-groove panel-to-panel connection (Figure 3.9 (c)). The same polymer concrete wearing surface provided by the manufacturer was applied on the slots after the bonding of the panel-to-panel connections.

The field joint fabrication protocol developed in Chapter 2 was followed during fabrication of the deck joints in the field. The fabrication of the actual deck joints went smoothly and therefore validates the use of the developed protocol on other FRP deck installations.

(a) New deck/beam/girder system

(b) FRP deck panel positioned by a crane

(c) Construct adhesively bonded panel-to-panel joint

(d) Bridge after rehabilitation

Figure 3.9 The Hawthorne Street Bridge rehabilitation

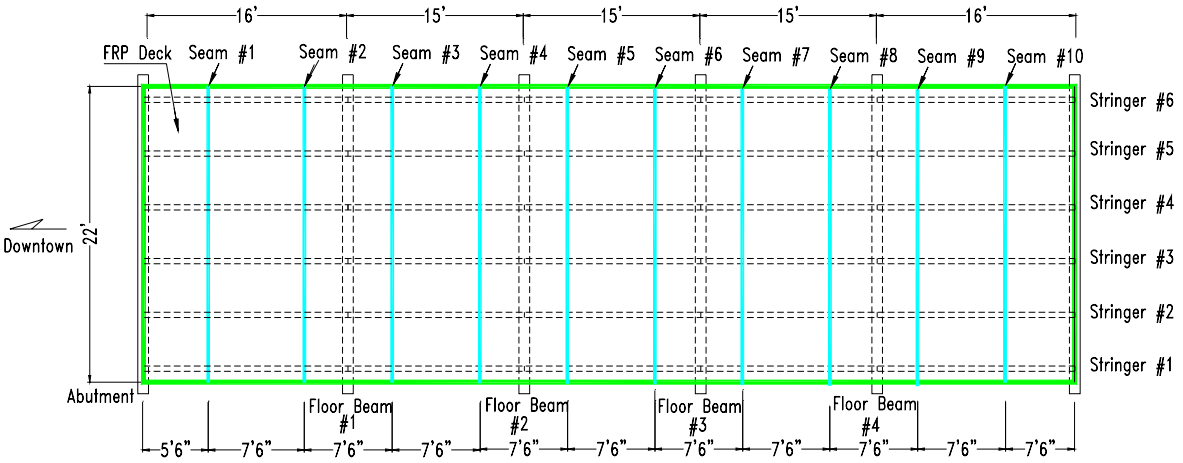

Figure 3.10 Plan view of deck and supporting steel superstructure

3.2.3 Field Testing Objectives

The field testing was performed on May 2nd, 2007. The structural performance of the FRP-on-steel-superstructure system was examined by monitoring a number of critical responses due to controlled live load, such as global structural stiffness, strain level in the deck, and load distribution factors.

The objectives of this portion of the research are as follows:

(1) examine the global structural performance of the FRP-on-steel-superstructure system;

(2) investigate the performance of the adhesively bonded panel-to-panel joints;

(3) measure the composite action of the FRP-on-steel-stringer system;

(4) determine appropriate distribution factors for the FRP-deck-on-steel-superstructure system;

(5) collect field data for calibrating a finite element model to further investigate the performance of the bridge deck system.

3.2.4 Instrumentation

A schematic of the instrumentation plan is shown in Figure 3.11. The stringers and floor-beams are referred to as “Stringer #1” through “Stringer #6” and “Floor Beam #1” through “Floor Beam #4.” For consistency throughout the discussion, all references to

“longitudinal” and “transverse” are given with respect to the bridge deck orientation; thus, “longitudinal” implies parallel to the pultruded tube direction of the FRP deck system, and the “transverse” direction refers to the traffic flow direction (perpendicular to the tube axis).

All instrumentation was installed at four locations along the span during bridge construction. These locations are referred to alphabetically as A through D. These locations were selected to meet the objectives of the testing as described in the previous section and challenges of the inaccessibility of the underside of the bridge after construction was complete.

Location A is at the mid-span of the first bay. A temporary wood platform made it possible to access this location. Transverse (along traffic direction) strain gauges were applied to the top of the bottom flange of Stringers #1 to #3 and both top of the bottom flange and bottom of the top flange for Stringers #4 to #6 as indicated in Figure 3.11. These gauges are intended to investigate any composite action between deck and stringers and load distribution factor at mid-span of the first bay.

The mid-span of the bridge is referred as Location B. Transverse strain gauges were applied to the top of the bottom flange of all the stringers as indicated in Figure 3.11 to investigate the load distribution factors at mid-span of the bridge. Due to the relative inaccessibility of the underside of the bridge, the strain gauges were mounted from the top of the steel superstructure before the FRP deck was installed.

Location C is at the mid-span of the last bay. Strain gauges were applied to the soffit of the FRP deck, midway between the instrumented girders as indicated in Figure 3.11. Gauges at these locations were oriented in both the longitudinal and transverse directions to investigate the global structural performance of the FRP deck.

The instrumentation plan at Location D is designed to measure the performance of the adhesively bonded panel-to-panel connection. As shown in Figure 3.11, at the soffit of the FRP deck, two strain gauges were used to measure longitudinal strains at both sides of the joint midway between Stringer #3 and #4. The instrumentation pattern was repeated for another two locations, midway between Stringer #4 and #5 and midway between Stringer #5 and #6. Two strain gauges were also selected to measure the transverse strains at both sides of the joint midway between Stringer #3 and #4.

Since the bridge crosses three railway lines, direct measurement of deflections was not allowed. Vertical deflections of the stringers at mid-span of the bridge were measured

using optical surveying techniques. Steel scales were installed on the top of the FRP deck and over each steel stringer. A high-precision level was used during testing to determine vertical deflections with a precision of approximately 0.04 in.

A total of 29 strain gauges (Measurement Group CEA-06-375UW-350) were used, 15 placed on steel stringers and 14 placed on the FRP deck (see Figure 3.11). Conventional, general purpose, uniaxial foil-strain gauges (Model EA-06-250AE-350), manufactured by Measurements Group, Inc, were used to measure strains during the testing. The strain gauges were bonded to the steel and FRP deck with M-Bond 200 adhesive and then environmentally and mechanically protected by M-Coat F system for long-term monitoring use. All data was collected using a portable data acquisition system, the CR9000, capable of high speed data measurement.

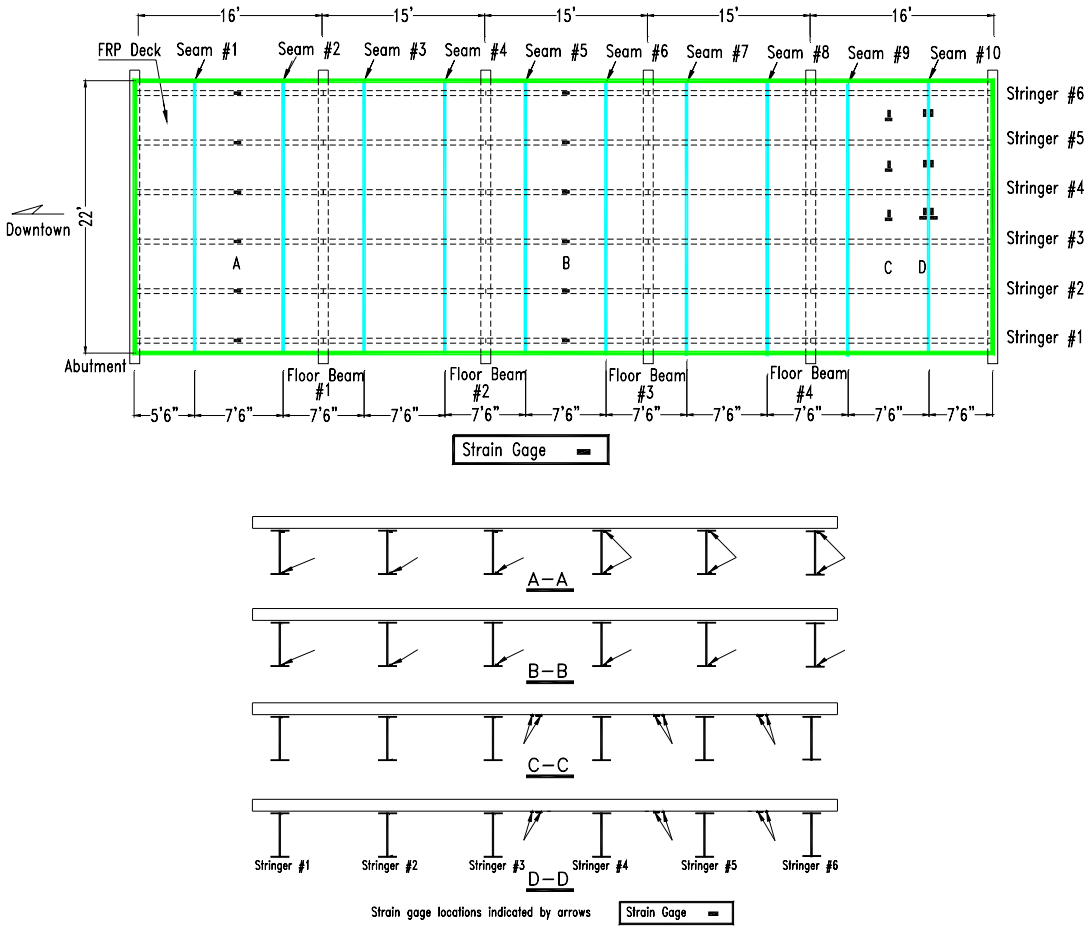

Figure 3.11 Location of instrumentation for field testing

3.2.4.1 Test Method

In situ load tests were conducted using a typical 3-axle dump truck loaded with aggregate provided by Virginia Department of Transportation (VDOT); truck loads were determined by weighing each wheel set individually (Figure 3.12). The weight of the rear tandem axles was measured as 40 kips and front axle was 10 kips. A total of six load paths were considered as shown in Figure 3.13. These configurations were intended to apply the worst-case load scenario to the FRP deck and superstructure.

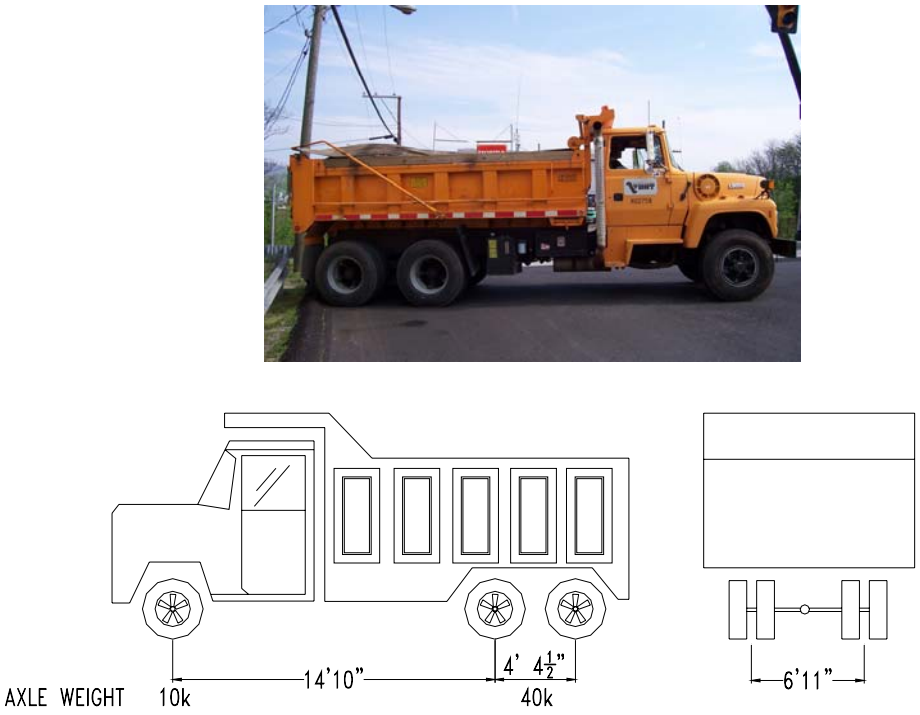

Figure 3.12 Field Test Truck

Load paths 1 to 4 (path 2 and 4 are the mirror cases of path 1 and 3, respectively) were selected in an attempt to produce the maximum deflection and load distribution factor (LDF) in the interior and exterior stringers for single and two lane load cases. Load path 1+2 and 3+4 were not actually performed, but used to simulate 2-lane trucks being simultaneously loaded by superimposing results from load paths. This method was deemed acceptable in the absence of a second truck because the bridge remained in the elastic range throughout the

testing. It should be note that load path 1+2 and 3+4 do not exactly follow the truck spacing specified by AASHTO LRFD (2004) specification. Due to the center to center distance of tires of the back axle is 6 ft–11 in., which is not 6 ft described in AASHTO LRFD specification. Therefore, when two lane trucks are located transversely to the traffic, the distances between two trucks are smaller (for path 1+2, 2 ft-2 in. and for path 3+4, 3 ft-4 in. as shown in Figure 3.13) than the 4 ft defined in AASHTO LRFD specification. These arrangements are used to conservatively evaluate the LDF for the interior stringers because less distance between two trucks means more load are transferred to interior stringers. Load paths 1, 5 and 6 were the critical cases for flexure of an FRP deck transverse to the traffic, with a wheel located at mid-span between two stringers.

For all load paths, the trucks were driven slowly, 5 mph or less across the bridge following lines marked on the bridge deck while strain data was recorded at a rate of 20 scans/second. For each load path, the truck crossing was repeated five times. For mid-span deflection measurements, the dump truck was parked following load path 1 and 2 perpendicular to the traffic direction with the center of back axle was as close as possible to mid-span (33 in.) of the bridge along the traffic direction, as shown in Figure 3.14. The vertical elevations of the six steel scales located on the top of the FRP deck over steel stringers were read using a high-precision level. These elevations are compared to base line readings taken before and after each load path to determine overall bridge deflections due to the applied truck loads.

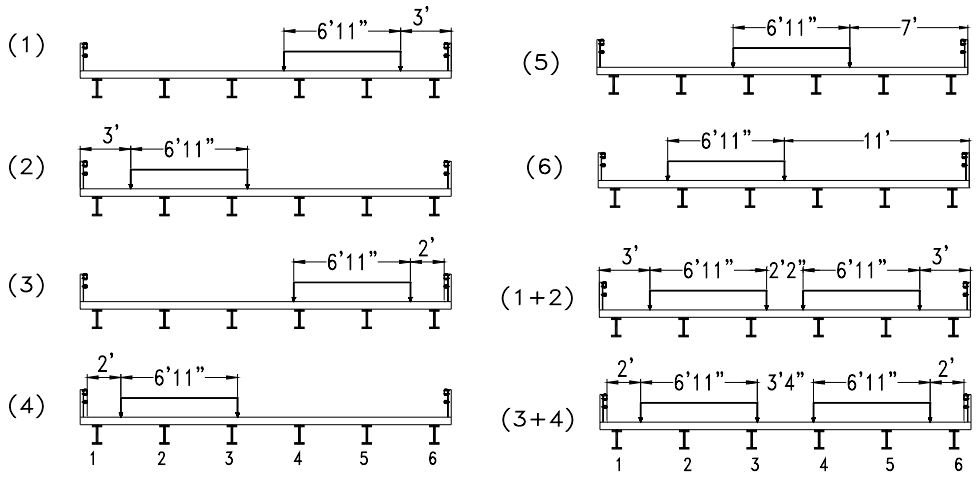

Figure 3.13 Summary of Loading Paths for Live Load Tests

Figure 3.14 Mid-span deflection measurement during field test

3.2.4.2 Test results

3.2.4.2.1 Bridge Deflection

Vertical deflections of the stringers at mid-span of the bridge were measured using optical surveying techniques. Superimposing load paths 1 and 2, to simulate two lanes loaded, yield a maximum deflection of Stringers #3 and #4 equal to 0.71 in. (18 mm). All deflections are tabulated in Table 3.4 and plotted in Figure 3.15 for comparison. The live load deflection of the bridge was approximately L/1270, which is within the deflection limit (L/800) specified in AASHTO LRFD Bridge Design Specification (AASHTO 2004). It also should be note that the superimposed load path 1+2 is more conservative than the real case as discussed earlier (due to the smaller truck spacing).

Table 3.4 Stringer deflections at mid-span of the bridge in field test (unit: in.)

Stringer #	S1	S2	S3	S4	S5	S6
Path 1	0.12	0.24	0.31	0.39	0.31	0.20
Path 2	0.20	0.35	0.39	0.31	0.24	0.16
Path 1+2	0.31	0.59	0.71	0.71	0.55	0.35

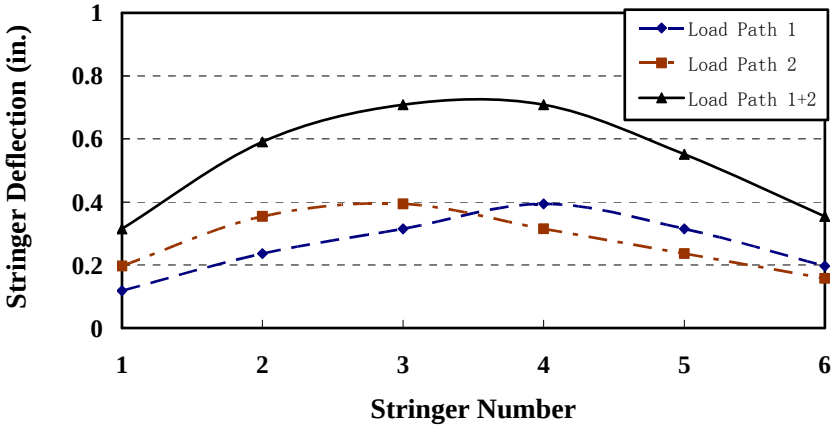

Figure 3.15 Mid-span stringer deflections

3.2.4.2.2 Effectiveness of deck-to-stringer connection

Previous laboratory test presented in Section 3.1.4.3 has indicated that little composite action was attained, which fulfilled the design intention. The design intention of no composite action was further checked with the field experimental data. One method to prove composite or non-composite action of the FRP-on-steel-stringer system is to locate the neutral axis of the stringers. Since the bridge remained in the elastic range under service loads, the strain in the stringer would change from compression to tension at or near the neutral axis of the stringer with little composite action (plan sections remain plane and linear strain behavior). At Location A, Stringers #4 to #6 were instrumented with strain gauges on the top and bottom flange as indicated in Figure 3.11. This instrumentation was aimed to locate the position of the neutral axis. A representative plot of the strain reading from the top and bottom flange of the Stringer #5 following load path 2 is shown in Figure 3.16. Top and bottom flange average strains (average of five load repetitions) of Stringer #5 under all load paths are listed in Table 3.5. It can be observed that strains in bottom and top flanges are almost the same except for the sign. This indicates that the neutral axis of the girder was still located near mid-depth of the

stringers and little composite action was attained, which fulfilled the design intention. Before the field test, the strain gauges mounted on Stringer #4 and #6 were vandalized and no data could be recorded.

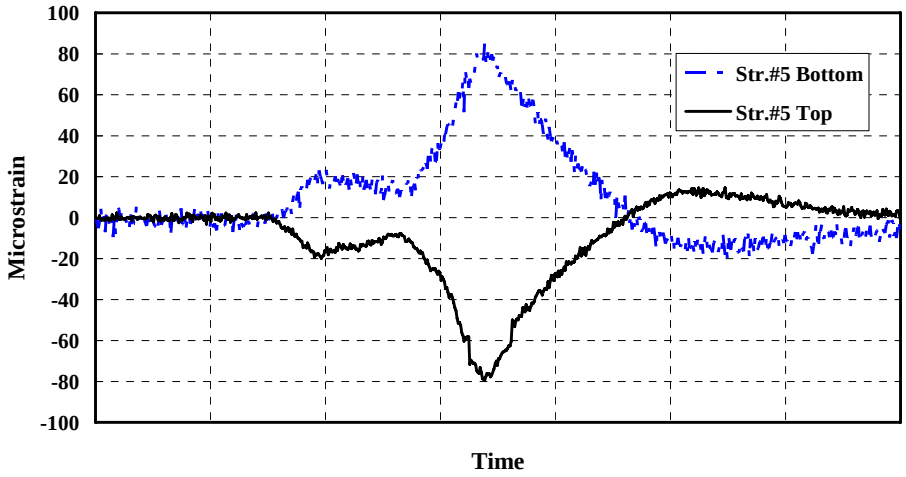

Figure 3.16 Top and bottom flange strains of Stringer #5 following load path 2

Table 3.5 Top and bottom flange average strains of Stringer #5

		Load Path 1	Load Path 2	Load Path 3	Load Path 4
Strain (με)	Stringer #5 Top	148	85	170	62
	Stringer #5 Bottom	150	80	175	55

3.2.4.2.3 Global FRP deck performance

The instrumentation plan at Location C and D is selected to measure the FRP deck strains at the soffit of the FRP deck, midway between stringers at various locations, as shown in Figure 3.11. The representative deck transverse and longitudinal strains at Location C between Stringer #3 and #4 following Load Path 3 are plotted in Figure 3.17. It was observed that the deck strains directly under truck wheels are a combination of both global and local bending. The local effects play an important role in the performance of FRP deck. Local effects make deck strains change rapidly when the wheels of loading truck pass the instrumented location. Also due to the local effects, the transverse strain (along traffic direction) of the deck changed from negative (compression) to positive (tension). This indicates that the cellular deck

system experienced double curvature when the wheel of a loading truck moving across the instrumented area.

The average peak longitudinal and transverse strains at Location C and D are summarized in Table 3.6. All deck strains recorded during field testing are included in Appendix D.1. The peak longitudinal strain on the bottom plate was 340 με, which is only 2% of the estimated ultimate strain of the bottom plate listed in Table 2.7. The peak transverse (traffic direction) strain was 330 με under the truck loading, which was nearly as high as the longitudinal strain at this load. This number is also consistent with the field testing results from Coleman's thesis (341 με, listed in Table 2.2). This number is smaller than the service strain of 501 με used in the Chapter 2 Stage II test, indicating that 501 με is a conservative service strain for Stage II test. Above results also show that the strain experienced in the material did not come close to reaching the ultimate strain in the material.

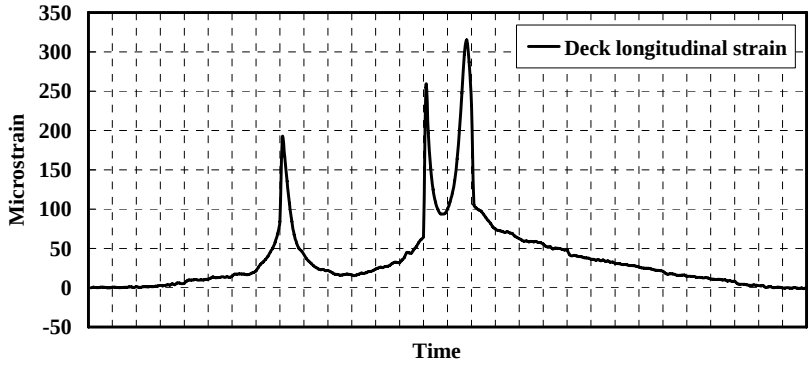

(a) Longitudinal Strain

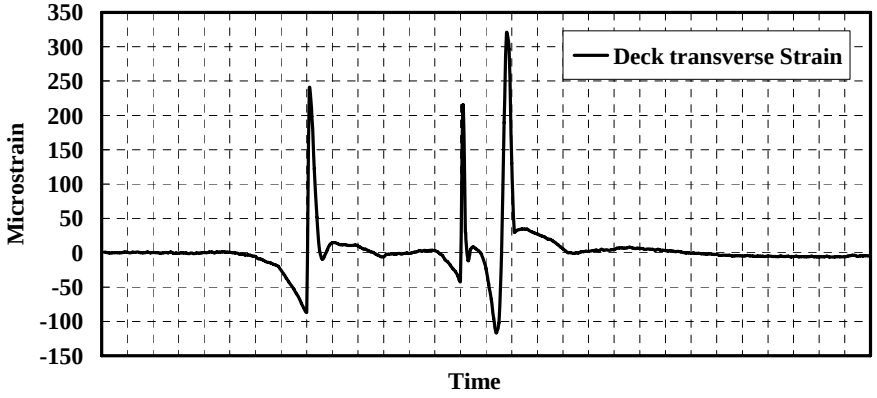

(b) Transverse Strain

Figure 3.17 Deck longitudinal and transverse strains at Location C between Stringer #3 and #4 following Load Path 6

Table 3.6 The average maximum longitudinal and transverse strains at Location C and D

		Maximum Strain (με)[1]	
		Transverse	Longitudinal
Location C	Between Stringer #3 and #4	330	310
	Between Stringer #4 and #5	260	N/A[2]
	Between Stringer #5 and #6	120	260
Location D	Between Stringer #3 and #4	320	340
	Between Stringer #4 and #5	N/A[2]	310
	Between Stringer #5 and #6	N/A[2]	250

Note: 1. Average maximum strain of five runs followed the control load path.
2. Strain gauges were either vandalized or not installed.

3.2.4.2.4 Performance of panel-to-panel connection

The development and evaluation of the adhesively-bonded panel-to-panel joint has been presented in chapter 2. The proposed FRP bridge deck was installed on the Hawthorne St. Bridge in August, 2006. A controlled live load field test has been conducted on the bridge after rehabilitation and the response of the adhesively bonded panel-to-panel connection is monitored and reported in this section.

There are ten panel-to-panel joints in this bridge. The instrumentation plan at Location D (Seam #10) is designed to measure the effectiveness of the adhesively bonded panel-to-panel connection. Two strain gauges were used to measure transverse strains at both sides of the joint at the soffit of the FRP deck, midway between stringers, as shown in Figure 3.11. If the panel-to-panel joint behaves as intended, then the longitudinal strains recorded on both sides of the joint should be about the same. Test results of the longitudinal strains at both sides of the joint between stringer #3 and #4 are shown in Figure 3.18. All other peak longitudinal strains at both sides of the joint are summarized in Table 3.7. Detailed data are included in Appendix D.1. The peak longitudinal strains at both sides of the joint are almost the same when front and back axles of the loading truck passed the joint, which indicate that the panel-to-panel joint is effectively transferring loads from one deck panel to the other. Due to the deck experiencing double curvature when the wheel of a loading truck moving across the area, transverse strains were found to be very sensitive to the exact location of both the gauge

and the applied loads, and more difficult to interpret. Due to their variability, such measurements are less suitable for performance assessment and will not be used in joint performance evaluation.

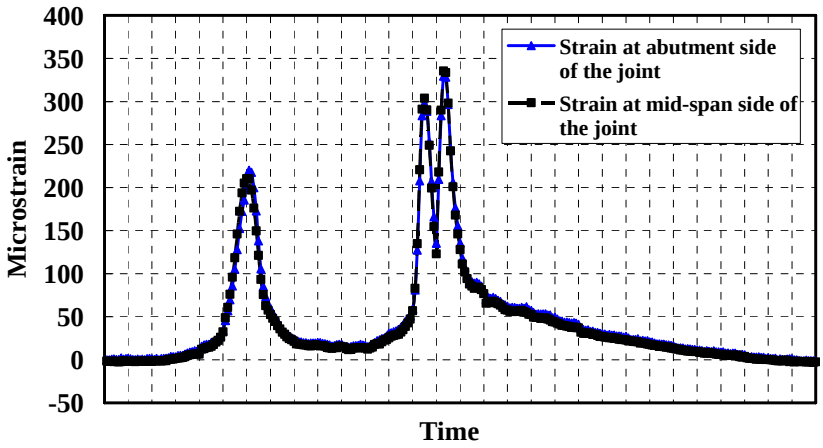

Figure 3.18 Longitudinal strain on both sides of the panel-to-panel joint

Table 3.7 Longitudinal strain on both sides of the panel-to-panel join

		Peak Longitudinal Strain (με)[1]	
		Rear tandem axle	Front axle
Between Stringer #3 and #4	Abutment side	250	150
	Mid-span side	240	110
Between Stringer #4 and #5	Abutment side	300	190
	Mid-span side	270	170
Between Stringer #5 and #6	Abutment side	340	220
	Mid-span side	330	210

Note: 1. Average maximum strain of five runs followed the control load path.

3.2.4.2.5 Load distribution factors

In the design of deck-on-steel-girder bridges, determination of the live load distribution is essential for the design of adequate and economical steel structures. LDFs allows engineers to predict the bridge response by treating the longitudinal and transverse effects as uncoupled since it takes a three-dimensional bridge system and reduces it to an equivalent two-dimensional structure. LDFs were calculated from the recorded strains on the stringers in the field test by assuming that the response of the bridge was elastic under each

load path. The distribution factor, DF was calculated as the ratio of the strain in a given stringer to the total strain of all the stringers.

All stringer strains measured under each load path during field test are included in Appendix D.2. Calculated DFs for the structure are shown in Table 3.8. From this table, it can be observed that the distribution factors for the 2-lane case are generally greater than those of the single truck; which indicates that the 2-lane case is critical for both the interior and exterior stringers.

Design equations provided in AASHTO Standard (AASHTO 2002) and LRFD (AASHTO 2004) specifications for determining the LDF are practical approaches for design deck-on-steel-girder bridges. However these equations only cover the conventional categories of reinforced concrete, wood and steel decks. No appropriate provisions from these specifications are available to determine the LDF of FRP deck-on-steel-girder bridges. To gain some insight about how existing design codes can be applied to FRP deck-on-steel-superstructure bridges, the FRP deck was assumed to behave similar to two types of decks contained as categories in both AASHTO specifications: (1) a 4000 psi compressive strength reinforced concrete deck of similar thickness supported by steel stringers; (2) a glue laminated wood deck of similar thickness on steel stringers; this allowed for a generic comparison of the AASHTO code predictions to results from field test.

The LDF from field and laboratory mock-up tests, code equations, and from lever rule are compared in Table 3.9. It should be note that the critical LDFs induced by superimposed load path 1+2 is more conservative than the real case as discussed earlier (less distance between two trucks, 2 ft-2 in. compared to 4 ft defined in AASHTO LRFD specification, which means more loads are distributed to interior stringers, i.e. larger LDFs). This reasoning is confirmed by comparing LDFs from field test with those from laboratory test (Table 3.9). The LDFs from field test are 2% and 6% larger than those from laboratory test at bridge mid-span and mid-span of the first bay, respectively, as expected.

It is also observed that both AASHTO code equations for a similar thickness concrete deck underestimate the LDF of the FRP deck. The Standard and LRFD equations produce a LDF from 20% to 28% and 2% to 12% less than the LDF from field results, respectively. However, both AASHTO equations for the category of glued laminated timber deck on steel girders give good estimations. The differences are within 12% (the actual difference is smaller

by considering the LDFs are more conservative as discussed earlier). This indicates that the FRP deck provides similar stiffness as a glued laminated timber deck rather than a concrete deck in the direction transverse to traffic.

Meanwhile it is observed that as a simplified method, the appropriately conservative LDF may be found using lever rule by assuming no load transfer across an interior girder (deck is hinged at each girder). This is in agreement with the finding from Moses et al. (2006). The lever rule produces a LDF from 0% to 11% larger than the LDF from field test.

The preceding discussion indicates that the FRP deck has a lower flexural stiffness in the primary direction (perpendicular to traffic direction) as compared to a similar depth concrete deck, which results in larger DFs for the FRP deck. The FRP deck can provide stiffness similar to a laminated timber deck. Both AASHTO LDFs for the category of glued laminated wood panels on steel stringers can give good estimations in design purposes. Also as a simplified method, appropriately conservative design DFs may be found using lever rule.

Table 3.8 Live Load Test Distribution Factors

Location	Load Path	Stringer number					
		Exterior			Interior		Exterior
		1	2	3	4	5	6
Bridge mid-span (B)	1	0.04	0.07	0.17	0.28	0.27	0.17
	3	0.03	0.05	0.14	0.26	0.26	0.23
	1+2	0.21	0.34	0.45	0.45	0.34	0.21
	3+4	0.27	0.33	0.41	0.41	0.33	0.27
Mid-span of the first bay (A)	1	0.03	0.08	0.19	0.31	0.20	0.18
	3	0.03	0.08	0.17	0.29	0.21	0.26
	1+2	0.21	0.28	0.50	0.50	0.28	0.21
	3+4	0.28	0.28	0.44	0.44	0.28	0.28

Note: Load path 2 and 4 are symetric path of 1 and 3, respectively; hence,not listed.

Table 3.9 Summaries of critical distribution factors

Location	Load Path	Field Test Results	Laboratory Mock-up Test Results / % difference	AASHTO Spec.for glued laminated timber deck[c] / % difference	AASHTO Standard (concrete deck)/ % difference	AASHTO LRFD (concrete deck)/ % difference	Level rule/ % difference
Bridge mid-span (B)	1+2	0.45[a]	0.44[b]/-2%	0.44 / -2%	0.36 / -20%	0.44 / -2%	0.50 / 11%
Mid-span of the first bay (A)	1+2	0.50[a]	0.47 / -6%	0.44 / -12%	0.36/ -28%	0.44 / -12%	0.50 / 0%

Note: a. Load Path 1+2.

b. At the mid-span of the second bay, not exactly at bridge mid-span.

c. Both AASHTO Specs use the same equations for the glued laminated timber deck on steel stringers.

3.2.5 Summary

Various design issues related to global structural performance of the FRP-deck-on-steel-superstructure system in laboratory and in field are investigated and discussed in this chapter. Following conclusions are drawn from this study:

1. The clip-type of panel-to-stringer connection provides little composite action as expected, which fulfilled the design intention.
2. The peak longitudinal strains (perpendicular to traffic direction) at both sides of the joint are almost identical when front and back axles of the loading truck passed the joint in the field test, which indicate that the panel-to-panel joint is effectively transferring loads from one deck panel to the other.
3. Neither AASHTO LDF equations for concrete deck systems are appropriate for the FRP-deck-on-steel-superstructure systems.
4. The FRP deck provides similar stiffness as a glued laminated timber deck rather than a concrete deck in the direction transverse to traffic. The AASHTO LDFs equations for the category of glued laminated timber deck on steel stringers can give good estimations on LDFs of FRP-deck-on-steel-girder bridges.
5. The lever rule can be used as an appropriately conservative design method to predict the LDFs of FRP-deck-on-steel-girder bridges.
6. The local effects play a important role in the performance of FRP deck. It makes the strains of the cellular type of deck system change rapidly and experienced transverse (traffice direction) double curvature when loading truck crossed the instrumented area.

However, the average peak longitudinal and transverse strains under truck loading did not even come close to reaching the ultimate strain in the material.

7. The live load deflection of the bridge in field test is approximately L/1270, which was within the deflection limit (L/800) specified in AASHTO LRFD Bridge Design Specification (AASHTO 2004).

CHAPTER 4 DESIGN RECOMMENDATIONS FOR FRP BRIDGE DECK SUPPORTED ON STEEL SUPERSTRUCTURE

4.1 Objectives

Because FRP decks typically have low modulus of elasticity, previous research has shown that their design is mostly driven by stiffness and not strength like traditional concrete deck (Bakis et al. 2002; Henry 1985; Karbhari and Zhao 2000; Temeles 2001; Zureick 1997). Therefore, the key design issue for FRP decks is the determination of deck relative deflection under live load to meet the required deflection limit. A detailed literature review shows that currently no such simplified structural analysis method with reasonable accuracy is available to design engineers. Complicated approximate orthotropic plate series solutions proposed by Qiao et al. (2000) and Salim et al. (2006) are not practical to design engineers. Finite element analysis (FEA) often requires specialized training, is time consuming and not always accessible to design engineers. Thus, there is a need for a simplified design procedure to predict the stiffness of FRP decks. This research seeks to extend the applicability of the strip method, an approximate method of analysis used within the AASHTO LRFD (AASHTO 2004) for the design of concrete, steel grid and wood decks to unconventional FRP deck systems. In the analysis, the deck is assumed to be subdivided into a series of strips perpendicular to the longitudinal support girders. In determining the strip widths, the effects of flexure in the secondary direction, shear and torsion effects are accounted for to obtain flexural force effects approximating those that would be provided by a more refined method of analysis. Once the strip width and stiffness are known, the strip is treated as a continuous beam and analyzed by classical beam theory. The supporting components are assumed to be infinitely rigid and the wheel loads are modeled as concentrated loads.

In the design of deck-on-steel-girder bridges, determination of the lateral load distribution is essential for the design of adequate and economical steel structures. Lateral load distribution factors (LDFs) allow engineers to predict the bridge response by treating the longitudinal and transverse effects as uncoupled since it reduces a three-dimensional bridge system to an equivalent two-dimensional structure. Although refined methods of analysis such as FEM and grillage have been proven to be the more accurate, they are usually time

consuming and not practical in the design phase. Design equations provided in AASHTO Standard (AASHTO 2002) and LRFD (AASHTO 2004) Specifications for determining the LDFs are used as the general approach for design deck-on-steel-girder bridges. However, these equations are only applicable to conventional bridge categories, such as reinforced concrete, wood and steel decks. No appropriate provisions in these specifications are available to determine the LDFs of FRP deck-on-steel-girder bridges. This research seeks to provide the appropriate LDF equations for bridge engineers to use for the implementation of FRP deck in bridges. Of particular interest is how existing design codes can be applied to FRP deck-on-steel-superstructure bridges.

The objective of this chapter is to address the above two design issues, namely deck relative deflection and LDFs and give design recommendations. To achieve this, three-dimensional (3-D) finite element (FE) simulations have been employed, since laboratory and field testing would be prohibitively expensive. The developed 3-D model has been verified using the results from laboratory tests and field measurements.

4.2 Strongwell FRP Deck System

The general information about Strongwell FRP deck is presented in Section 2.4.2 and not repeated here.

4.3 Bridge Finite Elment Model

A number of finite element bridge models were created and studied using the general-purpose finite element software package ANSYS® 9.0 (ANSYS 2004). A 3-D FE model using shell elements for the deck with eccentrically stiffened beam elements for the girder was selected for use. This model has been shown to give accurate results while retaining simplicity for practical use (Chan and Chan 1999; Chung and Sotelino 2006). The 8-node Mindlin type SHELL 93 element is selected in the present study to model the FRP deck with the one layer elastic equivalent plate (EEP) theory (Zhou 2002). Table 4.1 shows the material properties for the deck's top and bottom plates (Strongwell Inc. 2002), the equivalent material properties of the tube assembly and the equivalent orthotropic plate properties of the deck. The BEAM188

Element (three-node Timoshenko beam elements) was used to model the steel girders. The deck-to-girder non-composite action was modeled using constraint equations between mid-surface of the FRP deck and the centroid of the girders, which only consider the coupling at the vertical direction between a deck node and its corresponding beam node and is given by

$$U_z^g = U_z^d \qquad \text{Eq. 3.1}$$

where the superscripts g and d represent girder and deck, respectively; and U_z is the nodal displacement in the vertical direction. Girders are simply supported by pin-roller joints. Boundary conditions are assigned at the location where bearing exists. Figure 4.1 shows the developed FE model.

Two experiments are used for verification of the developed FE model. The first one is a two-bay full-scale laboratory investigation, which was conducted in the Structures Laboratory at Virginia Tech to ensure proper construction, serviceability, and strength of the FRP deck system used to rehabilitate an historical cast iron thru-truss bridge (Hawthorne St. Bridge in Covington, Virginia). Figure 4.2 gives an overview of the test setup and instrumentation plan. The six stringers (W14x34, transverse spacing of 4 ft on-center) and two floor beams (W14x120, supported by four pedestals that simulated the hangers in the through-truss bridge) are referred to as "Stringer #1" to "Stringer #6" and "Floor Beam #1" to "Floor Beam #2," respectively. Stringers and floor beams were joined together using moment resisting connections.

All instrumentation (strain gauges (Measurement Group CEA-06-500UW-350) and displacement transducers) was installed at cross-section A-A and B-B. Section A-A is located 7 ft-8 in. from the abutment, where the maximum live load moment of the first bay occurred. Section B is located at mid-span of the second bay. Strain gauges were mounted at the top face of the bottom flange for each stringer at all locations. In addition, displacement transducers (wire pots) were used to measure the vertical deflection of the six stringers and deflections of the FRP deck midway between the instrumented stringers. The symmetric, paired truck loading configuration followed HL-93 (AASHTO 2004) truck rear wheel weights and dimensions is applied at Section A-A and B-B by hydraulic actuators respectively, as shown in Figure 4.2.

Table 4.1 FRP deck material properties summary

Property[1]	Top Plate[2] (E^T)	Tube Assembly[3] (E^I)	Bottom Plate[2] (E^B)	Equivalent Deck[3] (E^e)
E_X (ksi)	1400	239	1400	368
E_Y (ksi)	1800	1002	1800	1088
E_Z (ksi)	1400	800	1400	840
G_{XY} (ksi)	623	66	623	128
G_{XZ} (ksi)	543	99	543	109
G_{YZ} (ksi)	611	788	611	763
ν_{xy}	0.31	0.33	0.31	0.33
ν_{yz}	0.31	0.33	0.31	0.33
ν_{xz}	0.29	0.1	0.29	0.12

1: X-longitudinal direction, Y-transverse direction, Z-vertical direction;
2: properties from design manual (Strongwell 2002);
3: Calculated equivalent elastic properties.

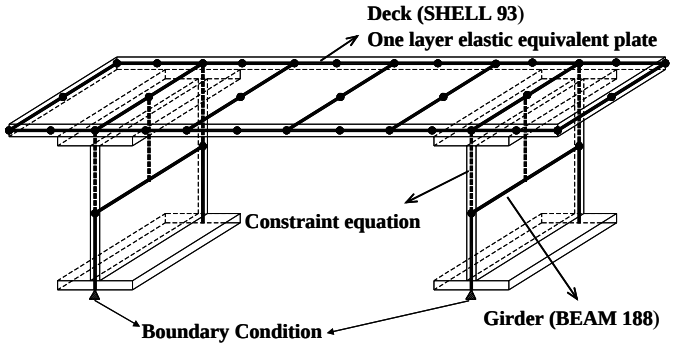

Figure 4.1 Finite Element Model

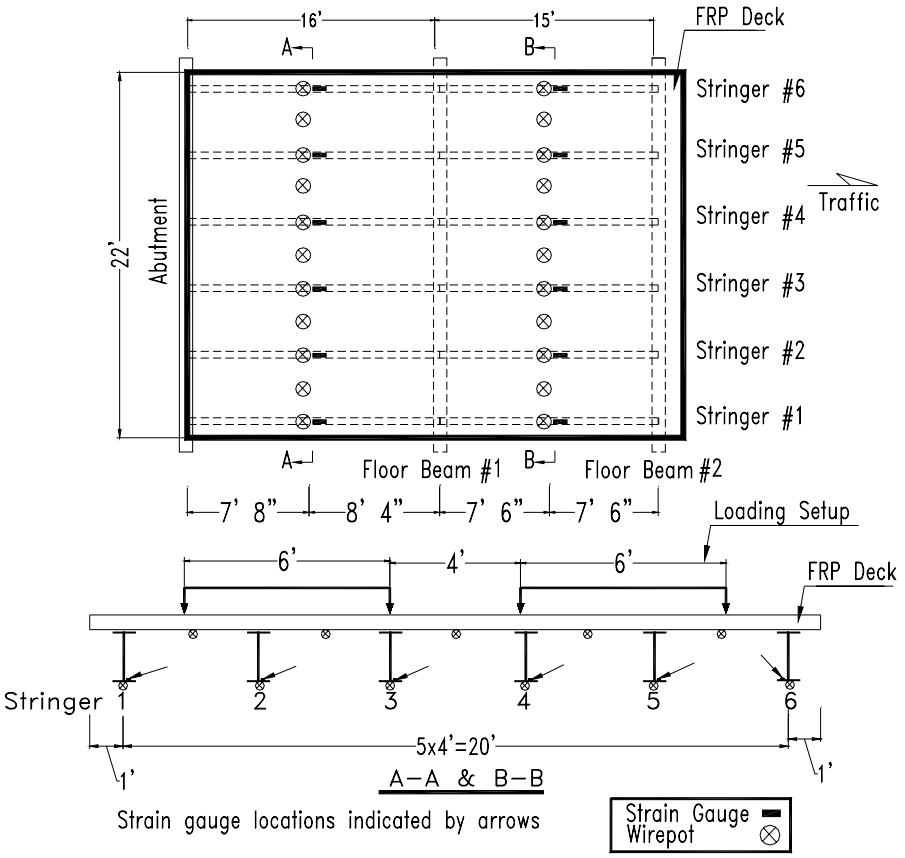

Figure 4.2 Test setup and instrumentation plan for a full-scale laboratory investigation.

The stringer bottom flange deflections and strains at Section A-A and B-B are plotted in Figure 4.3 and also listed in Table 4.2. It is observed that the FEM analytical results of stringer deflections show good agreement with the average lab measured deflections. The maximum difference between predicted and measured deflections is within 15%, as can be seen in Figure 4.3(a). The FE model is also able to accurately predict the strains in the stringers. In particular, for the center stringers (#3 and #4) where experience the largest strains, the FE model predicts the results within 10% of the measured values, as shown in Figure 4.3(b).

Since this study seeks to address the design issue concerning FRP decks, namely deck relative deflection, the capability of the FE model to predict deck relative deflections is also investigated. Values of the average measured and predicted deck relative deflections are shown in Table 4.3. The deck relative deflection is calculated as the difference between the deflection of the deck at mid-span of supporting stringers (under the loading patch) and a corresponding

reference deflection. The reference deflection is calculated as the average deflections of the two supporting stringers. As can be seen, the FEM results give reasonable predictions to the measured values with the predicted values being generally smaller than the measured ones. This is because the local behavior of the thin-walled cellular deck system under concentrated load, such as the patch load, can not be accurately predicted by the single layer EEP model. The EEP model is usually good at predicting deck deflection under distributed load. However these differences are considered not significant. Thus the EEP model can still be used as a practical method to calculate deck maximum relative deflections.

The FE model is further verified with the results from the field test conducted on the Hawthorne St. Bridge after rehabilitation. This historical cast iron thru-truss bridge has a 75 ft clear span with a roadway width of 21 ft-2 in. The same steel stringer, floor-beam and framing system are used as the two-bay full-scale laboratory investigation discussed earlier. The difference is that the bridge has five bays instead of two bays used in the laboratory characterization. Stringer displacements and strains at the top of the bottom flange at mid-span of the bridge were measured under several load paths using a tandem axle dump truck weighting 50 kips. For Load Path 1, the truck was located 2 ft-6 in. from the right curb and Load Path 2 is the symmetric case of Path 1 with the truck being 2 ft-6 in. from the left curb. The Load path 1+2 was not actually performed, but used to simulate 2-lane trucks being simultaneously loaded by superimposing results from load path 1 and 2. Details about the field tests can be found in Section 3.3.

The stringer displacement comparisons between the results from FE models and field test are shown in Figure 4.4 and listed in Table 4.4. The definitions of Load Paths are shown in Figure 3.13. The FE model generally gives good predictions, especially for center stringers (#3 and #4, where the maximum numbers exist). The deflection differences for Stringer #3 and #4 are within 10% for all load paths. The predicted strains are compared to those obtained from the field test in Figure 4.5. The correlations between calculated and average measured strains are overall very good. The maximum difference is within 13%. From above model verifications, it can be concluded that the one layer elastic equivalent plate with eccentric beam model, used in this study, predicts the global deck and stinger deflections and stringer strain within an acceptable level of accuracy.

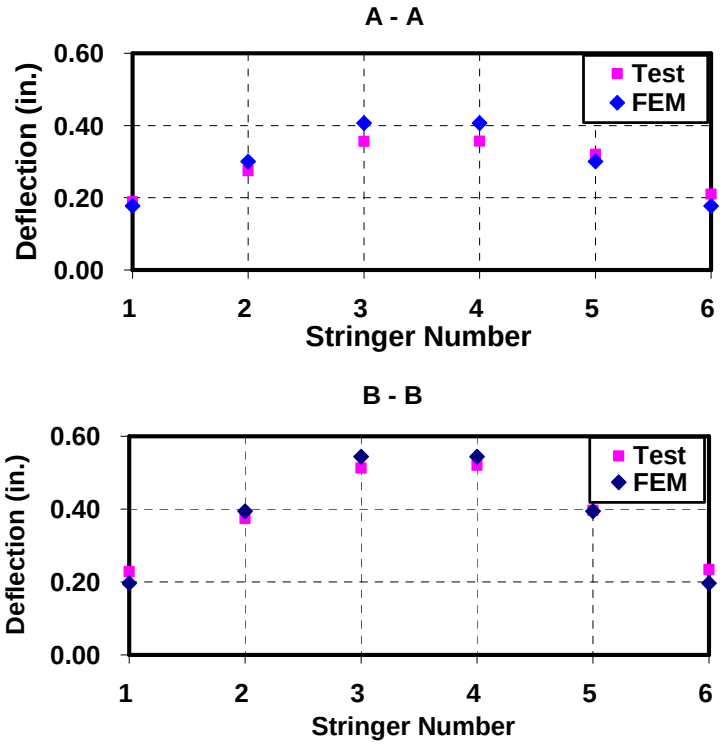

(a) Bottom Flange Deflection

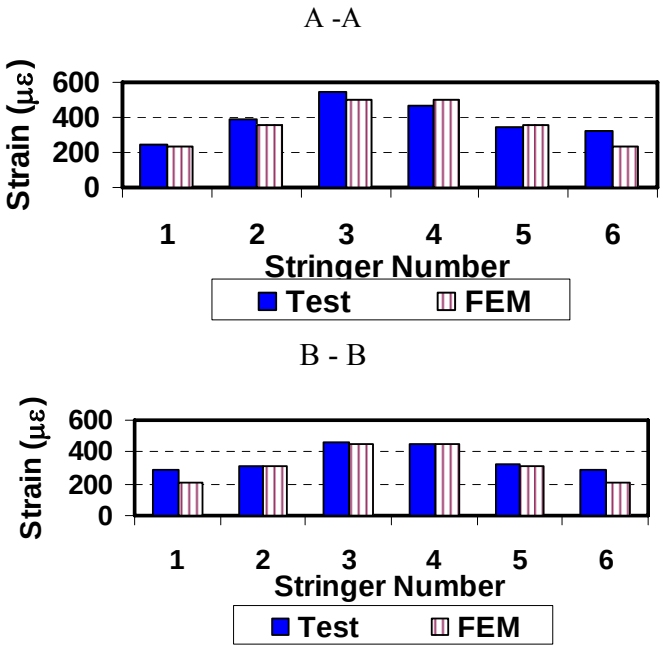

(b) Bottom Flange Strain

Figure 4.3 Comparison of FEM results to experimental measurements (mock-up test)

Table 4.2 Stringer deflections and strains: FEM vs. average experimental results (mock-up test)

Location	Stringer	Defelction (in.)			Strain (με)		
		Measured	FEM	difference (%)	Measured	FEM	difference (%)
A	1	0.189	0.181	-4	249	238	-4
	2	0.275	0.300	9	394	359	-10
	3	0.356	0.406	14	547	499	-10
	4	0.357	0.406	14	470	499	6
	5	0.321	0.300	-6	341	359	5
	6	0.210	0.181	-14	318	238	-33
B	1	0.228	0.200	-12	289	247	-17
	2	0.374	0.395	5	307	315	3
	3	0.513	0.544	6	464	446	-4
	4	0.521	0.544	4	446	446	0
	5	0.397	0.395	-1	328	315	-4
	6	0.234	0.200	-15	290	247	-17

Table 4.3 Deck relative deflection: FEM vs. average test results (mock-up test)

Section	Measured [a] (in.)	FEM (in.)	%difference
A-A	0.093	0.083	-11.6
B-B	0.102	0.087	-15.0

a. Average value at mid-span between Stringer #1 to #2.

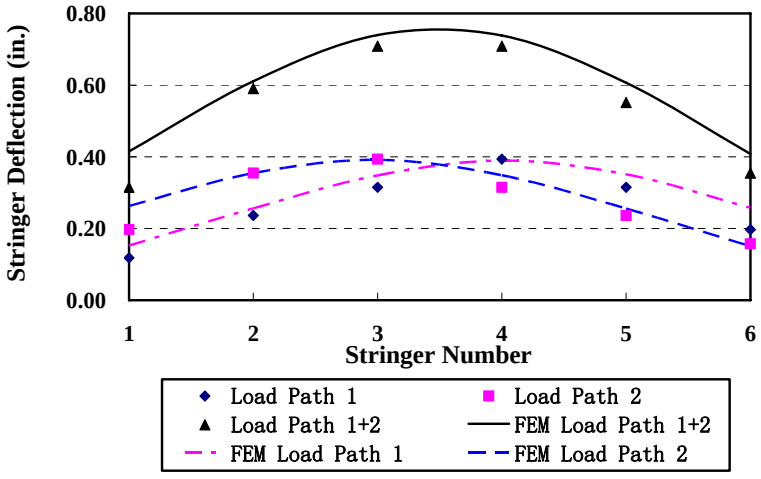

Figure 4.4 Comparison of Stringer deflections: FEM analysis vs. average field measurements

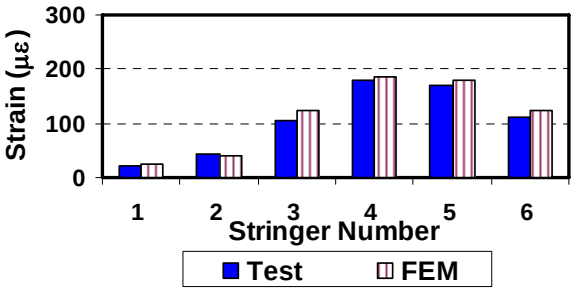

(a) Load Path 1

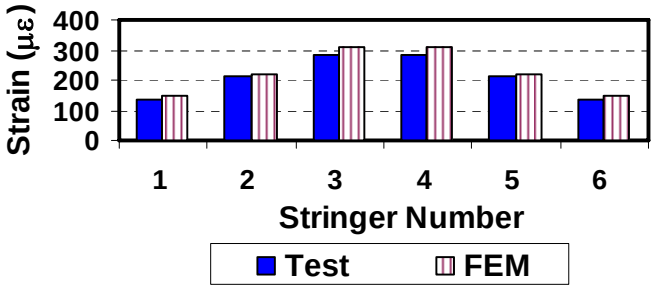

(b)Load Path 1+2

Figure 4.5 Comparison of Stringer strains: FEM analysis vs. average field measurements

Table 4.4 Stringer deflections and strains: FEM vs. average experimental results (field test)

Load Path	Stringer	Defelction (in.)			Strain (με)		
		Measured	FEM	difference (%)	Measured	FEM	difference (%)
1	1	0.118	0.152	22	23	23	4
	2	0.236	0.256	8	44	40	-9
	3	0.315	0.348	9	107	123	13
	4	0.394	0.390	-1	180	185	3
	5	0.315	0.351	10	170	180	5
	6	0.197	0.258	24	110	123	11
1+2	1	0.315	0.415	24	133	146	9
	2	0.591	0.611	3	214	220	3
	3	0.709	0.740	4	287	308	7
	4	0.709	0.738	4	287	308	7
	5	0.551	0.607	9	214	220	3
	6	0.354	0.408	13	133	146	9

4.4 FRP Deck Design – Deck Relative Defleciton

4.4.1 Design Procedures and its limitations for FRP Decks

FRP deck design is usually deflection controlled due to its relative low stiffness; therefore the design procedure is based on the serviceability limit state. Such a design procedure includes: 1) Determining the allowable deflection limit based on the serviceability design criteria; 2) Calculating the maximum deck relative deflection for the trial deck section under the worst live loading scenario and appropriate boundary conditions; 3) Changing deck stiffness by varying FRP deck components and support conditions until the maximum deck relative deflection can meet the limiting deflection. An alternative design procedure consists of setting the deflection equal to the limiting deflection and solving for the required stiffness for the deck. Then from the required stiffness, the FRP deck components can be selected.

The AASHTO LRFD Bridge Design Specifications (AASHTO 2004) has recommended limits of live load deflection for concrete, steel and wood construction, as shown in Table 4.5. The purpose of these limits are to provide rider comfort under vibrations induced by vehicular traffic, prevent excessive deflection causing problems with wearing surface and loosen connections between the beam and the deck. However, AASHTO does not establish deflection limitations for FRP decks. There is no current consensus on this deflection limit in the design of these systems. Composite bridges constructed for demonstration projects have been designed for allowable deflections from a range of L/425 to L/1,000 (Demitz et al. 2003). The cost of the structure increases with more restrictive design deflection limits, and thus makes using composites a less attractive option. However, if one can show that a less restrictive deflection limitation will provide the users of the bridge the similar level of comfort as a traditional bridge, the composite bridge can be a strong competitor to traditional bridges (Demitz et al. 2003).

To avoid excessive deflection causing problems with wearing surface and loosen connections between the beam and the deck, AASHTO (2004) [A2.5.2.6.2] outlines optional deflection limits in the design of timber decks (Barker and Puckett 1997). Since an FRP deck has similar stiffness, load distribution capability and similar deck-to-stringer connection system as a glued laminated timber deck, the limit of live load deflection for wood construction under vehicular and pedestrian loads (Span / 425) is considered to be also appropriate for FRP

deck application. To further justify the above argument, future research should focus on human tolerance on static deflection or dynamic motion due to vehicular traffic. Also, the proper deflection limit should be investigated with regard to any wearing surface applied on FRP deck. This is not the interest of this paper and will not be discussed here.

Table 4.5 Recommended limits of live load deflection in AASHTO LRFD Bridge Design Specifications

Steel, aluminum, and concrete construction	Vehicular load, general: Span/800 Vehicular and/or pedestrian loads: Span/1,000 Vehicular and/or pedestrian loads on cantilever arms: Span/375
Wood construction	Vehicular and pedestrian loads: Span/425 Vehicular load on wood planks and panels relative deflection between adjacent edges: 0.10 in.

A very important design step in both procedures is the calculation of the deck live load deflection to meet the required deflection limit. A detailed literature review shows that currently no simplified structural analysis method with reasonable accuracy for FRP decks is available to design engineers. Complicated approximate orthotropic plate series solutions proposed by Qiao et al. (2000) and Salim et al. (2006) are not practical. Finite element analysis (FEA) often requires specialized training, is time consuming and not always accessible to design engineers. Thus, there is a need for a simplified design procedure to predict the stiffness of the FRP deck.

4.4.2 Strip Method

The strip method is an approximate method of analysis specified in Article 4.6.2.1 of AASHTO LRFD Specification (AASHTO 2004) for the design of concrete, steel grid and wood decks. The deck is assumed to be subdivided into a series of strips perpendicular to the longitudinal support girders. In determining the strip widths, the effects of flexure in the secondary direction, shear and torsion effects are accounted for to obtain flexural force effects

approximating those that would be provided by a more refined method of analysis. Once the strip width and stiffness are know, the strip is treated as continuous beams and analyzed by classical beam theory. The supporting components are assumed to be infinitely rigid and the wheel loads are modeled as concentrated loads. As shown in Table 4.6, for cast in place reinforced concrete decks, the strip widths are based on the girder spacing (S) and the distance from the load to the point of support (X). For stress-laminated wood decks, strips widths are based on girder spacing (S) and categorized by the parallel and perpendicular directions to the traffic.

Table 4.6 Equivalent Strip (unit: in.)

Deck Type	Equivalent Strip Width
Concrete (cast in place)	Overhang: $45.0+10.0X$ M^+: $26.0+6.6S$ M^-: $48.0+3.0S$
Wood (Stress-laminated)	Parallel: 0.8S+108.0 Perpendicular: 10.0S+24.0

This research seeks to extend the applicability of the strip method to FRP decks. Similar to wood deck, the strip width W is based on the deck relative deflections. This is different from strip width determination for concrete deck, which is based on stresses inside the deck. The deck relative deflections of FRP decks are investigated through an extensive parametric study using FE model discussed previously to collect experimental data. The outcome of this study is a procedure that enables the determination of equivalent strip widths for FRP decks. The study is described in detail in the following section.

4.4.3 Parametric Study and Strip Width Determination

A total of 60 different bridge models were developed and investigated. Each model has a specific combination of girder span, spacing and stiffness. The girder span of these models ranges from 15 ft to 50 ft and girder spacing ranges from 4 ft to 8 ft. These are considered to be typical spans and spacings for current FRP bridge deck application. Two values of girder stiffness were investigated. The lower bound is the minimal required girder stiffness which corresponds to a global girder deflection of L/800 (L is girder span) as

specified in AASHTO LRFD Specification (AASHTO 2004). The higher bound is an infinitely stiff girder, which corresponds to the case where the supporting girders do not deflect. The FRP decks were designed for non-composite action and continuously supported by the girders.

All steel girders are simply supported, equally spaced and loaded with HL-93 loading (AASHTO 2004). To apply the worst-case scenario and get the maximum deck relative deflection, three loading cases were investigated for each model. The first and second case are one wheel of a truck loading located on the 0.4 span length and mid-span of the first span (between girder 1 and 2), respectively. The third case is one wheel located on the mid-span of the second span (between girder 2 and 3). All cases were intended to find the critical deck relative deflections. In the longitudinal (traffic direction), the middle axle with 42.6 kips load (include the impact factor) was set directly on the mid-span of the girders.

The results from the parametric study are summarized in Figure 4.6 (only shows 4 ft, 6 ft and 8 ft spacing cases for clear comparison). It can be observed that with increase in girder spacing, the deck relative deflection increases significantly. The increase of the girder span reduces the deck relative deflection (Figure 4.6). This seems reasonable since the longer girder span the larger deck area to resist the load, thus leading to smaller deck deflection. However, when the span lengths reach around 25 ft, the deck relative deflections only vary within a small range for all cases. With smaller girder spacing, the effect of girder span on deck relative deflection is, thus, less significant. Also from the figure, it becomes evident that increasing the girder stiffness reduces the deck relative deflection, as expected.

From the parametric study presented previously, it can be concluded the largest contributor to the deck relative deflection in FRP deck-on-steel-girder bridges is girder spacing with lesser contributions from parameters such as span length, and girder stiffness. In order to simplify the design process, the equation for deck strip width is considered to be a function only of girder spacing (S). The critical deck relative deflections are conservatively picked from the upper bound of all deck relative deflections with the same girder spacing, as shown in Figure 4.6.

Based on the critical deck relative deflections from the parametric study, the width of the equivalent strip of a deck for specific girder spacings are extracted and the results are plotted in Figure 4.7. A second polynomial equation is used to curve fit the data points. The equation is listed as following:

$$W = 0.0046S^2 - 0.47S + 28 \qquad \text{Eq. 3.2}$$

S: Girder spacing (in).

This equation is proposed as the strip width equations for determining the deck relative deflections of this type of FRP deck.

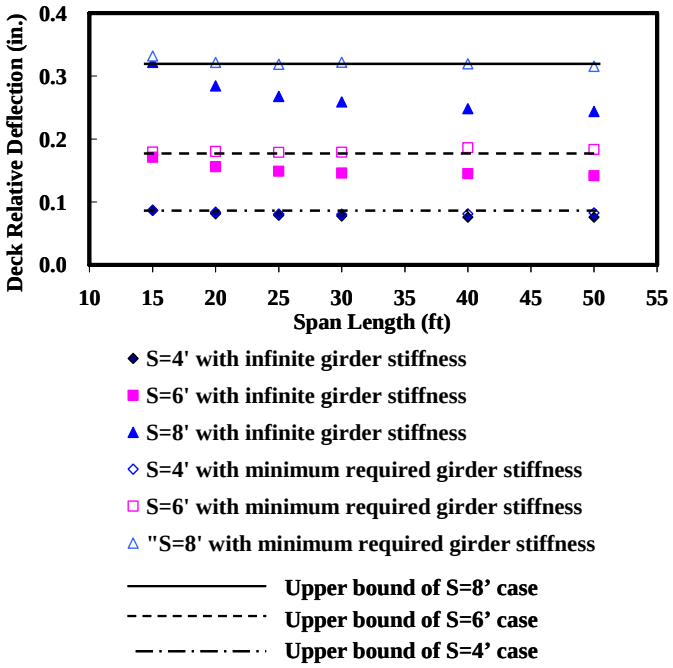

Figure 4.6 Deck relative deflection comparison

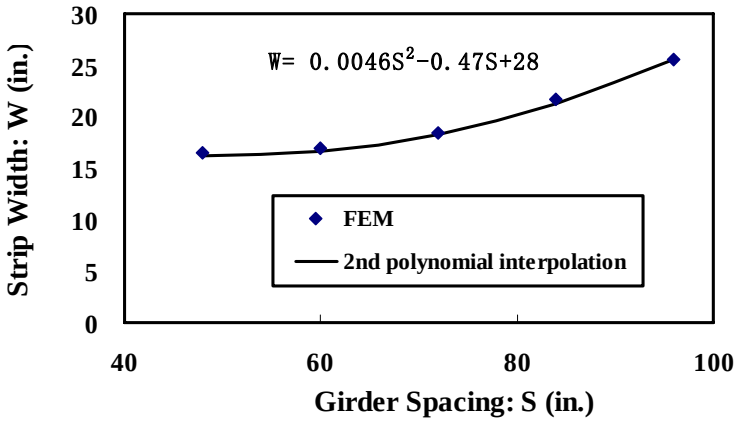

Figure 4.7 Strip width curve fit

4.4.4 Example: Live Load Deflection Determination

The previous sections have already investigated how to choose the proper strip width to account for the effects of flexure in the secondary direction, of shear on the deformation in both directions and of torsion on the distribution of internal force effects without using more refined methods of analysis.

This example shows the steps necessary to determine FRP deck relative deflections. Step 1: choose FRP deck system including deck thickness and girder spacing; Step 2: Determine equivalent deck strip width by using Eq. 3.2; Step 3: Calculate equivalent Young's modulus for the FRP deck in the transverse direction (perpendicular to traffic direction); Step 4: The strip is treated as continuous beams and analyzed by classical beam theory. The supporting components will be assumed to be infinitely rigid and the wheel loads are modeled as concentrated loads.

Step 1:

Choose 6.75 in. deck and the spacing for five equally spaced supporting girders is 4 ft. HL-93 Loading (21.3 kips per wheel).

Step 2:

For 6.75 in. thick deck, use Eq. 3.2.

Strip width $W= 0.0046S^2 - 0.47S + 28 = 0.0046*(48)^2 - 0.47*(48) + 28 = 16$ in.

Step 3:

The equivalent Young's modulus for the FRP deck in the transverse direction (perpendicular to traffic direction) can be reasonably obtained from the deck components' properties (Table 4.1). The equivalent Young's modulus E_{11} and moment of inertia for two types of Strongwell's FRP decks are listed in Table 4.7.

Table 4.7 Equivalent Young's modulus E_{11} and moment of inertia for Strongwell's FRP deck

Material Properties of 6.75 in. thick deck	
E_{11}(ksi)	1088
I(in^4)	25.6

Step 4:

The supporting girders are assumed to be infinitely rigid and the wheel loads are modeled as concentrated loads. The critical live load deck deflection occurs when the left wheel is near the mid-span of the first bay, that is, 2 ft from girder 1.

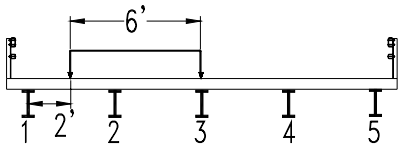

Figure 4.8 Design truck positioned for maximum deck relative deflection

The strip is treated as a continuous beam and analyzed by classical beam theory. If only the first bay is considered to be simply supported, the simple beam deflection is:

$$\Delta = \frac{PS^3}{48EI} = \frac{(\frac{21.3}{16})(1.2)(48)^3}{48(1088)[\left(\frac{1}{12}\right)(6.75)^3]} = 0.132\ in.$$

Note the design truck HL-93 wheel load include IM factor, which is 21.3 kips as discussed before. The multiple presence factor of 1.2 is included per AASHTO LRFD Bridge Design Specification (2004).

Next the deflection due to the continuity moments is determined. The continuity moments are calculated with the aid of the influence coefficients in Appendix A in "*Design of Highway Bridges*" (Barker and Puckett 1997).

The moment over girder 2 is

$$M_{LL} = 21.3kips(-0.1004)(S = 48in.) + 21.3kN(0)(S = 48in.) = -102.7\ kips\text{–}in$$

In 1in width:

$$m_{LL}^2 = \frac{-102.7\ kips\ in.}{16\ in.} = \text{-6.4 kips in.}/in.$$

The deflection due to the continuity moments is

$$\Delta = \frac{S^2}{16EI}[m_{LL}^1 - m_{LL}^2] = \frac{(48)^2}{16(1088)[\left(\frac{1}{12}\right)(6.75)^3]}[0-(-6.4)](1.2) = 0.04\ in.$$

Note m_{LL}^{1} is moment over girder 1, equal zero. This equation can be found as Eq. 9.32 in "*Design of Highway Bridges*" (Barker and Puckett 1997). The multiple presence factor of 1.2 is also included.

The total deck relative deflection is

$\Delta = 0.132 - 0.04 = 0.092\ in.$

Step 5:

This span/deflection ratio = 48 in. / 0.092 in. = 522.

The 4-ft stringer spacing indicates an L/522 response at design service load. It did not meet the desired deflection index of less than L/800, which is the recommended limit of live load deflection for steel, aluminum and concrete construction by AASHTO LRFD Bridge Design Specifications (AASHTO 2004). However, it could meet the recommended deflection limit for wood construction (L/425).

4.4.5 Comparison: values from strip methods vs. laboratory measurements

Based on the strip width equations (Eq. 3.2) provided in the preceding discussion, deck relative deflections for different girder spacings are calculated as continuous beams with concentrated loads pattern. Results from calculation and laboratory measurements (if available) are listed in Table 4.8 for comparison. By comparing these values, it is observed that the deck relative deflections from strip method generally show good agreement with the lab measurements for the cases when lab measurements are available.

It should be noted that although the above study is only based on a single FRP deck type (Strongwell FRP Deck), it gives a general approach, which can be used for other type of FRP deck systems. Different strip width equations can be determined following the same procedures presented in this study. It can be concluded that the strip method specified in AASHTO LRFD specification (AASHTO 2004) as an approximate method of analysis for the design of concrete, steel grid and wood decks can also be applied to unconventional FRP decks as a practical method in conjunction with the proposed strip width equation.

Table 4.8 Deck relative deflection: strip method vs. laboratory measurement

Girder spacing ft.	Deck relative deflection (in.)	
	Strip method Second Polynomial	Lab measurement
4	0.092	0.087 to 0.105[a]
6	0.193	N/A
6. 5	0.220	0.165 to 0.193[b]
8	0.339	N/A

a. from the two-bay laboratory test dicussed earlier (Table 3.1), data scatter due to different axle orientations

b. from Zhou et al. 2005, data scattered due to different locations and under different loading patches (steel patch and rubber patch).

4.5 Steel Girder design - Load Distribution Factor

4.5.1 Need for research

In the design of deck-on-steel-girder bridges, the determination of the lateral load distribution factor is essential for the design of adequate and economical steel girders. LDFs allow engineers to predict the bridge response by treating the longitudinal and transverse effects as uncoupled, since it reduces the three-dimensional bridge system into an equivalent two-dimensional structure. Although refined methods of analysis such as FEM and grillage analysis have been proven to be the more accurate, they are usually time consuming and not practical in the design phase. Design equations provided in AASHTO Standard (AASHTO 2002) and LRFD (AASHTO 2004) specifications for determining the LDF are the general practical approach for the design of deck-on-steel-girder bridges. However, these equations only cover conventional decks, i.e., reinforced concrete, wood and steel decks. No appropriate provisions from these specifications are available to determine the LDF for FRP deck-on-steel-girder bridges. This research seeks to provide the appropriate LDF equations for bridge engineers to use for the implementation of FRP deck in bridges.

4.5.2 LDF equations in current provisions

To gain some insight into how existing design codes can be applied to FRP deck-on-steel-superstructure bridges, the FRP deck was assumed to behave similarly to two types of

decks contained as categories in both AASHTO specifications: (1) a 4000 psi compressive strength reinforced concrete deck of similar thickness supported by steel stringers; (2) a glue laminated wood deck of similar thickness on steel stringers; this allowed for a generic comparison of the AASHTO code predictions to the results from a FEM parametric study.

Equations specified by both AASHTO bridge design specifications to calculate LDF for interior stringers are summarized in Table 4.9. Due to the relative low modulus of FRP deck, only short deck overhangs are typically used in FRP deck applications (the overhang was, thus, assumed to be 12 in. all the model bridges throughout this study). Therefore, the distribution factors for exterior stringers are generally smaller than those for interior girders, which do not control the design and thus are not discussed here. In Table 4.9, all LDF values are normalized as the percentage of a lane load (total truck load) resisted by the most heavily loaded stringer and the multiple presence factors are included in the approximate equations for one lane traffic case. It can be observed that both AASHTO specifications use the same equations for the category of glued laminated timber deck on steel stringers.

4.5.3 Parametric study

Four different models, named M1 to M4, are developed and investigated. Each model has a different girder spacing and span. All models have six wide flange steel girders which are simply supported. To apply the worst-case scenario and obtain meaningful LDFs, three loading cases are investigated for Model M1 and M3 (Figure 4.9 (a)), five loading cases for Model M2 and M4 (Figure 4.9 (b)) with all cases using HL-93 truck axle loads. In the traffic direction, the mid-axle is located at the mid-span of the girders for all cases to get the maximum moment at mid-span. The front axle, middle axle and rear axle are 11 kips, 42.6 kips, and 42.6 kips, respectively, which include the impact factor (33%) as defined in AASHTO LRFD Bridge Design Specification (2004). The distances between front axle, middle axle and rear axle are 14 ft, respectively.

Table 4.9 Summary of equations for calculating interior girders' LDFs

Spec.	Type	Lane	DF	Range of Applicability
AASHTO Standard	Concrete deck on steel I beam stringers	One lane traffic	S/11.7	S<10, otherwise lever rule
		Two or more traffic lanes	S/11.0	S<14, otherwise lever rule
	glued laminated wood panels on steel stringers with 6"or more thickness	One lane traffic	S/8.8	S<5.5, otherwise lever rule
		Two or more traffic lanes	S/9.0	S<7, otherwise lever rule
AASHTO LRFD	Concrete deck on steel I beam stringers	One lane traffic	$0.06+\left(\frac{S}{14}\right)^{0.4}\left(\frac{S}{L}\right)^{0.3}\left(\frac{K_g}{12.0Lt_s^3}\right)^{0.1}$	$3.5\le S\le 16.0$ $4.5\le t_s\le 12.0$ $20\le L\le 240$ $N_b\ge 4$ $10{,}000\le K_g\le 7\times 10^6$
		Two or more traffic lanes	$0.075+\left(\frac{S}{9.5}\right)^{0.6}\left(\frac{S}{L}\right)^{0.2}\left(\frac{K_g}{12.0Lt_s^3}\right)^{0.1}$	
	glued laminated wood panels on steel stringers	One lane traffic	S/8.8	$S\le 6$
		Two or more traffic lanes	S/9.0	

Note: 1. S = spacing of beams (ft);

2. L = span of beam (ft);

3. t_s =depth of concrete slab (in.);

4. $K_g = n(I + Ae_g^2)$, in which $n = \frac{E_B}{E_D}$ where E_B=modulus of elasticity of beam material (ksi); E_D= modulus of elasticity of deck material (ksi); I= moment of inertia of beam (in^4); e_g=distance between the centers of gravity of the basic beam and deck (in.); A= area of beam (in^2).

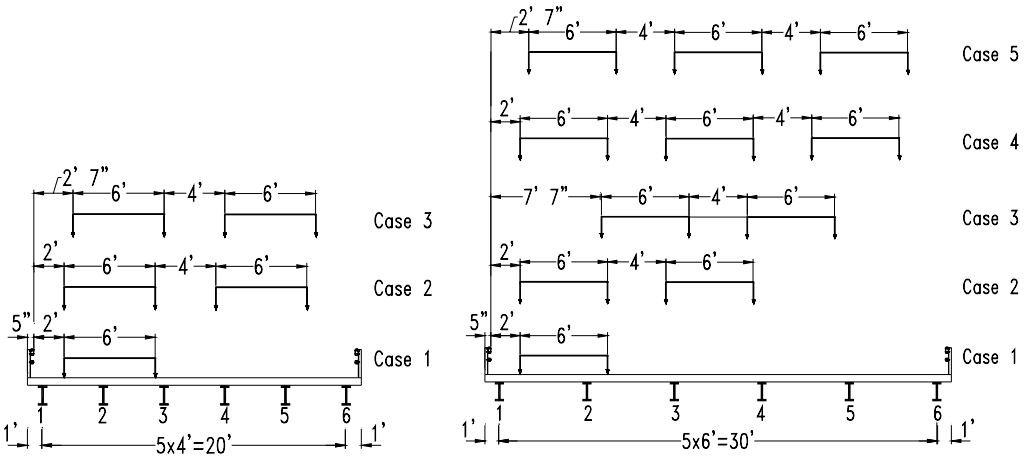

(a) Model M1 and M3 (b) Model M2 and M4

Figure 4.9 Loading cases for model M1 to M4

The FRP decks in the models were of the same type as the one discussed in Section 2.4.2 and were designed with no composite action with supporting girders. The span, spacing and girder type are shown in Table 4.10. For these four models, the spans ranged from 30 ft to 60 ft and girder spacings ranged from 4 ft to 6 ft. Girder spacings larger than 6 ft, such as 8 ft were not considered since they would result in large deck relative deflection, as shown in Figure 4.6 (as high as L/290, where L is girder span). Also, the girder sizes (stiffness) are chosen to meet the global girder deflection limit of L/800 as specified in AASHTO LRFD Specification (2004).

Table 4.10 Bridge models used to investigate LDFs

Model Name	M1	M2	M3	M4
Span	30 ft	30 ft	60 ft	60 ft
Spacing	4 ft	6 ft	4 ft	6 ft
Girder Size	W24x55	W24x94	W24x76	W24x103

The comparisons between the LDFs obtained from FEM, code equations, and from lever rule are shown in Figure 4.10 and listed in Table 4.11 for the four bridge models. It is observed that both AASHTO code equations for a similar thickness concrete deck underestimate the LDF of FRP decks. The Standard and LRFD equations produce LDFs 15% to 20% and 4% to 20% lower than the LDF obtained from FEM, respectively. However, both

AASHTO equations for the category of glued laminated timber deck on steel girders give good estimations with the differences within 4%. This can be attributed to the fact that the modulus of elasticity of the FRP deck is closer to that of a glued laminated timber deck than that of a concrete deck in the direction transverse to traffic. The equivalent E_Y =1088 ksi for FRP deck (shown in Table 4.1) is 99% to 66% of E_Y for glued laminated timber deck (E_Y =1100-1650 ksi for different types of glued laminated timber decks (Barker and Puckett 1997)) and is only 28% of E_Y =4020 ksi for a 4000 psi compressive strength reinforced concrete deck. E_Y is the modulus of elasticity of decks perpendicular to the traffic direction. Meanwhile it is observed that as a simplified method, the appropriately conservative LDF may be found using lever rule by assuming no load transfer across an interior girder (deck is hinged at each girder). This is in agreement with the findings from Moses et al. (2006). The lever rule produces a LDF from 3% to 16% larger than the LDF obtained from FEM. Another noteworthy point is that the girder span has much less influence on the LDF compared to the girder spacing, as shown in Figure 4.10.

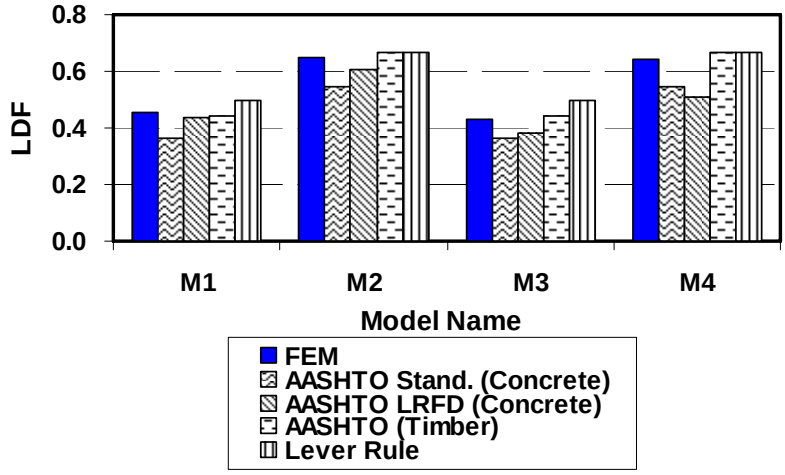

Figure 4.10 Comparison of LDFs: FEM results vs. design estimations

The measured data from the full-scale laboratory test and field test discussed earlier further confirms the above findings as seen in Table 4.12. Design values are 6% smaller and 0% larger than the critical tested values at Section A-A and B-B in the laboratory test. For these sections, the lever rule produces a reasonable and appropriately conservative method to

predict LDFs. Design values are 6% and 14% larger than critical tested values at Section A-A and B-B. In field test, the predicted LDFs are 0-7% larger than the critical tested values at mid-span of the first bay and mid-span of the bridge. The lever rule is a little conservative giving 14% to 22% larger than the tested values at these two locations.

Table 4.11 LDFs: FEM results vs. design estimations

Model Name	M1	M2	M3	M4
FEM	0.46	0.65	0.43	0.64
AASHTO Stand. (concrete)	0.36	0.55	0.36	0.55
% difference	-20	-16	-15	-15
AASHTO LRFD (concrete)	0.44	0.61	0.38	0.51
% difference	-4	-6	-12	-20
AASHTO Spec.(Timber)	0.44	0.67	0.44	0.67
% difference	-2	3	3	4
Lever Rule	0.50	0.67	0.50	0.67
% difference	10	3	16	4

The preceding discussion indicates that the FRP deck has a lower flexural stiffness in the primary direction (perpendicular to traffic direction) as compared to a similar depth concrete deck, which results in larger DFs for the FRP decks. FRP decks have stiffness similar to laminated timber decks. Both AASHTO LDFs for the category of glued laminated wood panels on steel stringers provide good estimations for design purposes. Also as a simplified method, the appropriately conservative design DFs may be found using lever rule.

Table 4.12 Summaries of critical distribution factors (interior stringers)

Location		Test Results[a]	AASHTO Spec.for glued laminated timber deck / % difference	Lever rule/ % difference
Full scale laboratory test	A	0.47	0.44 / -6%	0.5 / 6%
	B	0.44	0.44 / 0%	0.5 / 14%
Field test	Midspan of the bridge	0.41[b]	0.44 / 7%	0.5 / 22%
	Midspan of the first bay	0.44[b]	0.44 / 0%	0.5 / 14%

Note: a. LDF is calculated as the ratio of the strain in a given stringer to the total strain of all the stringers.
b. LDF under Load Path 3+4, similar to AASHTO LRFD HL-93 2-lane case.

4.6 Summary

In this research, an extensive parametric study was conducted to examine the structural behavior of FRP deck-on-steel-superstructure systems. Based on the FEM results, two design issues concerning the FRP decks, namely deck relative deflection and LDF of supporting steel girders, are investigated. The following findings can be drawn from this study.

1. The strip method specified in AASHTO LRFD specification (AASHTO 2004) as an approximate method of analysis for the design of concrete, steel grid and wood decks can also be applied to unconventional FRP decks as a practical method. However, different strip width equations have to be determined by either FEM or experimental methods for different types of FRP decks. In this study, one such an equation has been derived for the Strongwell deck.
2. Both AASHTO code equations for a similar thickness concrete deck underestimate the LDF of FRP deck-on-steel-superstructure systems (up to 20% lower than the LDFs obtained from FEM). This may be due to the fact that flexural stiffness of an FRP deck in the primary direction (perpendicular to traffic) is much smaller than that of a concrete deck with similar thickness.
3. Both FEM results and experimental measurements show that the AASHTO LDFs equations for glued laminated timber decks on steel stringers provide good estimations of LDFs for FRP-deck-on-steel-girder bridges. This is because the FRP deck in this study has similar stiffness to a laminated timber deck. These equations are recommended as a practical method in determining LDFs of this type FRP-deck-on-steel-superstructure bridges.
4. The lever rule can be used as an appropriately conservative design method to predict the LDFs of FRP-deck-on-steel-girder bridges. This is in agreement with the finding from Moses et al. (2006).
5. No secondary elements, such as bracing and parapets, were considered in this study. Since these elements generally help the transverse distribution of moment and result in smaller LDFs, the above methods will produce conservative LDFs.
6. The above conclusions are based on non-composite behavior between FRP deck and girders. Because the composite behavior in FRP deck-on-steel-superstructure bridges will degrade with time and can not be considered in the strength limit states (Moses et al. 2006;

Zhang and Cai 2006), the above methods may be used in a long-term basis and for conservative design purposes.

The reader should be cautioned that this research is based on a single FRP deck type (Strongwell FRP Deck). Different deck systems may exhibit different behavior and the application of the present results would need to be investigated thoroughly.

CHAPTER 5 CONCLUSIONS AND RECOMMENDATIONS FOR FUTURE RESEARCH

5.1 Conclusions

The purpose of this research is to develop and investigate the performance of an FRP deck system (Strongwell Decks) used to rehabilitate the Hawthorne St. Bridge in Covington, Virginia. Based on the findings of this research, the author seeks to address some of the technical needs and questions to advance FRP deck application. The desired goals of the research are as follow:

1. Develop an effective panel-to-panel connection in a four-stage study and investigate the performance and failure mechanism of the final-proposed adhesively-bonded tongue-and-groove, panel-to-panel connection under service, strength and fatigue loads. Explore various issues related to constructability of FRP deck systems. Establish construction and installation procedures for this adhesively bonded panel-to-panel connection.
2. Monitor and examine global structural performance of the FRP-deck-on-steel-superstructure system both in laboratory and in field. Various issues concerning design of the FRP-deck-on-steel-superstructure bridges are investigated, such as global structural deflections and strains, effectiveness of the clip-type deck-to-stringer connections and load distribution factors under service load.
3. Address two important design issues concerning the FRP deck design, namely deck relative deflection and steel structure design, i.e. LDF of supporting steel stringers based on the extensive experimental investigation and FE study. Provided relevant practical design recommendations to help design engineers to overcome any reluctance to adopt FRP decks due to limited experience and design approaches.

Chapter 1 is the introduction and literature review of the research, which briefly introduces the general background, status and technologies in FRP bridge deck application. The objectives and needs for research are also provided in this part.

Chapter 2 presents four-stage development and evaluation of an adhesively-bonded panel-to-panel connection for the FRP bridge deck system to rehabilitate the Hawthorne St. Bridge. The panel-to-panel connections were finally accomplished using full width, adhesively

(structural urethane adhesive) bonded tongue and groove splices with scarfed edges. Test results showed that no crack initiated in the joints under service load and no significant change in stiffness or strength of the joint occurred after 3,000,000 cycles of fatigue loading.

In Chapter 3, various design issues related to global structural performance of the FRP-deck-on-steel-superstructure system in laboratory and in field are investigated and discussed, which included global structural deflections and strains, effectiveness of the clip-type deck-to-stringer connections and load distribution factors under service load.

In Chapter 4, an extensive FEM parametric study was conducted to examine two design issues concerning the FRP deck design, namely deck relative deflection and steel structural design, i.e. LDF of supporting steel stringers. The design recommendations for FRP bridge deck supported on steel superstructure are provided to help design engineers to overcome any reluctance to adopt FRP decks due to limited experience and design approaches.

The present chapter briefly summarizes contributions of this research including the notable conclusions in each of the areas of study and provides recommendations for future research in this field.

5.1.1 Development and Evolution of an Adhesively-bonded Panel-to-panel connection for an FRP Bridge Deck System

The following conclusions can be drawn from the four-stage study on the development and evolution of an adhesively-bonded, panel-to-panel connection for an FRP bridge deck system.

1. The findings from Stage I research show that although mechanical connections have the advantage of easy disassembly for repair, adhesively-bonded connections are more efficient in load transfer and fatigue resistance and are easier and cheaper to construct. Thus Stages II through IV research focus on developing and evaluating a redesigned adhesively-bonded tongue and groove joint.
2. Stage II tests indicated the adhesive bonding was a viable technique in using with panel-to-panel joint for FRP decks. Stage III research was aimed to further optimize this design.
3. In Stage III, results show that under a four-point bending configuration, FRP samples with a scarfed edge have better performance than those having a butt joint (90°). The critical

load and displacement (at crack initiation) increased as scarf angle decreased. In addition, no significant advantage or difference in behavior was found using double seam connection (using I-connectors) compared to single seam connection for the deck joints tested. Since the double seam connection involves developing a new, special pultruded shape (I-connector), the single seam connection with scarfed edge was used in the Stage IV study: a two-bay mock-up test of the Hawthorne St. Bridge.

4. Finally in Stage IV, a full-scale two-bay section of the bridge was constructed and tested in the Structures Laboratory at Virginia Tech. Static, fatigue, and failure tests were conducted on the adhesive panel-to-panel connections to evaluate their performance. The following conclusions can be drawn from the static and fatigue tests conducted on the adhesively-bonded, panel-to-panel connections of an FRP bridge deck system in Stage IV study.
   - The proposed full-length, adhesively-bonded tongue and groove panel-to-panel joints can meet the necessary strength performance criteria. No failure was observed in the adhesive layer or in the joint interface, which indicates the adhesive layer and adhesive-substrate interface are stronger than the FRP components. Thus adhesive bonding will not control the design strength of this FRP deck system.
   - The average first failure load was 100 kips in the strength tests on the adhesive joints, about five times the design service load of 21.3 kips. This value is close to the first failure load found in strength tests of as-received decks. This indicates the adhesive joint will not influence the strength of the deck.
   - The failure in the top plate and the top flange of the tube was characterized by weak-axis bending, with cracking parallel to the tube webs. This is also consistent with the failure mode in strength tests of as-received decks.
   - The strain and displacement showed linear elastic behavior up to design service load. The test results revealed an average deflection of span/664, which is slightly larger than the span/800 criteria in the AASHTO LRFD Bridge Design Specifications (AASHTO 2004). It should be noted that this limit is not intended for application to FRP composite bridge decks. However, no appropriate design limit is presently available.
   - No significant change in stiffness or strength of the deck after 3,000,000 cycles of a fatigue load at a minimum/maximum load ratio of R=0.1, with the maximum load of 22

kips and the minimum load of 2 kips. This demonstrated the durability of the adhesive joint under repetitive loading.

- The mock-up test in the laboratory provided valuable insights into the constructability of the adhesive panel-to-panel connections. These results will help develop a protocol for adhesive construction during the future bridge installation. Furthermore, the data collected during the test will be used to compare with later test data from an in-situ bridge test.

Based on the results of this four-stage study, it was concluded that this adhesive bonding technique is suitable for use with Strongwell's FRP deck system to replace the deteriorated RC deck in the Hawthorne St. Bridge. Future research will focus on the long-term durability of the FRP deck system.

5.1.2 Global Structural Performance of the FRP-deck-on-steel-superstructure system

Various design issues related to global structural performance of the FRP-deck-on-steel-superstructure system were investigated both in laboratory and in field. Following conclusions are drawn from this study:

1. Results from both laboratory and field indicate that the clip-type of panel-to-stringer connection provides little composite action as expected, which fulfills the design intention.
2. The peak longitudinal strains (perpendicular to traffic direction) at both sides of the joint are almost identical when front and back axles of the loading truck passed the joint in the field test, which indicate that the panel-to-panel joint is effectively transferring loads from one deck panel to the other.
3. Test results from both laboratory and field show that both AASHTO LDF equations for concrete deck systems are not appropriate for the FRP-deck-on-steel-superstructure systems.
4. The FRP deck provides similar stiffness as a glued laminated timber deck rather than a concrete deck in the direction transverse to traffic. The AASHTO LDFs equations for the category of glued laminated timber deck on steel stringers can give good

estimations on LDFs of FRP-deck-on-steel-girder bridges as suggested by the results from both laboratory and field tests.

5. The lever rule can be used as an appropriately conservative design method to predict the LDFs of FRP-deck-on-steel-girder bridges.
6. The local effects play a important role in the performance of FRP deck. It makes the strains of the cellular type of deck system change rapidly and experienced transverse (traffice direction) double curvature when loading truck crossed the instrumented area. However, the average peak longitudinal and transverse strains under truck loading do not even come close to reaching the ultimate strain in the material.
7. The live load deflection of the bridge in field test is approximately L/1270, which is within the deflection limit (L/800) specified in AASHTO LRFD Bridge Design Specification (AASHTO 2004).

5.1.3 Design Rcommendations for FRP Bridge Deck Supported on Steel Superstructure

An extensive parametric study was conducted to examine the structural behavior of FRP deck-on-steel-superstructure systems. Based on the FEM results, two design issues concerning the FRP decks, namely deck relative deflection and LDF of supporting steel girders, are investigated. Practical design recommendations are provided to help design engineers to overcome any reluctance to adopt FRP decks due to limited experience and design approaches. The following conclusions can be drawn from this study.

1. The strip method specified in AASHTO LRFD specification (AASHTO 2004) as an approximate method of analysis for the design of concrete, steel grid and wood decks can also be applied to unconventional FRP decks as a practical method. However, different strip width equations have to be determined by either FEM or experimental methods for different types of FRP decks. In this study, one such an equation has been derived for the Strongwell deck.
2. Both AASHTO code equations for a similar thickness concrete deck underestimate the LDF of FRP deck-on-steel-superstructure systems (up to 20% lower than the LDFs obtained from FEM). This may be due to the fact that flexural stiffness of an FRP deck in

the primary direction (perpendicular to traffic) is much smaller than that of a concrete deck with similar thickness.

3. Both FEM results and experimental measurements show that the AASHTO LDFs equations for glued laminated timber decks on steel stringers provide good estimations of LDFs for FRP-deck-on-steel-girder bridges. This is because the FRP deck in this study has similar stiffness to a laminated timber deck. These equations are recommended as a practical method in determining LDFs of this type FRP-deck-on-steel-superstructure bridges.
4. The lever rule can be used as an appropriately conservative design method to predict the LDFs of FRP-deck-on-steel-girder bridges. This is in agreement with the finding from Moses et al. (2006).
5. No secondary elements, such as live bracing and parapets, were considered in this study. Since there elements generally help the transverse distribution of moment and result in smaller LDFs, the above methods will produce conservative LDFs.
6. The above conclusions are based on non-composite behavior between FRP deck and girders. Because the composite behavior in FRP deck-on-steel-superstructure bridges will degrade with time and can not be considered in the strength limit states (Moses et al. 2006; Zhang and Cai 2006), the above methods may be used in a long-term basis and for conservative design purposes.

The reader should be cautioned that this research is based on a single FRP deck type (Strongwell FRP Deck). Different deck systems may exhibit different behavior and the application of the present results would need to be investigated thoroughly.

5.2 Recommendations for Future Research

The recommended areas of future research presented in this section address several aspects of FRP bridge deck to overcome any reluctance to adopt FRP deck into mainstream bridge application,

1. High initial cost is the first concern that hinders the use of FRP bridge deck systems. This cost is more than twice that typically quoted for the new construction or replacement of a deck with conventional materials. To help FRP deck get widely accepted in

the civil engineering field, technology of production quantities and manufacturing advances helps to reduce the high initial project costs is greatly needed.

2. There is uncertainty in defining the deflection limits in existing design guidelines for FRP composites construction. For the time being, FRP bridge deck designers quantify deck performance in terms of criteria developed for conventional materials. Since an FRP deck has similar stiffness, load distribution capability and similar deck-to-stringer connection system as a glued laminated timber deck, the limit of live load deflection for wood construction under vehicular and pedestrian loads (Span / 425) is consider to be also appropriate for FRP deck application. To further justify the above argument, future research should focus on human tolerance on static deflection or dynamic motion due to vehicular traffic. Also, the proper deflection limit should be investigated with regard to any wearing surface applied on FRP deck.

3. Research on investigation and evaluation the durability of the FRP bridge deck system. Damage accumulation induced by environmental effects, such as moisture, temperature and UV light exposure should be monitored by extensive visual and non-destructive evaluation in a long-term basis. Deck fire retardant is another important topic needs further investigation.

4. Fatigue behavior of FRP bridge deck system. The damage and failure of the deck system observed from field test indicates that research on the fatigue cracking and damaging for the deck system is necessary.

5. For bridge decks made from traditional material (concrete, steel etc.), a dynamic load allowance percent is used to account for dynamic loading of traveling vehicles. However, it is not clear whether this method can be applied to thin-walled multi-cellular bridge decks made from FRP composite materials. Research needs to be done to investigate the dynamic traveling loading on the FRP deck's performance.

REFERENCES

(MDA) Market Development Alliance. (2000). *Product selection guide: FRP composite products for bridge applications, edited by J. P. Busel and J. D. Lockwood.*, Market Development Alliance, Harrison, New York, USA.

American Association of State Highway and Transportation Officials (AASHTO). (2002). *Standard specifications for highway bridges 17th Edition*, American Association of State Highway and Transportation Officials, Washington, D.C.

American Association of State Highway and Transportation Officials (AASHTO). (2004). *AASHTO LRFD bridge design specifications*, American Association of State Highway and Transportation Officials, Washington, D.C.

ANSYS. (2004). "ANSYS Release 9.0 Documentation." version 9.0, Swanson Analysis System, Inc.

Ashland. (2003). "Ashland Pliogrip 8000/6660 Urethane Adhesive System Work Sheet."

Bakeri, B., and Sunder, S. S. "Concepts for hybrid FRP bridge deck system." *Proceedings of 1st Materials Engineering Congress, ASCE*, Denver, CO. 1990, 1006-1014.

Bakis, C. E., Bank, L. C., Brown, V. L., Cosenza, E., Davalos, J. F., Lesko, J. J., Machida, A., Rizkalla, S. H., and Triantafillou, T. C. (2002). "Fiber-reinforced polymer composites for construction-state-of-the-art review." *Journal of Composites for Construction*, 6(2), 73-87.

Barker, R. M., and Puckett, J. A. (1997). *Design of Highway Bridges*, John Wiley & Sons, Inc.

Brown, B. J. (1998). "Design analysis of single-span advanced composite deck-and-stringer bridge systems," MS thesis, West Virginia University, Morgantown, West Virginia.

Brown, R. T., and Zureick, A. (1999). "Lightweigh composite truss section decking." 3rd International Workshop on Very Large Floating Structures, Honolulu, Hawaii, U.S.,paper 7-1-3.

Cassity, P., Richards, D., and Gillespie, J. (2002). "Compositely Acting FRP Deck & Girder System." *Structural Engineering International*, 12(2), 71-75.

Chan, T. H. T., and Chan, J. H. F. (1999). "The use of eccentric beam elements in the analysis of slab-ongirder bridges." *Struct. Eng. Mech.,*, 8(1), 85-102.

Chung, W. S., and Sotelino, E. D. (2006). "Three-dimensional finite element modeling of composite girder bridges." *Engineering Structures*, 28(1), 63-71.

Coleman, J. T. (2002). "Continuation of Field and Laboratory Tests of a Proposed Bridge Deck Panel Fabricated from Pultruded Fiber-Reinforced Polymer Components," M.S. Thesis, Virginia Polytechnic Institute and State University, Blacksburg,VA.

Composite Growth Initiative of the American Composites Manufactures Association (ACMA). (2004). "Global FRP Use for Bridge Applications: statistics." <http://www.mdacomposites.org> (Sep, 7, 2006).

Coogler, K., Harries, K. A., Wan, B., Rizos, D. C., and Petrou, M. F. (2005). "Critical Evaluation of Strain Measurements in Glass Fiber-Reinforced Polymer Bridge Decks." *J. Bridge Eng*, 10(6), 704–712.

Davalos, J. F., Qiao, P., Xu, X. F., Robinson, J., and Barth, K. E. (2001). "Modeling and characterization of fiber-reinforced plastic honeycomb sandwich panels for highway bridge applications." *Composite Structures*, 52(3-4), 441-452

Demitz, J. R., Mertz, D. R., and Gillespie, J. W. (2003). "Deflection Requirements for Bridges Constructed with Advanced Composite Materials." *J. of bridge eng.*, 8(2), 73-83.

Ehlen, M. A. (1999). "Life-cycle costs of fiber-reinforced-polymer bridge decks." *Journal of Materials in Civil Engineering*, 11(3), 224-230.

Federal Highway Administration and United States Department of Transportation (FHWA/USDOT). (2002). "Corrosion costs and preventative strategies in the United States." A Supplement to Materials Performance (MP), NACE International, Houston.

Federal Highway Administration and United States Department of Transportation (FHWA/USDOT). (2006). "FRP Decks and Superstructures: Current Practice." http://www.fhwa.dot.gov/BRIDGE/frp/deckprac.htm.

GangaRao, H. V. S., and Siva, H. R. V. (2002). "Advances in fibre-reinforced polymer composite bridge decks." *Prog. Struct. Engng Mater* 4, 161–168.

GangaRao, H. V. S., Thippeswamy, H. K., Shekar, V., and Craigo, C. (1999). "Development of glass fiber reinforced polmer composite bridge deck." *SAMPE Journal*, 35(4), 12-24.

Harik, I., Alagusundaramoorthy, P., Siddiqui, R., Lopez-Anido, R., Morton, S., Dutta, P., and Shahrooz, B. "Static testing on FRP bridge deck panels." *Proceedings of the 44th International Sampe Symposium and Exhibition*, Long Beach, California, U.S., 1643-1654.

Hayes, M. D., Ohanehi, D., Lesko, J. J., Cousins, T. E., and Witcher, D. (2000). "Performance of tube and plate fiberglass composite bridge deck." *J. Compos. Constr.*, 4(2), 48–55.

Henry, J. (1985). "Deck girders system for highway bridges using fiber reinforced plastics," MS thesis, North Carolina State Univ., Raleigh, N.C.

Jones, R. (1999). *Mechanics of composite materials*, Taylor & Francis, Philadelphia, PA, USA.

Karbhari, V. M., and Zhao, L. (2000). "Use of composites for 21st century civil infrastructure." *Computer Methods in Applied Mechanics and Engineering*, 185(2-4), 433-454.

Keller, T. (2001). "Recent all-composite and hybrid fiber-reinforced polymer bridges and buildings." *Struct. Engng Mater.*, 3, 132-140.

Keller, T., and Gurtler, H. (2005). "Quasi-static and fatigue performance of a cellular FRP bridge deck adhesively bonded to steel girders." *Composite Structures*, 70(4), 484-496.

Keller, T., and Gurtler, H. (2006). "Design of hybrid bridge girders with adhesively bonded and compositely acting FRP deck." *Composite Structures*, 74(2), 202-212.

Keller, T., and Schollmayer, M. (2004). "Plate bending behavior of a pultruded GFRP bridge deck system." *Composite Structures*, 64(3-4), 285-295.

Keller, T., and Schollmayer, M. (2006). "In-plane tensile performance of a cellular FRP bridge deck acting as top chord of continuous bridge girders." *Composite Structures*, 72(1), 130-140.

Link, C. T. (2003). "Development of Panel-to-Panel Connection for use with a Pultruded Fiber-Reinforced-Polymer Bridge Deck System," M.E.Report, Virginia Polytechnic Institute and State University, Blacksburg, Virginia.

Lopez-Anido, R. (2002). "Life-Cycle Cost Survey of Concrete Bridge Decks– A Benchmark for FRP Bridge Deck Replacement." Transportation Research Board, Washington D.C.

Lopez-Anido, R., GangaRao, H., Vedam, V., and Overby, N. "Design and evaluation of a modular FRP bridge deck." *Proc., Int. Composites Expo '97*, SPI-Composites Institute, Nashville, TN, 3(E)1–6.

Mallick, P. K. (1993). *Fiber-reinforced composites: materials, manufacturing, and design*, M. Dekker, New York, NY, USA.

McGhee, K. K., Barton, F. W., and Mckeel, W. T. "Optimum Design of CompositeBridge Deck Panels. Advances Composites Materials in Civil Engineering Structures,." *Proceedings of the Specialty Conference, A.S.C.E.*, Las Vegas, Nevada,Jan. 31-Feb. 1, 1991, 360-370.

Meggers, D. "Fiber reinforced polymer bridge decks—The Kansas experience." *Rep. Prepared for the Kansas Department of Transportation (CD-ROM), 2000*, Topeka, Kan.

MMC. (2002). *DuraSpan Fiber-reinforced Polymer Bridge Deck Systems*, Martin Marietta Composites (MMC), Raleigh, NC,USA.

Moon, F. L., and Gillespie, J. W. (2005). "Experimental validation of a shear stud connection between steel girders and a fiber-reinforced polymer deck in the transverse direction." *Journal of Composites for Construction*, 9(3), 284-287.

Moses, J., Harries, K., Earls, C., and Yulismana, W. (2006). "Evaluation of Effective Width and Distribution Factors for GFRP Bridge Deck Supported on Steel Girders." *J. Bridge Eng.*, 11(4), 401-409.

Munley, E. (2000). "FHWA's program in FRP composites. Eastern Resource Center Bridge Technology Workshop notes." Federal Highway Administration, Baltimore, Maryland, USA (On-line Internet web: http://www.fhwa.dot.gov/resourcecenters/eastern/infrastr/Boston.ppt).

Qiao, P. Z., Davalos, J. F., and Brown, B. (2000). "A systematic analysis and design approach for single-span FRP deck/stringer bridges." *Composites Part B-Engineering*, 31(6-7), 593-609.

Reising, R. M. W., Shahrooz, B. M., Hunt, V. J., Neumann, A. R., and Helmicki, A. J. (2004a). "Performance comparison of four fiber-reinforced polymer deck panels." *J. Compos. Constr.*, 8(3), 265-274.

Reising, R. M. W., Shahrooz, B. M., Hunt, V. J., Neumann, A. R., Helmicki, A. J., and Hastak, M. (2004b). "Close look at construction issues and performance of four fiber-reinforced polymer composite bridge decks." *Journal of Composites for Construction*, 8(1), 33-42.

Righman, J., Barth, K., and Davalos, J. (2004). "Development of an efficient connector system for fiber reinforced polymer bridge decks to steel girders." *Journal of Composites for Construction*, 8(4), 279-288.

Salim, H. A., Barker, M., and Davalos, J. F. (2006). "Approximate series solution for analysis of FRP composite highway bridges." *Journal of Composites for Construction*, 10(4), 357-366.

Salim, H. A., Davalos, J. E., Qiao, P., and Kiger, S. A. (1997). "Analysis and design of fiber reinforced plastic composite deck-and-stringer bridges." *Composite Structures*, 38(1-4), 295-307.

Soto J, Lesko, J., Case, S., Majumdar, P., and Liu, Z. (2004). "Design and Testing of Adhesively Bonded FRP Deck Joints." National Science Foundation (NSF) and Research Experience for Undergraduates (REU) Summer Undergraduate Research Program (SURP),Department of Engineering Science and Mechanics, Virginia Polytechnic Institute and State University, Blacksburg, VA 24061.

Strongwell Inc. (2002). *Extren Design Manual*, Bristol, VA. <http://www.strongwell.com/literature/design_manual/> (May, 20, 2007).

Taly, N. (1998). *Design of Modern Highway Bridges*, McGraw-Hill, New York, New York.

Tang, B., and Podolny, W. "A Successful Beginning for Fiber Reinforced Polymer (FRP) Composite Materials in Bridge Applications." *Proceedings of International Conference on Corrosion and Rehabilitation of Reinforced Concrete Structures, Dec. 7-11, 1998*, Orlando, Florida (Online: http://www.fhwa.dot.gov/bridge/frp/frp1298.htm).

Temeles, A. B. (2001). "Field and Laboratory Tests of a Proposed Bridge Deck Panel Fabricated from Pultruded Fiber-Reinforced Polymer Components," M.S. Thesis, Virginia Polytechnic Institute and State University, Blacksburg, Virginia.

Transportation Research Board. (2006). "National coooperative Highway Research Program (NCHRP) Report 564: Field Inspection of In-Service FRP Bridge Decks." Transportation Research Board, Washington, D.C.

Tsai, S. W. (1992). *Theory of Composites Design*, Think Composites, ISBN 0-9618090-3-5.

Turner, M. K., Harries, K. A., Petrou, M. F., and Rizos, D. (2004). "In situ structural evaluation of a GFRP bridge deck system." *Composite Structures*, 65(2), 157-165.

Wan, B. L., Rizos, D. C., Petrou, M. F., and Harries, K. A. (2005). "Computer simulations and parametric studies of GFRP bridge deck systems." *Composite Structures*, 69(1), 103-115.

Zetterberg, T., Astrom, B. T., Backlund, J., and Burman, M. (2001). "On design of joints between composite profiles for bridge deck applications." *Compos. Struc.*, 51(1), 83–91.

Zhang, Y., and Cai, C. S. (2006). "Load distribution and dynamic response of multi-girder bridges with FRP decks." *Engineering Structures*, In Press, Corrected Proof.

Zhou, A. (2002). "Stiffness and strength of fiber reinforced polymer composite bridge deck systems," PhD dissertation, Virginia Polytechnic Institute and State University, Blacksburg, Virginia, USA.

Zhou, A., and Keller, T. (2005). "Joining techniques for fiber reinforced polymer composite bridge deck systems." *Composite Structures*, 69(3), 336-345.

Zhou, A. X., Coleman, J. T., Temeles, A. B., Lesko, J. J., and Cousins, T. E. (2005). "Laboratory and field performance of cellular fiber-reinforced polymer composite bridge deck systems." *Journal of Composites for Construction*, 9(5), 458-467.

Zureick, A. "Fiber-reinforced polymeric bridge decks." *Proceedings of the National Seminar on Advanced Composite Material Bridges*, FHWA, 1997.

APPENDICES

Appendix A: Testing Results of Stage III (Plate Bending Test)

A.1 Results of Service Load Tests

Specimen		Deck #1		Deck #2	
		First Seam	Second Seam	First Seam	Second Seam
Load (kip)		22	22	22	22
Strain (με)	ASG1	141	-78	404	N/A
	ASG2	-932	8	-766	N/A
	ASG3	700	105	905	N/A
	ASG4	409	144	604	N/A
	ASG5	N/A	N/A	221	N/A
	ASG6	N/A	N/A	-166	N/A
	BSG1	35	244	N/A	557
	BSG2	-15	-834	N/A	-984
	BSG3	19	490	N/A	826
	BSG4	11	349	N/A	577
	BSG5	N/A	N/A	N/A	292
	BSG6	N/A	N/A	N/A	-127
Deflection (in) under loading patch	AWP1	0.1214	N/A	0.1436	N/A
	BWP1	N/A	0.1268	N/A	0.186

A.2 Results at Crack Initiation

Specimen		Deck #1		Deck #2	
		First Seam	Second Seam	First Seam	Second Seam
Load (kip)		27.6	41.7	30.4	36.6
Strain (με)	ASG1	127	-133	479	N/A
	ASG2	-924	-26	-1007	N/A
	ASG3	697	192	1150	N/A
	ASG4	427	263	754	N/A
	ASG5	N/A	N/A	245	N/A
	ASG6	N/A	N/A	-194	N/A
	BSG1	38	440	N/A	723
	BSG2	-14	-1347	N/A	-1280
	BSG3	22	913	N/A	1131
	BSG4	14	656	N/A	789
	BSG5	N/A	N/A	N/A	351
	BSG6	N/A	N/A	N/A	-164
Deflection (in) under loading patch	AWP1	0.1274	N/A	0.167	N/A
	BWP1	N/A	0.1661	N/A	0.226

A.3 Results at Ultimate Failure

Specimen		Deck #1		Deck #2	
		First Seam	Second Seam	First Seam	Second Seam
Load (kip)		22	22	22	22
Strain (με)	ASG1	141	-78	404	N/A
	ASG2	-932	8	-766	N/A
	ASG3	700	105	905	N/A
	ASG4	409	144	604	N/A
	ASG5	N/A	N/A	221	N/A
	ASG6	N/A	N/A	-166	N/A
	BSG1	35	244	N/A	557
	BSG2	-15	-834	N/A	-984
	BSG3	19	490	N/A	826
	BSG4	11	349	N/A	577
	BSG5	N/A	N/A	N/A	292
	BSG6	N/A	N/A	N/A	-127
Deflection (in) under loading patch	AWP1	0.1214	N/A	0.1436	N/A
	BWP1	N/A	0.1268	N/A	0.186

Appendix B: Testing Results of Stage IV (Full-scale Mock-up Test)

B.1 Results of Strength Test on the As-received Deck

At crack initiation		Case A	Case B	Case C
Load (kip)		94	148	158
Maximum Strain (με)	Longitudinal	3950	N/A	N/A
	Transverse	2360	N/A	N/A
Maximum Deflection (in)	Stringer 1	0.393	0.375	0.258
	Stringer 2	0.509	0.891	0.604
	Stringer 3	0.410	1.388	0.934
	Stringer 4	0.339	1.126	1.196
	Stringer 5	0.241	0.754	1.212
	Stringer 6	0.103	0.336	0.525
	Under load patch	0.966	N/A	N/A
	Under load patch (Left)	N/A	1.627	1.753
	Under load patch (Right)	N/A	1.594	1.689
	Relative deflection	0.515	0.222	0.517

Note: For case A, deck relative deflection is defined as deck deflection under loading patch with respect to the two supporting stringers.
For case B and C, deck relative deflection is defined as the average deck deflection at two sides of the stringer with respect to the stringer under loading patch.

B.2 Results of Strength Test on Panel-to-panel Connections

At crack initiation		Without fatigue		After fatigue
		Seam 2	Seam 3	Seam 3
Load (kip)		93	107	94.4
Maximum Strain (με)	Longitudinal	2886	3386	2980
Maximum Deflection (in)	Stringer 1	N/A	0.165	0.418
	Stringer 2	N/A	0.400	0.513
	Stringer 3	0.819	0.636	0.395
	Stringer 4	0.720	0.867	0.305
	Stringer 5	N/A	0.754	0.196
	Stringer 6	N/A	0.301	0.072
	Under load patch	1.211	1.267	0.868
	Relative deflection	0.441	0.457	0.403

Note: deck relative deflection is defined as deck deflection under loading patch with respect to the two supporting stringers.

Appendix C: Global Structural Performance of the Hawthorne St. Bridge

C.1 Results of Stringer and Deck Deflection under Service Load Case 1 to 5 at Location A

Location A

		Load Case 1				Load Case 2			
		Run 1	Run 2	Run 3	Ave.	Run 1	Run 2	Run 3	Ave.
Wheel Load (kip)		22	22	22	22	22	22	22	22
Stringer Deflection (in)	Str.1	0.181	0.186	0.163	0.177	0.125	0.114	0.117	0.119
	Str.2	0.229	0.229	0.233	0.230	0.236	0.229	0.222	0.229
	Str.3	0.231	0.229	0.213	0.224	0.264	0.253	0.249	0.255
	Str.4	0.148	0.151	0.153	0.151	0.244	0.232	0.226	0.234
	Str.5	0.088	0.087	0.085	0.087	0.143	0.141	0.141	0.141
	Str.6	0.028	0.028	0.027	0.027	0.054	0.055	0.054	0.054
Deck absolute deflection (in)		0.293	0.288	0.277	0.286	0.347	0.333	0.336	0.339
Deck relative defleciton (in)		0.088	0.081	0.079	0.082	0.093	0.091	0.099	0.094

		Load Case 3				Load Case 4			
		Run 1	Run 2	Run 3	Ave.	Run 1	Run 2	Run 3	Ave.
Wheel Load (kip)		22	22	22	22	22	22	22	22
Stringer Deflection (in)	Str.1	0.097	0.091	0.094	0.094	0.082	0.076	0.075	0.078
	Str.2	0.207	0.207	0.213	0.209	0.189	0.187	0.185	0.187
	Str.3	0.268	0.253	0.249	0.257	0.277	0.262	0.255	0.265
	Str.4	0.257	0.262	0.264	0.261	0.303	0.289	0.292	0.295
	Str.5	0.164	0.164	0.161	0.163	0.191	0.185	0.184	0.186
	Str.6	0.065	0.067	0.068	0.067	0.073	0.077	0.078	0.076
Deck absolute deflection (in)		N/A	N/A	N/A	N/A	0.318	0.309	0.309	0.312
Deck relative defleciton (in)		N/A	N/A	N/A	N/A	0.085	0.084	0.089	0.086

		Load Case 5			
		Run 1	Run 2	Run 3	Ave.
Wheel Load (kip)		22	22	22	22
Stringer Deflection (in)	Str.1	0.191	0.191	0.184	0.189
	Str.2	0.269	0.276	0.271	0.275
	Str.3	0.361	0.346	0.348	0.356
	Str.4	0.372	0.340	0.360	0.357
	Str.5	0.328	0.321	0.324	0.321
	Str.6	0.209	0.206	0.208	0.210
Deck absolute deflection (in)		0.355	0.352	0.351	0.359
Deck relative defleciton (in)		0.086	0.088	0.085	0.086

Note: Deck deflections are not listed for Load Case 3 because the load patch is not at the mid-span of two supporting stringers.

C.2 Results of Stringer and Deck strains under Service Load Case 1 to 5 at Location A

		Load Case 1				Load Case 2			
		Run 1	Run 2	Run 3	Ave.	Run 1	Run 2	Run 3	Ave.
Wheel Load (kip)		22	22	22	22	22	22	22	22
Stringer Strain (με)	Str.1	243	244	245	244	91	91	91	91
	Str.2	344	342	341	342	377	376	376	376
	Str.3	381	377	377	378	400	398	398	399
	Str.4	118	117	117	117	220	223	223	222
	Str.5	24	23	24	24	44	44	45	44
	Str.6	1	3	2	2	52	16	14	28
Deck Strain under loading patch (με)	Long.	761	760	761	761	842	836	837	838
	Trans.	178	182	181	180	473	461	461	465

		Load Case 3				Load Case 4			
		Run 1	Run 2	Run 3	Ave.	Run 1	Run 2	Run 3	Ave.
Wheel Load (kip)		22	22	22	22	22	22	22	22
Stringer Strain (με)	Str.1	47	48	47	47	24	25	25	25
	Str.2	329	329	329	329	280	277	276	278
	Str.3	392	392	392	392	406	401	399	402
	Str.4	287	292	290	290	349	341	341	343
	Str.5	65	66	66	66	97	96	96	96
	Str.6	1	16	16	11	7	39	41	29
Deck Strain under loading patch (με)	Long.	N/A	N/A	N/A	N/A	730	715	709	718
	Trans.	N/A	N/A	N/A	N/A	425	399	380	401

		Load Case 5			
		Run 1	Run 2	Run 3	Ave.
Wheel Load (kip)		22	22	22	22
Stringer Strain (με)	Str.1	242	245	245	244
	Str.2	400	389	390	393
	Str.3	550	545	545	547
	Str.4	471	468	473	471
	Str.5	340	338	344	341
	Str.6	322	318	320	320
Deck Strain under loading patch (με)	Long.	838	827	839	835
	Trans.	390	388	391	390

Note: Deck strains are not listed for Load Case 3 because the load patch is not at the mid-span of two supporting stringers.

C.3 Results of Stringer and Deck Deflection under Service Load Case 1 to 5 at Location B

		Load Case 1				Load Case 2			
		Run 1	Run 2	Run 3	Ave.	Run 1	Run 2	Run 3	Ave.
Wheel Load (kip)		22	22	22	22	22	22	22	22
Stringer Deflection (in)	Str.1	0.212	0.215	0.210	0.212	0.132	0.126	0.127	0.128
	Str.2	0.271	0.273	0.264	0.270	0.247	0.247	0.253	0.249
	Str.3	0.317	0.319	0.319	0.319	0.319	0.313	0.306	0.313
	Str.4	0.246	0.239	0.235	0.240	0.294	0.285	0.282	0.287
	Str.5	0.145	0.142	0.141	0.142	0.168	0.164	0.167	0.166
	Str.6	0.056	0.055	0.056	0.056	0.069	0.068	0.068	0.068
Deck absolute deflection (in)		0.343	0.345	0.338	0.342	0.406	0.404	0.399	0.403
Deck relative defleciton (in)		0.101	0.101	0.101	0.101	0.099	0.105	0.105	0.103

		Load Case 3				Load Case 4			
		Run 1	Run 2	Run 3	Ave.	Run 1	Run 2	Run 3	Ave.
Wheel Load (kip)		22	22	22	22	22	22	22	22
Stringer Deflection (in)	Str.1	0.118	0.118	N/A	0.118	0.097	0.098	0.099	0.098
	Str.2	0.271	0.264	N/A	0.268	0.240	0.229	0.231	0.233
	Str.3	0.350	0.337	N/A	0.344	0.341	0.335	0.335	0.337
	Str.4	0.335	0.332	N/A	0.334	0.351	0.346	0.339	0.345
	Str.5	0.203	0.195	N/A	0.199	0.212	0.208	0.209	0.209
	Str.6	0.075	0.076	N/A	0.075	0.085	0.086	0.083	0.084
Deck absolute deflection (in)		N/A	N/A	N/A	N/A	0.404	0.397	0.397	0.399
Deck relative defleciton (in)		N/A	N/A	N/A	N/A	0.113	0.115	0.114	0.114

		Load Case 5			
		Run 1	Run 2	Run 3	Ave.
Wheel Load (kip)		22	22	22	22
Stringer Deflection (in)	Str.1	0.228	0.229	0.228	0.229
	Str.2	0.381	0.374	0.374	0.374
	Str.3	0.519	0.511	0.513	0.514
	Str.4	0.527	0.516	0.521	0.521
	Str.5	0.404	0.397	0.397	0.397
	Str.6	0.239	0.233	0.234	0.236
Deck absolute deflection (in)		0.402	0.405	0.404	0.403
Deck relative defleciton (in)		0.097	0.103	0.103	0.102

Note: Deck deflections are not listed for Load Case 3 because the load patch is not at the mid-span of two supporting stringers.

C.4 Results of Stringer and Deck strains under Service Load Case 1 to 5 at Location B

		Load Case 1				Load Case 2			
		Run 1	Run 2	Run 3	Ave.	Run 1	Run 2	Run 3	Ave.
Wheel Load (kip)		22	22	22	22	22	22	22	22
	Str.1 (top)	287	286	286	286	107	109	109	109
	Str.1 (bottom)	-237	-239	-238	-238	-110	-111	-111	-111
	Str.2 (top)	273	271	272	272	266	266	268	267
	Str.2 (bottom)	-320	-318	-318	-319	-303	-302	-303	-303
	Str.3 (top)	338	337	337	337	299	300	300	300
Stringer	Str.3 (bottom)	-325	-324	-325	-324	-277	-276	-277	-277
	Str.4 (top)	129	132	127	129	220	220	221	221
Strain	Str.4 (bottom)	-128	-126	-124	-126	-206	-207	-207	-206
(με)	Str.5	22	21	23	22	51	49	49	49
	Str.6	0	0	-1	-1	2	2	2	2
Deck Strain under	Long.	812	782	778	791	869	866	871	869
loading patch (με)	Trans.	641	613	607	620	662	648	648	653

		Load Case 3				Load Case 4			
		Run 1	Run 2	Run 3	Ave.	Run 1	Run 2	Run 3	Ave.
Wheel Load (kip)		22	22	22	22	22	22	22	22
	Str.1 (top)	74	72	N/A	73	41	42	42	41
	Str.1 (bottom)	-84	-83	N/A	-83	-55	-56	-54	-55
	Str.2 (top)	256	255	N/A	256	200	202	201	201
	Str.2 (bottom)	-293	-291	N/A	-292	-224	-223	-223	-224
	Str.3 (top)	320	321	N/A	320	310	311	312	311
Stringer	Str.3 (bottom)	-299	-297	N/A	-298	-287	-287	-288	-287
	Str.4 (top)	296	295	N/A	295	333	333	335	333
Strain	Str.4 (bottom)	-274	-273	N/A	-273	-309	-307	-308	-308
(με)	Str.5	76	76	N/A	76	103	103	104	103
	Str.6	8	8	N/A	8	17	16	17	17
Deck Strain under	Long.	N/A	N/A	N/A	N/A	877	872	875	875
loading patch (με)	Trans.	N/A	N/A	N/A	N/A	557	545	541	548

		Load Case 5			
		Run 1	Run 2	Run 3	Ave.
Wheel Load (kip)		22	22	22	22
	Str.1 (top)	290	290	289	290
	Str.1 (bottom)	-249	-251	-249	-250
	Str.2 (top)	309	309	307	308
	Str.2 (bottom)	-351	-352	-349	-351
	Str.3 (top)	466	464	464	465
Stringer	Str.3 (bottom)	-435	-436	-434	-435
	Str.4 (top)	442	444	446	444
Strain	Str.4 (bottom)	-412	-415	-415	-414
(με)	Str.5	332	325	328	328
	Str.6	292	288	290	290
Deck Strain under	Long.	811	803	812	809
loading patch (με)	Trans.	560	556	557	558

Note: Deck strains are not listed for Load Case 3 because the load patch is not at the mid-span of two supporting stringers.

Appendix D: Field Testing

D.1 Results of Deck Strains under different load paths

	Deck Span Center Strain (Loacation C)		
	Btw Str.5 & 6	Btw Str.4 & 5	Btw Str.3 & 4
Run1	245		
Run2	273		
Run3	267		
Run4	264		
Run5	263		
AVG	262		
Run1	123		
Run2	126		
Run3	116		
Run4	127		
Run5	125		
AVG	123		
Run1		N/A	
Run2		N/A	
Run3		N/A	
Run4		N/A	
Run5		N/A	
AVG		N/A	
Run1		257	
Run2		263	
Run3		266	
Run4		261	
Run5		252	
AVG		260	
Run1			N/A
Run2			316
Run3			315
Run4			310
Run5			298
AVG			310
Run1			N/A
Run2			331
Run3			319
Run4			339
Run5			329
AVG			330

	Joint strain (Location D)		
	Btw Str. 5 & 6	Btw Str.4 & 5	Btw Str.3 & 4
	Abutment side/mid-span side	Abutment side/mid-span side	Abutment side/mid-span side
Run1	245 / 232		
Run2	253 / 210		
Run3	256 / 250		
Run4	251 / 253		
Run5	254 / 260		
AVG	252 / 241		
Run1	N/A		
Run2	N/A		
Run3	N/A		
Run4	N/A		
Run5	N/A		
AVG	N/A		
Run1		306 / 290	
Run2		309 / 265	
Run3		308 / 275	
Run4		309 / 285	
Run5		290 / 250	
AVG		304 / 273	
Run1		N/A	
Run2		N/A	
Run3		N/A	
Run4		N/A	
Run5		N/A	
AVG		N/A	
Run1			N/A
Run2			347 / 340
Run3			334 / 345
Run4			325 / 310
Run5			343 / 330
AVG			337 / 331
Run1			N/A
Run2			341 / 290
Run3			332 / 299
Run4			284 / 280
Run5			323 / 295
AVG			320 / 291

D.2 Results of Stringer Strains under different load paths

Strain			S1	S2	S3	Strain		S1	S2	S3
Path 1	Bridge Mid-span	Run1	23	46	110	First bay mid-span	Run1	24	50	116
		Run2	22	44	104		Run2	22	52	119
		Run3	24	42	106		Run3	23	56	145
		Run4	23	42	106		Run4	22	52	118
		Run5	21	44	107		Run5	21	58	144
		AVG	22.6	43.6	106.6		AVG	22.4	53.6	128.4
Path 2	Bridge Mid-span	Run1	106	170	182	First bay mid-span	Run1	126	148	216
		Run2	108	175	183		Run2	78	91	175
		Run3	113	167	178		Run3	137	133	213
		Run4	112	168	176		Run4	128	140	206
		Run5	111	170	181		Run5	129	151	212
		AVG	110	170	180		AVG	119.6	132.6	204.4
Path 3	Bridge Mid-span	Run1	19	35	88	First bay mid-span	Run1	19	52	117
		Run2	20	34	86		Run2	19	54	106
		Run3	22	36	86		Run3	20	55	114
		Run4	21	34	85		Run4	20	52	117
		Run5	20	35	85		Run5	19	46	110
		AVG	20.4	34.8	86		AVG	19.4	51.8	112.8
Path 4	Bridge Mid-span	Run1	145	168	164	First bay mid-span	Run1	147	176	177
		Run2	146	167	164		Run2	186	119	185
		Run3	144	167	163		Run3	179	111	195
		Run4	141	166	163		Run4	170	138	197
		Run5	140	170	168		Run5	171	135	190
		AVG	143.2	167.6	164.4		AVG	170.6	135.8	188.8

VITA

Zihong Liu was born and grew up in a mountain city, Zhangjiakou, Hebei (located 200 km northwest to Beijing), China and pursued his undergraduate education at the Tongji University, Shanghai, China. He graduated with a BS in Bridge Engineering in Aug. 1995 before working in the Guangdong Highway Design Institute, Guangdong China as a bridge design engineer.

He continuously worked for eight years and designed bridges ranging from short-span girder to long-span cable-stayed bridges. At the mean time, he studied part-timely and received an ME in Civil Engineering (Structures) in August 2002 from South China University of Technology. He started pursuing his Ph.D. at Virginia Tech in August, 2003. He completed his studies in the field of Fiber Reinforced Polymer (FRP) bridge deck system in June 2007. He will now go to Calgary, Canada to continue his professional career in bridge engineering.